COMBUSTION ANOMALIES IN STOP-RESTART FIRING OF HYBRID ROCKET ENGINES

****

Michael A. Saraniero

Princeton University
School of Engineering and Applied Science
Aerospace and Mechanical Sciences Department

Route	Init	
2123		Cataloging Dept. (for formal cataloging)
2127		Processing Dept. Note: After processing route worksheet, catalog cards, & excess copies of thesis to 2125. Route one copy of thesis, together with this sheet, to 2124.
2124		Technical Reports Section (for SABIR3 processing) Note: See Manual Letter 133, Part A.
2125		Reader Services Dept. Note: Shelve thesis & discard attached sheet.
Comments, etc.		

COMBUSTION ANOMALIES IN STOP-RESTART FIRING OF HYBRID ROCKET ENGINES

by

Michael A. Saraniero
LTJG USN

Submitted in partial fulfillment
of the requirements for
the degree of Master of Science in Engineering
from Princeton University, 1970

Signature of Author

ACKNOWLEDGMENTS

At this time I would like to express my appreciation to Prof. M. Summerfield, under whose advisorship this investigation has proceeded. His personal enthusiasm and interest has been a constant source of motivation for me.

Special thanks are offered to Dr. L. H. Caveny who diligently guided the experimental program and who helped immeasurably in developing the computer solutions for this study. Without his administrative forethought and experimental experience, I could not have accomplished as much within the alloted time.

I wish to thank Mr. P. L. Stang for directing my initial interests into the field of hybrid rockets. I am very grateful to Prof. H. Isoda who acted as technical advisor to the program. The careful proofreading provided by Dr. E. G. Plett is also appreciated.

The experimental apparatus could not have been built without the assistance and moral support of the technical staff. In particular, I am indebted to: Mr. C. R. Felsheim for building the experimental apparatus; Mr. S. O. Morris for designing and instrumenting the electrical system; Mr. J. H. Semler for fabrication of the motor parts and fuel grains; and Mr. E. R. Crosby who has ably provided the professional photography of the experimental apparatus. To Mr. J. Slade, an undergraduate, I am also grateful for his assistance in the day-to-day experimental firings during the academic year.

Mr. J. Lamendola has contributed many hours of conscientious effort to this work. His patience and assistance in preparing this thesis are warmly acknowledged. The skillful typing of this thesis has been accomplished by numerous personnel, all of whom I wish to thank. In particular, the typing done by Mrs. D. Morris and Miss C. Hartman was greatly appreciated.

This study has been made possible through the financial support of the Daniel and Florence Guggenheim Foundation and the National Aeronautics and Space Administration under NASA Grant NGR31-001-009. This thesis carries the report designation AMS No.945 in the records of the Department of Aerospace and Mechanical Sciences.

ABSTRACT

An experimental investigation of the restart process of an oxygen-Plexiglas hybrid rocket demonstrated that preheating the fuel (as a consequence of a previous ignition and a temporary extinguishment) significantly increases the rate of chamber pressurization and produces regression rate overshoots during reignition. Higher rates of chamber pressurization measured during the restart transient imply faster instantaneous regression rates of the fuel during restart. Transient periods following the initial ignition and the restart after a two-second shut-down were observed for four experimental tests which were conducted at two oxidizer flow rates, 0.078 lbm/sec and 0.039 lbm/sec, and two chamber pressures, 80 psig and 320 psig. Thermocouples made from 0.001 inch diameter chromel-alumel wire were embedded in the fuel to record subsurface temperature histories.

A mathematical model of the thermal processes in the fuel and the events that occur during an experimental firing was developed to calculate the regression rate transients. Quantitative agreement with experimental results was obtained by making nominal corrections to the calculated convective and radiative heating rates. A parametric study investigated the influence of the fuel's thermal characteristics (thermal conductivity, surface temperature, and heat of gasification) and the shut-down duration on the transient responses. The calculated results showed that instantaneous regression rate overshoots were as high as 29% when high energy fuels are reignited.

The results of this study indicate that the transient behaviors of pressure and regression rate during reignition after shut-down (the duration of which has been varied over a range of 0.9 to 4.0 sec) can be anticipated and predicted once the regression characteristics of individual fuel/oxidizer combinations have been established. Thus, extensive experimental firings of full scale rocket motors will not be required to adequately predict pressure-time histories and fuel consumption following reignition if proper attention is given to understanding the thermal distributions during shut-down periods.

TABLE OF CONTENTS

TABLE OF CONTENTS - cont'd.

LIST OF TABLES

List of Figures

NOMENCLATURE

a	coefficient in burning rate law, $r=aP^n$	
A	area of the motor port	(in^2) (cm^2)
B	linear pyrolysis law pre-exponential factor (when used in Chapter VI)	(cm/sec)
B	mass transfer number	
C_H	Stanton number	
C_{H_o}	Stanton number in the absence of blowing	
C_H/C_{H_o}	blowing coefficient	
C_p	specific heat of gas (Btu/lbmF)	(cal/gC)
C_s	heat capacity of the solid fuel	(cal/gC)
d	diameter	(in)
E	activation energy	(cal/g-mole)
G	total mass flux per unit area	(lbm/in^2sec)
G_{O_2}	oxygen mass flux per unit area based on initial diameter of the motor port	(lbm/in^2sec)
h_{conv}	convective heat transfer coefficient (Btu/ft^2sec F)	(cal/cm^2sec K)
h	enthalpy	(cal/g)
Δh	sensible enthalpy difference between the flame and the wall	(cal/g)
Δh_s	heat required to gasify condensed phase after vaporization temperature is achieved	(cal/g)
ΔH	effective heat of gasification of solid fuel, latent heat (Btu/lbm)	(cal/g)
K	constant	
k	thermal conductivity	(cal/cm sec K)
Le	Lewis number	
M	Mach number	
n	pressure exponent of simple burning rate law	

Nu	Nusselt number	
P	pressure	(psi) (atm)
Pc	steady-state chamber pressure	(psi) (atm)
Pr	Prandtl number	
Q	net heat flux to the surface	(Btu/sec)
q	heat transfer rate	(Btu/ft^{2}sec)
$\dot{q}_s$	rate of energy released associated with chemical reactions and phase changes at the gas-solid interface.	(cal/cm^{2}sec)
r	radius	(cm) (in)
$\dot{r}$	regression rate (in/sec)	(cm/sec)
R	universal gas constant, 1.9867	(cal/g mole K)
R_e	Reynolds number	
R_{e_z}	Reynolds number based on z	
R_{e_d}	Reynolds number based on diameter	
ΔR	total regression	(in)
t	time	(sec)
t_{ign}	igniter duration	(sec)
t_{run}	initial firing duration	(sec)
t_{rei}	firing duration following reignition	(sec)
t_{shd}	shut-down duration	(sec)
T	temperature,	(C)
T_s	surface temperature	(C)
T_f	temperature in the flame or in combustion zone at the fully reacted state	(C)
u	axial velocity component	(ft/sec)
V	free stream gas velocity	(ft/sec)
z	longitudinal coordinate in stream direction	(in)
Z	pre-exponential factor	(cal/cm^2 sec)

Greek Symbols

α_g	absorptivity of gas		
β	coefficient in Beer's Law		(cm^{-1})
δ	depth in significant heating		(in)
ϵ	emissivity		
χ	thermal diffusivity		(in^2/sec)
μ	viscosity coefficient		(g/cm sec)
ρ	mass density	(lbm/ft^3)	(g/cm^3)
σ	Stefan-Boltzman constant	$(cal/sec\ cm^2\ C^4)$	

Subscripts

b	bulk		
c	solid (i.e. condensed) phase		
e	edge of boundary layer		
f	fuel		
g	gas		
r	radiation		
s	gas-solid interface		
t	instantaneous		
w	wall		
x	distance from initial surface in direction of surface regression	(in)	(cm)
r	steady-state		
0	ambient conditions deep in fuel		

Superscripts

*	evaluated at reference temperature defined by Eq. VI-9	

CHAPTER I

INTRODUCTION TO THE CONCEPT OF THE HYBRID COMBUSTION MOTOR

I-A: Preliminary Remarks

Research and development programs have advanced the hybrid rocket motor state-of-the-art to the point that it is at times competitive and, in several applications, superior to either conventional liquid or solid propellant rocket motors. The application of hybrid rocket motors in advanced propulsion systems is imminent. The hybrid rocket features the advantages of a high specific impulse in a storable system, a wide range of thrust modulation, stop-start capabilities, and the safety of separate fuel and oxidizer storage. A hybrid rocket consists of a gaseous or vaporized oxidizer passing over a solid fuel. The high specific impulse is obtained through the use of special high energy ingredients in the solid fuel and by using high energy fluid oxidizers. The inverse of this configuration has been demonstrated; the inverse hybrid consists of a solid oxidizer and liquid or gaseous fuel. Conceptual representations of both the conventional and inverse hybrids are shown in Fig. 1.

The combustion processes of a hybrid rocket may be considered to consist of a reacting boundary layer with heat and mass transfer as well as chemical reactions occuring simultaneously. The combustion model for an oxidizer flowing over a flat plate of fuel is shown in Fig. 2. After ignition is achieved, the injected gaseous oxidizer and the fuel vapor (vaporized from the solid fuel by the heat feedback from the flame zone) are mixed in the boundary layer and form a turbulent diffusion flame zone.

The combustion rate of the hybrid rocket motor ingredients depends on a complex interplay of the following: (1) total mass flux of the oxidizer, (2) total mass flux of the fuel, (3) convective and diffusive mass transfer of the reactants and products in the turbulent boundary layer, (4) convective and radiative heat transfer from the flame to the surface and (5) motor and chamber configurations that may promote or retard the combustion processes. The resulting interactions that exist between fuel regression rate and fuel geometry, wherein the point regression rate is a function of the upstream regression rates and the flow conditions, posed serious problems to the development of hybrid motors. No simple regression rate expression, such

as $\dot{r} = aP^n$ as applied to conventional solid propellants, could be prescribed by previous hybrid researchers; rather, a complex combustion model is needed to predict the rate of regression of the solid phase as a function of the geometry of the motor, the flow rate of the oxidizer, the operating pressure, and the characteristics of the fuel. Because of the complexities of the combustion process, considerable difficulty is being experienced in the development of rocket motor configurations that produce uniform regression of the solid fuel.

A large portion of the hybrid rocket research has focused on the following two aspects of this surface regression problem: (a) a physical model describing the reaction in the boundary layer as a function of the physical properties of the propellant ingredients to yield a thermal driving force and (b) a mathematical model of the regression rate that encompasses the thermodynamic properties of the propellant and the fluid dynamics of the flow.[1] The development of these regression rate models has coincided with advances made in the fundamental investigations of the hybrid combustion mechanism. The results of more recent studies are reviewed in Chapter II.

I-B: Problems in Connection with Ignition, Shut-down and Restart

While researchers have made significant advances in fundamental investigations of the combustion mechanism [2,3], the development of more sophisticated, high energy propellant combinations with additives and high metal loading in polymer fuels has produced new developmental problems. Of particular interest to practical hybrid configurations are the problems that might occur during ignition, shut-down, and restart periods. They may arise as a result of one or more of the following factors:

1. A high loading of metal powder used in some hybrid fuels imparts a high thermal conductivity to the fuel. Thus, more heat must be transferred to the subsurface regions to achieve ignition. As a result, pronounced delays in achieving steady-state operation are encountered.

2. When partially oxidized fuel charges are employed for enhancement of specific impulse or for enhancement of regression rate, the exothermic reactions induced by the burning process during the normal thrust period continue rather vigorously after oxidizer shut-off, and so sharp thrust termination becomes uncertain.

3. The slow regression rate characteristic of most hybrid fuels produces a thick heated layer that remains on the fuel surface after shut-off of the oxidizer at thrust termination, and this residual heat can produce continued charring, surface reaction, and/or hot fuel vapor evolution for some time afterward.

4. If the state of the surface is altered considerably as a result of a continued reaction and residual heating after combustion termination, the restart process may be adversely affected. For example, if a deep heated region is produced in the fuel, significant overpressures may result during the reignition transient.[4]

A complete understanding of these factors and the ability to predict their influence on the ignition and restart processes is a prerequisite to the design of a high performance, rapidly responding hybrid rocket. Overpressurization and excessive rates of pressurization during the reignition transient period may lead to increases in the weight of structural components and erratic thrust versus time histories.

In particular, the restart or reignition process requires additional considerations as a result of the thermochemical processes and thermophysical changes that may occur in the fuel binder during the shut-down period. Because both the total redistribution of heat (by convection, conduction, and radiation) throughout the motor and the degree of preheatedness of the fuel are functions of time during the shut-down duration, a formidable problem evolves in predicting the pressure transients during the restart process.

Out of this description emerge the problems that require both theoretical and experimental considerations that are essential to gain an understanding of the ignition and restart processes. Also, because of the continuing trend toward larger, more sophisticated, and more costly hybrid motors, experimental results that can be applied to practical hybrid rockets must be achieved using laboratory scale rocket motors. Therefore, a study has been conducted to determine the effects of the following factors on the restart process: (1) temperature profiles in the fuel, (2) heat redistribution to the fuel from the motor following oxidizer termination and (3) the duration of the shut-down interval.

CHAPTER II

LITERATURE SURVEY

No simple regression rate law is available to the hybrid rocket designer and analyst. Instead, previous researchers have formulated difficult to use, qualitative expressions that describe the processes occurring in the reacting boundary layer adjacent to the regressing fuel. Numerous studies in which both simple and complex approaches to the reacting boundary layer have provided various regression rate expressions. The purpose of the following discussion is not to give a complete account of all the previous hybrid regression rate studies (this has been expertly done in Ref. 1) but rather, to indicate to the reader the general direction and scope of previous research on regression rate models for hybrid rockets. In Chapter III, a discussion of the factors influencing the problems connected with shut-down and restart will be treated.

II-A: Hybrid Combustion Models

The nature of combustion within a hybrid rocket, wherein combustion is controlled by convective and radiative heat transfer, rather than a direct reaction between the oxidizer and the fuel, suggests that a combustion model could be similar to that of a turbulent diffusion flame within the boundary layer with mass addition. As a result of this similarity, the sought after regression rate law describing such a combustion model would naturally contain terms coupling it to the aerothermodynamics of the boundary layer. Attention has therefore been focused on the chemically reacting boundary layer. Lees[5] presented a comprehensive study of convective heat transfer from reacting boundary layers by considering the influence of fuel mass addition from the wall.

Marxman and Gilbert[6] applied Lees' generalized category of a reacting boundary layer to the combustion process in a hybrid rocket. They found that if Le=1 when the boundary layer is laminar, and if Reynold's analogy is valid when the boundary layer is turbulent, the regression rate is proportional to heat flux reaching the surface from the turbulent boundary layer adjacent to the fuel. The result was a regression rate equation based on an ideal turbulent boundary layer. The combustion model, as shown in Fig. 3, assumes a thin flame combustion layer above the solid fuel. Marxman and Gilbert's

regression rate law illustrates the coupling between the fluid dynamics of the flow and the aerodynamics of the boundary layer. The complete equation is given below:*

$$\dot{r} = \frac{KG\,Re_x^{-0.2}}{\rho_f} \frac{C_H}{C_{H_0}} \frac{u_e}{u_g} \frac{\Delta h}{\Delta H} + \frac{\sigma \epsilon_w (\epsilon_g T_f^4 - \alpha_g T_w^4)}{\rho_f \Delta H} \qquad (1)$$

Three important parameters are included in the equation. The first parameter is the blowing coefficient ratio, C_H/C_{H_0}, relating the coupling between regression rate and boundary layer flow by accounting for the partial blockage of heat transfer to the fuel surface as a result of mass addition from the fuel surface. The second parameter is the independent variable, $\Delta h/\Delta H$, coupling the regression rate equation to a thermodynamic parameter dependent on only the fuel-oxidizer combination and its gasification process. The third parameter is the velocity ratio, u_e/u_g, leading to a solution locating the flame position relative to the boundary layer thickness. Marxman and Gilbert have also included a radiation term to include any additional heat transfer as a result of radiative energy. However, during normal operating conditions, the radiative addition is likely to be small in comparison to the convective heat transfer. Applying Eq. 1, less the radiation term, to an oxygen-Plexiglas system, Marxman and Gilbert have correlated regression rates over a wide range of oxidizer mass fluxes and Reynolds numbers and obtained agreement with experimental values within a factor of two. However, as noted by Marxman and Gilbert, experimental and theoretical work is still needed to clarify the influences of the parameters in the equation.

It is convenient at this time to introduce and define the mass transfer number $B = (u_e/u_g)(\Delta h/\Delta H)$. This parameter plays a dual role in hybrid combustion. Initially, B may be considered as a thermodynamic constant characterized by the physical properties of the solid and the gas phase of the particular propellants. Further, it has also been shown that $B' = Pr^{-0.67} B$ is the similarity parameter of a boundary layer with mass injection. Thus, if B' is constant along the wall, the velocity, species concentration, and enthalpy profiles are similar in the boundary layer. Since the Prandtl number of the gas is near unity, B' and B are not only similar, but also approximately equal.

---

*All symbols are defined in the nomenclature.

Thus, B serves to couple the regression rate equation to a particular propellant combination and the fluid dynamics of the flow.[1]

An empirical analysis of the regression rate equation was performed by Anderson.[7] Anderson[7] applied the Dittus-Boelter heat transfer equation to turbulent flow over a fuel sample in a blast tube. Using the Dittus-Boelter equation

$$Nu = \frac{h_{CONV}\, d}{k} = K\, Re_d^{0.8}\, Pr^{0.4} \tag{2}$$

and a constant Prandtl number of unity

$$Pr = \frac{c_p\, \mu}{k} = 1 \tag{3}$$

the heat transfer coefficient becomes

$$h_{conv} = K Re_d^{0.8} = K\left(\frac{\rho d V}{\mu}\right)^{0.8} \tag{4}$$

Anderson then applies the ideal gas law to express ρ, V, and μ (and thus R_{ed}) in terms of temperature, T, pressure, P, and Mach Number, M. The heat transfer rate is equal to the convective heat transfer coefficient multiplied by the temperature difference, $T_f - T_w$.

$$q = h_{CONV}\left(T_f - T_w\right) = K\left(M \cdot P\right)^{0.8}\left[\frac{T_f - T_w}{T_f^{0.8}}\right] \tag{5}$$

The regression rate will be directly proportional to the amount of heat reaching the surface and inversely proportional to the heat required to vaporize the solid. Hence, a simplified regression rate equation is given:

$$\dot{r} = \frac{K(MP)^{0.8}}{\rho_f\, \Delta H}\left[\frac{T_f - T_w}{T_f^{0.8}}\right] \tag{6}$$

In summary, Anderson related the regression rate equation to Mach number, pressure, and the heat of ablation of the solid fuel. The equation is independent of the oxidizer choice, and his results for the regression rate of Plexiglas as a function of the Mach number-pressure produce, M·P, is shown in Fig. 4. Anderson believes that this practical expression, in terms of easily obtained parameters, is a good approximation over a wide range of the oxidizers and is therefore a useful engineering tool for the design of hybrid motors.

In an extension of Anderson's work, Hurt and Anderson[8] arrived at Eq. 6 by an approach that included experimental and theoretical examination of the convective heat transfer through the laminar sublayer protion of the turbulent boundary layer. The laminar sublayer normally offers the greatest resistance to heat flow. Hurt and Anderson[8] postulated that the ablation of the solid fuel is controlled by the thickness of the viscous sublayer and that a heat transfer coefficient with zero fuel mass addition could be chosen and multiplied by a correction factor to account for the effect of fuel mass addition at the wall.

The pressure dependence of both metalized and non-metalized hybrid fuels has received considerable attention.[9,10,11] Smoot and Price concluded[9,10] that in regions of lower oxidizer flow rates the regression rates were independent of pressure and increased as the 0.8 power of specific total flow rate. However, at high flow rates, the regression rate was nearly independent of flow, but increased markedly with pressure. Thus, their expperimental results are in good agreement with those predicted by the turbulent heat transfer model for only the lower flow rates. It was therefore postulated by Smoot and Price[9,10] that rate limiting chemical kinetic processes were the cause of the observed pressure dependence.

It is important to mention that the approaches to modeling a regression rate law, whether it is the turbulent boundary layer combustion model or the M·P correlation, have primarily been directed at the steady-state condition. That is, the regression rate is directly proportional to the heat reaching the surface. Therefore, neither approach has been extended to consider a transient period when the instantaneous regression rate is changing to approach its steady-state value. A transient regression rate may arise as a result of any of the following: (1) after ignition, the burning conditions approach the steady-state value, (2) a throttling maneuver when a rapid change in oxidizer flow is followed by an increasing or decreasing

regression rate and (3) termination of the oxidizer flow when the regression rate approaches zero.

II-B: Time Dependent Operation

An analytical investigation of the time dependent transient period has been performed by Marxman, Wooldridge and Muzzy.[12] Their results are directed at only the transient period following initiation of heat to the surface (ignition). This transient period is related to the time required to achieve a steady-state thermal profile in the fuel. During this period, the regression rate is not proportional to the heat flux received at the surface since the thermal profile is developing to the steady-state conditions. During ignition transients the ratio of the heat conducted into the solid to the heat that gasifies the fuel is higher than for the steady-state conditions. As a result, regression rate equations based on steady-state thermal balances at the gas-solid interface do not apply during transient conditions. Thus, it is necessary to account for the developing thermal profiles in the fuel in order to predict the instantaneous regression rate.

Marxman, et al. continued their analysis to predict the depth of the thermal profile as a function of time. The steady-state penetration depth, δ_∞ , which the protile will reach is proportional to the thermal diffusivity and inversely proportional to the steady-state regression rate as approximated by Eq. 7.

$$\delta_\infty = 3\,\frac{\alpha}{\dot{r}_\infty} \tag{7}$$

The nomenclature associated with the steady-state thermal profile is shown in Fig. 5.

As a result of their analysis the transient behavior of the regression rate can be expressed as a function of the parameter $c_s (T_s - T_o)/\Delta H$ (assuming $\dot{r}_\infty^2/\alpha$ is constant) as shown in Fig. 6. Consequently, the transient periods are greater for fuels with a low ΔH or a high vaporization temperature. However, the possibility of decreasing the transient period arises as a result of increasing T_o, the initial fuel temperature. This is not considered by Marxman, Wooldridge and Muzzy. Although T_o is considered the constant temperature deep in the fuel, T_o may be increased as a result of a previous firing.

In conclusion then, the relationship established between the transient regression rate and the time to establish a thermal profile can be extended one step further.

As the steady-state thermal profile is established and more fuel mass is added to the combustion process, the rate of pressurization in the chamber increases and also depends, therefore, on the time to establish the steady-state thermal profile. This interdependence between the temperature profile of the fuel, regression rate transients, and the chamber pressurization rate will be discussed in more detail in the next chapter.

CHAPTER III

THE EFFECTS OF THE THERMAL ASPECTS OF A HYBRID FUEL ON THE SHUT-DOWN DURATION AND RESTART PROCESSES

III-A: Influence of a Preheated Fuel

The purpose of this discussion is to examine the problems that may arise in predicting the reignition process as a result of a nonuniform, nonsteady thermal profile in the fuel. A search of previous efforts revealed that insufficient emphasis has been placed on the factors influencing the reignition process.[13] Therefore, an experimental program was undertaken to determine the influence of a preheated fuel on the reignition process by comparing the pressure-time histories and subsurface temperature measurements of the ignition and reignition transients leading to steady-state operation.

As mentioned previously, problems connected with shut-down and reignition may arise as a result of many factors. By way of review, a few of the factors are: (1) charring of the fuel as a result of residual heat in the fuel, (2) continued exothermic surface reactions after termination of oxidizer flow and (3) heated subsurface layers causing significant overpressurizations during the reignition transients. Furthermore, the ignition criteria applied to the initial ignition model may become invalid for reignition as a result of nonuniform heat transfer to the fuel during shut-down.

Therefore, for the design of advanced maneuvering missiles to include accurate, predictable, stop-start operation, emphasis must be placed on the thermal aspects influencing the shut-down period and the reignition process.

III-B: Thermal Aspects of the Shut-down Period

The following sequence of events provides a model for considering the thermal aspects that influence the shut-down period:

1. A hybrid rocket motor is operating at steady-state conditions.
2. The flow of oxidizer into the motor ports is terminated, causing chamber pressure to decrease. As a result of this, heat transfer to the propellant surface is reduced. The net effect is extinguishment.

3. Heat contained in the fuel at the surface is conducted into the interior of the fuel.

4. The fuel may continue to receive conductive heat energy from continued exothermic reactions in a metal loaded fuel even after the cessation of oxidizer flow. Also, the flow of the hot premixed combustion gases remaining in the chamber will contribute to the convective heat transfer to the fuel.

5. The fuel may also receive heat in the form of radiant energy.

Since the propellant surface is cool in comparison to motor components, such as the nozzle, the redistribution of the total heat energy will proceed toward an equilibrium value. However, this redistribution of heat is both nonuniform and nonsteady. A model for the nonuniform distribution of heat transfer to the fuel is shown in Fig. 7. As a result of this redistribution, if excessive heat is conducted into the subsurface layers, a thick layer of the fuel is effected. For example, in a 70-percent lithium-fluorine hybrid system, melt layer depths of greater than 0.125 inches have been measured.[14] Reignition of this type of surface allows for much of the fuel to be stripped away from the surface and not vaporized before it is ejected from the motor. This can greatly reduce combustion efficiency and may hinder or even prevent reignition.

In conclusion, the degree of heating of the fuel at a given location is dependent upon motor geometry, temperature distribution throughout the motor, characteristics of the propellant, and duration of the shut-down period.

III-C: Thermal Aspects to be Considered in Formulating A Reignition Model

There is presently no model that can be used to predict the prerequisite igniter energy or delivery rate for the reignition of a preheated hybrid fuel. The purpose of the following discussion is not to develop such a model, but rather to incorporate the results gained from a thermal study of the shut-down period into a descriptive model that can be used to predict a satisfactory reignition process in practical hybrid rockets.

As the combined convective and radiant heat transfer to the fuel during shut-down is conducted into the fuel and away from the surface (as described in the previous section), a thermal wave travels through the fuel. Since

the fuel is no longer burning, i.e. surface is no longer regressing, the heating penetrates deeper into the fuel than for steady-state conditions.

The temperatures in the layers near the surface will decrease as the deeper sublayers are preheated. An example of the thermal profile established during the shutdown interval is compared to a steady-state profile in Fig. 8, curves 1 and 2 respectively. The slope and depth of curve 2 is particularly significant in the reignition model as they determine the amount of igniter energy needed to reignite the motor and also determine the transient regression rate behavior prior to the steady-state conditions.

It seems evident that if the same igniter energy as applied on the initial ignition is applied to the preheated fuel, the following sequence should occur:

1. Ignition delay will decrease because less energy is absorbed by the fuel before it reaches ignition conditions. The time between the onset of the ignition stimulus and the actual reignition event must be predictable to control accurate thrusting maneuvers.

2. As a result of the already preheated sublayers, a thermal profile (curve 3) is established which penetrates deeper into the fuel than the steady-state profile (curve 2). The preheated fuel requires less heat flux to the surface to bring the fuel to its vaporization point. Thus a greater fraction of the heat flux can be used for vaporizing the fuel. As a result, instantaneous regression rates will be higher. The transient behavior of the regression rate following reignition will rise more rapidly. If a sufficiently deep layer of fuel has been preheated, the regression rate may overshoot its steady-state value. Due to the nonuniformity of the thermal profile along the fuel, the regression rates along the fuel grain will not be uniform. The overall effect is to complicate the axial dependence of regression rate and to enhance the possibility of a local burn-out of the fuel, thereby prematurely exposing the motor case to the hot combustion gases.

3. If higher instantaneous regression rates are encountered, higher chamber pressures following the reignition stimulus will occur. These will result from higher rates of fuel mass addition to the combustion process. The reignition model

must, therefore, consider the degree of preheatedness of the fuel to account for the increased fuel mass addition in order to anticipate the chamber pressure within structural limits of the motor.

In summary, if the same ignition stimulus is applied to a preheated fuel, the degree of preheatedness influences the reignition process as follows: ignition will occur sooner, instantaneous regression rates will be higher, and chamber pressures will be greater. An experimental program must first determine to what extent a preheated fuel influences the restart of a hybrid motor and then investigate the effects of propellant properties, shut-down duration and igniter stimulus. An oxygen-Plexiglas hybrid motor was designed for this program and is described in Chapter IV.

CHAPTER IV

EXPERIMENTAL APPARATUS

IV-A: Overall Gas System

A hybrid rocket motor was designed and constructed for experimental investigations of the ignition and restart processes. Figs. 9 and 10 show schematic drawings of the hybrid motor and overall gas system respectively. The system consists of oxygen, methane and nitrogen sources and their associated regulators and gauges. Oxygen is stored in type 1A bottles containing 244 cu. ft. at 2200 psig, and its flow is regulated from the test cell by a nitrogen dome regulator. Immediately upstream of the solenoid and flow metering orifice, an oxygen reservoir holds 15 $in.^3$ at the system stagnation pressure. The pressure in this reservoir is registered on the oxygen reservoir gauge (0-2000 psig) in the test cell. The oxygen reservoir pressure and the orifice size are matched to achieve the desired oxidizer mass flows.

Methane is stored in type 1A bottles at 2200 psig and fed through a two stage regulator to the solenoid in the methane line. The pressure set on the second stage of the regulator and the orifice downstream of the solenoid were matched to achieve stoichiometry between the ignition gases, methane and oxygen.

The orifices used as flow metering devices were calibrated using a gas-water displacement apparatus. All the orifices tested were found to be $\pm 3\%$ of theoretically predicted flows.

Nitrogen, stored at 375 psig, was used to purge any residual burning and remove combustion gases from the system. The motor is shown in an exploded view in Fig. 11 with its components labeled.

IV-B: Description of the Hybrid Motor

The fuel consisted of a hollow cylinder of Plexiglas 10.0 inches in length and 3.0 inches in outer diameter. The initial port diameter was 1.0 inch for all experimental firings. Final port diameters were always less than 1.2 inches. Gaseous oxygen was used as the oxidizer. Experiments were conducted at two oxygen flow rates, 0.0785 lbm/sec and 0.0392 lbm/sec. Experiments were conducted over a range of steady-state chamber pressures between 60 and 700 psig. Ignition was achieved by a methane-oxygen torch igniter mounted on the forward housing. Igniter durations were varied between 50 msec and 500 msec. A plenum, or mixing chamber, located aft of the grain, was designed to receive the hot combustion products and eject them out the nozzle. The motor in Fig.12 is shown assembled and mounted for firing in the test cell.

A normal test firing consisted of one or two 5 to 10 sec successive firings with a predetermined shut-down duration. A photograph of the hybrid rocket in steady-state operation is shown in Figure 13.

IV-C: Timing System

Four automatically resetting timers were integrated on the firing console. Two, 0-30 sec, ATC timers (series 305D) provided selection of the firing duration and shut-down duration. The hybrid firing duration timer controlled power to the solenoid in the oxygen line. At the end of the firing duration, the timer would signal the solenoid to close and initiate the shut-down timer. The firing duration timer would reset automatically for a duplicate second firing duration.

Two other timers were available for setting the igniter durations. For single firing runs the #2 cam of the firing sequencer could provide the desired igniter duration. However, accurate positioning of the cam proved to be time consuming and not reproducible. For two successive firings, an initial igniter duration could be set on the sequence cam, while the restart igniter duration could be set on the igniter duration timer mounted on the console. This timer had a 0-1000 msec range. Single firing igniter durations sould also be set on the igniter duration timer. The timer controlled the opening and closing of the solenoid valve in the methane line. Figure 14 shows the electrical schematic drawing for the entire system.

IV-D: Hybrid Ignition System

The ignition of polymethylmethacrylate (commonly referred to as Plexiglas or PMM) was achieved with a methane-oxygen gas torch. The igniter system allowed both igniter mass flow rates and igniter durations to vary as a controlled experimental parameter. Methane was metered through a flow metering orifice in approximate stoichiometric proportion to the experimental oxygen flow rate. The igniter gases were then mixed and ignited in the forward housing and then injected into the motor port.

The actual ignition sequence occurred as follows: (1) two spark plugs were actuated for 500-700 msec, (2) methane valve was opened, (3) oxygen valve was opened, (4) hot igniter gases entered the motor, (5) ignition was achieved, (6) methane flow was terminated, and (7) constant oxygen flow was supplied for the duration of the firing.

IV-E: Description of the Hybrid Fuel

Plexiglas has been used extensively by other researchers, [15, 16, 17, 18, 19] before experimenting with high energy fuels. As a fuel, PMM provides a safe, practical, inexpensive

laboratory model. Results obtained from this model can be used as a guide for the development of analytical models for the prediction of ignition and restart transients of other hybrid engines.

A cylindrical shape was chosen for the motor configuration, rather than a normal flat slab model, because a cylindrical grain provides a realistic simulation to practical hybrid combustion motors. However, there are definite disadvantages inherent to the cylindrical configuration. They are: (1) photography of the burning mechanism is hampered by focusing through a burning surface and (2) measured regression rates on curved surfaces are inaccurate.*

IV-F: Components of the Aft Housing

The aft housing receives the hot combustion products from the oxidizer and Plexiglas reaction. In order to prevent high heat transfer rates to the pressure transducer housing, a high density graphite insert was inserted in the mixing chamber. The graphite insert was made in three sections. The first section, adjacent to the grain, had a slight taper to provide a gradual change from the port diameter to the mixing chamber diameter. Without this insert, complex flow patterns and undesired heating eddies would occur immediately aft of the grain.

Motor nozzles were fabricated from copper to prevent any measurable erosion in the throat section. Nozzles were designed with a slight convergent section leading to a precise throat diameter. Required pressure seals were maintained with rubber O-rings.

IV-G: Instrumentation

Chamber pressure measurements were recorded during all experimental firings. A Dynisco pressure transducer, Model PT-76, was mounted over the mixing chamber forward of the nozzle blocks. A 1/4 inch thick disk of General Electric RTV 580 rubber was bonded to the diaphram to protect the sensitive diaphragm from contact with the hot combustion gases.

The same model transducers were also placed downstream of the solenoid valves in the oxygen and methane flow lines for initial tests. These pressure recordings were used to determine flow rates and opening/closing times of the solenoid valves. The oxygen solenoid valve fully opened and closed in 25 msec. The methane solenoid valve opened to the full position in 40 msec and closed in 25 msec. The times measured for firing duration and igniter duration were measured from the time the oxygen and methane valve received

* The total regression, ΔR, was measured with an accuracy of ± 0.0005 inches which gave reliable regression rate measurements to $\pm 1\%$.

their respective electrical signals to open. The signals to open and close the valves were recorded by the visicorder.

The RTV shielded pressure transducer had a natural frequency of 22000 cps. It was reliable to a frequency-amplitude response to 8000 cps.[20] The transducers were driven with B & F Transducer Conditioning Modules. The pressure transducers were initially calibrated using the Amthor 0-2000 type 472 Deadweight Tester. Each experimental firing was accompanied by a pressure calibration of the motor with a regulated nitrogen supply.

Some experimental firings were instrumented with fine bare wire thermocouples embedded in the fuel. These thermocouples were made from chromel-alumel wire 0.001 inches in diameter. A detailed explanation of the technique developed to embed these thermocouples will be given in Appendix I.

Both pressure signals and thermocouple outputs were fed to Dana Model 3520 D. C. Amplifiers. At the Honeywell Model 1508 Visicorder, these signals were matched with Honeywell galvonometers (Model 1650) and were recorded at a visicorder speed of 12 in/sec with timing marks every 10 msec.

Thermocouple outputs were calibrated prior to the firing by using a potentiometer to input a desired voltage to the galvonometers. Amplifiers could then be adjusted to match the desired deflection per millivolt. Most thermocouple outputs were calibrated for 1/2 inch deflection per 3 millivolts.

High speed photography, using a 16mm Wollensak Fastex camera, provided observations of the ignition and restart phenomena. High speed films can locate the point of ignition, direction of flame spreading, and the rate of flame propagation over the surface.

Films taken at 1500 and 2000 frames per second were electronically sequenced to be at operational speeds at the time of ignition. Two neon marking lights were used to coordinate recorded data and filmed observations. One mark recorded simultaneously on both the film and visicorder served as a reference mark. The second mark was an oscillating timing light set at 100 Hz .

CHAPTER V

EXPERIMENTAL RESULTS AND DISCUSSION

V-A: Thermocouple Measurements

Thermocouples were embedded in the Plexiglas fuel for five experimental firings. At each experimental oxidizer flow rate, 0.078 lbm/sec and 0.039 lbm/sec, we attempted to investigate two operating pressures of approximately 80 and 360 psig. Four firings, Runs 17, 18, 22, and 23, were instrumented with four thermocouples per firing, each at a different depth in the fuel (see Table J). A fifth firing, Run 19, was conducted with five thermocouples spaced axially along the grain all at the same subsurface depth. All five firings were conducted with the same firing sequence, t_{run}=5.0 sec, t_{shd}=2.0 sec, and t_{rei}=5.0 sec.

The temperatures recorded during Runs 17, 18, 22, and 23, were plotted versus time, in Figs. 15-18. Focusing our attention on the shut-down duration (5-7 sec), it is evident that the temperatures in the subsurface layers continued to rise after termination of the oxidizer flow. This temperature rise is caused by continued heat conduction from higher temperature regions near the surface and radiation from the hot motor components.

However, as mentioned previously, this redistribution of heat during the shut-down period may not be uniform. The results obtained from Run 19, shown in Fig. 19, give supporting evidence to the nonuniformity of the heat distribution. More clearly, Fig. 19 shows the temperatures recorded at 1.75, 6.0 and 7.5 inches from the injector face increased 5, 3 and 6 degrees C respectively during the shut-down interval, while temperatures at 4.5 inches from the injector face decreased 3 degrees C during the first second of shut-down and increased 2 degrees C during the last second of shut-down. In conclusion, the results shown in Figs. 15-19 exhibit the nonsteady and nonuniform temperatures of the subsurface layers and confirm our earlier notions of the nonsteady, nonuniform heat distribution during the shut-down interval.

Thermocouple data was also used to measure the growth of the thermal profile following ignition and reignition stimuli and during the shut-down interval. In order to experimentally model a thermal profile, three factors were considered: (1) instantaneous regression rate, $\dot{r}_t$, (2) instantaneous location of the surface and (3) accurate knowledge of the thermocouple location.

The instant that the ablating surface passes each thermocouple bead can be approximated in two ways. First, an examination of voltage output from the thermocouple reveals a smooth voltage output while in the solid region, but as the temperature sensing bead enters the molten liquid or gas phase region, the voltage output becomes wavy or rippled. Two examples taken from different firings are shown in Fig. 20. Second, plots of recorded temperature data on a log T_x vs. time scale yield a straight line in the solid region during steady-state. However, a noticeable change in the slope, normally in the form of a departure from the straight line steady-state approximation, occurs when the thermocouple records the surface temperature, T_s. Temperature measurements and the times the thermocouple beads reach the surface are shown in Figs. 21 to 24.

By combining the two previous observations an empirical regression rate can be attained and applied to determine the location of the burning surface during the entire firing. An example of several experimental thermal profiles measured during initial steady-state operation, shut-down and reignition steady-state operation are shown in Fig. 25 for Run 18. It should be noted here that the maximum error in the thermocouple placement was 0.005 cm which represents the sum of the maximum errors of each individual measurement taken. For further analysis, the profiles will be represented as smooth curves to facilitate any comparisons.

The profiles shown in Fig. 25 particularly show the overheating of the subsurface layers deeper in the fuel as the shut-down duration proceeds. The entire heat capacity of the thermal wave is free to "cook" the deeper layers of fuel as little or no heat is used for ablation. It also appears that almost immediately after the reignition stimulus is applied at t = 7.00 sec, the thermal profile established at t = 7.12 sec is deeper than the steady-state profile at t = 4. This would imply faster instantaneous regression rates because a smaller fraction of the heat is transferred to the subsurface regions of the fuel and consequently more heat is available to vaporize more fuel. The results would imply higher transient regression rates as the preheated regions are consumed.

Further comparison of the measured penetration depth of the thermal profile during initial steady-state operation with the steady-state penetration depth predicted by Marxman, Wooldridge and Muzzy[12] in Eq. 7 show close agreement. However, the measured thermal profiles following the reignition stimulus penetrate deeper into the fuel with temperatures generally exceeding corresponding steady-state profiles (Fig. 25).

Furthermore, comparisons of the times to reach steady-state chamber pressure (as tabulated in Table 1) with the times to establish a steady-state thermal profile agree very closely. The time to establish a steady-state thermal profile may be estimated graphically from a plot of log T_x vs. time. When the temperature-time response from a thermocouple becomes linear, a steady-state thermal profile has been established as shown in Fig. 26.

V-B: Chamber Pressure Measurements

The major purpose of the experimental investigation was to determine the influence of a preheated thermal profile on the reignition transient by comparing the pressure-time histories of the ignition and reignition transients, respectively. These comparisons of pressure-time histories were made following a two second shut-down. The pressures during reignition transients were always greater than the respective initial pressures during the ignition transient, as shown in Figs. 27-30. However, both the ignition and reignition processes approached similar steady-state pressures in the chamber as shown in Figs. 31-34.

Reignition delays were up to 15% less than ignition delays. Furthermore, the times to reach 90% of steady-state pressures following reignition were one-fourth of the initial ignition times. Both ignition delays and the times to reach 90% of steady-state chamber pressure, $t_{.9Pc}$, are tabulated in the compendium given in Table 1.

V-C: Regression Rate Measurements

Average regression rates were measured on each experimental firing by measuring the change in web thickness per firing duration. Weight loss measurements were also recorded and compared with previous runs of the same durations. Regression rates were measured at nine stations, space at one inch intervals beginning from the injector face of the fuel. Only the regression rates measured at the 5th station, 5 inches from the injector face, are recorded in Table 1.

Experimental conditions precluded the measurement of instantaneous regression rates during the firing duration. From the results of the pressure measurements, we can infer that the instantaneous regression rates following reignition of a preheated fuel were faster than their respective regression rates following ignition of an ambient fuel. However, the results obtained from measuring average regression rates do provide meaningful information helpful in understanding other problems of hybrid combustion.

For example, total regression, ΔR, rather than regression rate $\dot{r}$, was plotted versus the distance from the injector face for three firings of the same duration, but at different operating pressures, 600, 325 and 80 psig respectively. The results in Fig. 35 show a definite x-dependence on regression rate with minimum burning occurring at midstream. Referring to the same figure, (Fig. 35) the pressure effect on regression rate is also noticeable. Runs 10 and 13 at higher pressures, 600 and 325 psig respectively, have similar total regressions; Run 15 at a lower pressure, 76 psig, has a smaller total regression. These results concur with the earlier mention of the pressure dependence and the chemical kinetics.

V-D: Photographic Observation

Extensive photographic observations of the ignition and reignition processes and the flame propagation during the pressure transients were made. Although no significant difference could be detected between the ignition event and reignition event, both processes were characterized by long flame spreading durations (usually 350 msec) very similar to the long chamber filling intervals. A flame spreading interval during hybrid ignition is shown in Fig. 36.

The most peculiar result of the photographic observation was the unusual distribution of flame intensity throughout the motor core. The high speed films show a nonsteady, almost pulsating, nonuniform flame distribution during steady-state operation. A sequence of photos in Fig. 37 show the flame. Similar pulsating flames were reported by Courtney[21] in a double-slab O_2-Plexiglas system. The nonuniform intensity seen in both Figs. 36 and 37 raises the question of complete combustion along the surface of the fuel. What appears to be a region of "spotty" higher intensity burning upstream indicates that upstream burning exhausts the oxygen supply. Accordingly, the oxygen concentration in the downstream boundary layer is not sufficiently high to burn the Plexiglas at the grain surface. One hypothesis is that hot combustion products passing over the downstream regions of the grain melts the Plexiglas and carries the melt to the plenum chamber where it is burned.

CHAPTER VI

A PARAMETRIC INVESTIGATION OF THE TRANSIENT REGRESSION RATE BEHAVIOR FOLLOWING A SHUT-DOWN

In order to gain a better understanding of the transient regression rate behavior on the restart process of a hybrid rocket motor, a mathematical model was developed to calculate the instantaneous regression rates of the fuel and the temperature profiles in the fuel. The model, in the form of an extension and modification to an existing computer program[22], calculates the temperature-time responses at locations corresponding to the thermocouples at subsurface depths. A discussion of the computer solution to the heat conduction equation used to compute regression rates is given in the following section. Subsequent to that section, the approach used in the parametric study will be treated, and the results presented.

VI-A: Formulation and Solution of the Mathematical Model

The mathematical model of the regressing fuel may be considered in two parts: 1) the thermal driving force to the fuel surface that gasifies, decomposes and transports the fuel into contact with the oxidizing species in the chamber and 2) the transient moving boundary heat conduction within the fuel.

VI-A.1: Heat Conduction Equation for the Fuel

The equation governing transient heat conduction within a nonstationary medium (in cylindrical coordinates) is

$$\rho c_s\left(\frac{\partial T}{\partial t}+\dot{r}\frac{\partial T}{\partial x}\right)=k\frac{\partial\left(\frac{\partial T}{\partial x}\right)}{\partial x}+\frac{k}{r}\left(\frac{\partial T}{\partial x}\right)+\beta\dot{q}_r\exp\left(-\beta x\right) \qquad \text{(VI-1)}$$

I II III IV V

The terms in Eq. (VI-1) have the following physical significance:

I Time rate of energy accumulation and temperature rise at a particular point

II Rate of energy convection due to motion of the coordinate system

III Energy transfer by thermal conduction in the solid

IV Term which accounts for effects of varying cross-sectional geometry in the cylinder on energy transfer by thermal conduction

V Rate of radiative heat transfer to the subsurface regions

The boundary condition at the gas-solid interface for the fuel is

$$\ddot{q}_{bs} + \ddot{q}_{bg}(T_s, T_f, P) = k\left(\frac{\partial T}{\partial x}\right)_{c,s} \qquad \text{(VI-2}$$

Where $\ddot{q}_{bg}$ is the convective heat flux from the combustion products flowing over the fuel. The quantity $\ddot{q}_s$ is the rate of heat release at the gas-solid interface due to gasification of the fuel. For conventional fuels the gasification at the gas-solid interface is generally considered to be endothermic. The quantity $\ddot{q}_{bs}$ is usually expressed in one of two ways, in terms of an Arrhenius relation

$$\ddot{q}_{bs} = Z_s \exp\left(\frac{-E_s}{RT_s}\right) \qquad \text{(VI-3}$$

or in terms of a net energy release per unit mass converted from the condensed phase to the gas phase

$$\ddot{q}_{bs} = \dot{r}_b \rho_c \Delta h_s \qquad \text{(VI-4}$$

The regression rate at the surface is controlled by both a linear pyrolysis law,

$$\dot{r}_b = B_s \exp\left(\frac{-E_s}{RT_s}\right) \qquad \text{(VI-5}$$

and a heat balance at the surface,

$$\dot{r}_b = \frac{\left[k_c\left(\frac{\partial T}{\partial x}\right)_{c,s} - k_g\left(\frac{\partial T}{\partial x}\right)_{g,s} + \ddot{q}_{br}\right]}{\rho_c \Delta h_s} \qquad \text{(VI-6}$$

When the pyrolysis law (Eq. VI-5) describes the regression rate, the temperature at the gas-solid interface, T_s, increases as the heat flux to the solid-phase surface increases. As T_s increases, by Eq. (VI-5), a corresponding increase in $\dot{r}_b$ occurs. However, we chose to adopt a simpler description of the pyrolysis process, namely

$$T_s = T_s' = \text{constant} \qquad \text{(VI-5)}'$$

The value of $\dot{r}_b$ will now be controlled by the other equations of the problem, but it will also increase as the heat flux increases.

The boundary condition for $x \to \infty$ is

$$\frac{\partial T(x,t)}{\partial x} = 0 \qquad \text{(VI-7)}$$

the initial condition is

$$T(x,t) = T_i \qquad \text{(VI-8)}$$

Because of the low thermal conductivity of the fuel and the rapid surface regression, the conditions of Eq. (VI-7) is reached just 0.01 cm below the gas-solid interface.

Ignition is assumed to occur when either the surface or the interface reaches a prescribed ignition temperature.

VI-A.2: The Thermal Driving Force to the Surface of the Fuel

The reactions and transport phenomena within the boundary layer adjacent to the fuel surface, if treated analytically, would be a most formidable aerothermochemical exercise. Several investigators have attempted such analyses with only limited success.[1, 6, 12] An examination of the bulk processes indicate that it may be both attractive and meaningful to consider the convective heat transfer from the reacting gases to the fuel using the same functional relationships as those developed for nonreacting turbulent boundary layers. There are two justifications for this: 1) the work of Anderson and Hurt[7, 8] demonstrated that the surface gasification rates of hybrid fuels can be correlated in terms of emperical turbulent boundary layer parameters and 2) the analytical relationships for the thermal driving force developed by Marxman and coworkers[1, 6, 12] have similar functional dependencies on free stream pressure and velocity as those dependencies on turbulent convective heating.

Accordingly, the thermal driving force used in the model was based on the empirical relationships* for high speed turbulent forced convection as presented by Eckert.[23]

* It should be pointed out that we understood why the simple convective boundary does not fully account for the diffusion blowing, and kinetic processes within the boundary layer. Rather it is used as a systematic means of correlating measured results within the budget limitations of the study.

The following general conditions were considered to prevail: 1) the boundary layer is steady and completely turbulent, 2) an inviscid flow field, external to the boundary layer, is imposed by the internal ballistic relationships of the chamber 3) the conditions at the fuel surface and in the inviscid flow field are quasi-steady and 4) the heat conduction within the fuel is unsteady. In an effort to account for the effects of temperature on the physical properties of the gases, they are evaluated at the following reference temperature

$$T^* = T_f + 0.5\left(T_f - T_s\right) \tag{VI-9}$$

The convective heat transfer coefficient based on the temperature difference, $T_f - T_s$, is

$$h_x = 0.0296\, C_c\, c_p\, \rho^* V\, Pr^{-2/3}\, Re^{*-1/5} \tag{VI-10}$$

The factor C_c is adapted to make the calculated steady-state regression rates agree with the measured steady-state regression rates.

VI-A.3: Solution to the Heat Conduction Equation

The method of explicit finite differences and relaxation were used to solve the differential equations, Eq. (VI-1). The several terms in the solid-phase energy equation are considered by writing the derivatives in terms of the corresponding finite differences. For example,

$$\frac{\partial T}{\partial x} = \frac{T(t+\Delta t) - T(t)}{\Delta t} = \frac{\Delta T}{\Delta t} \tag{VI-11}$$

and

$$\frac{\partial T}{\partial x} = \frac{T_{n+1} - T_{n-1}}{2\,\Delta x} \tag{VI-12}$$

or

$$\frac{\partial T}{\partial x} = \frac{\Delta T}{\Delta x} \tag{VI-13}$$

The differential temperature over the time interval, Δt, is

$$\Delta T = \dot{r}\left(\frac{T_{n+1} - T_{n-1}}{2\Delta x}\right)\Delta t + k\left[\frac{\left(\frac{\partial T}{\partial x}\right)_{x+\Delta x/2} - \left(\frac{\partial T}{\partial x}\right)_{x-\Delta x/2}}{\Delta x}\right]\frac{\Delta t}{\rho C_s}$$

$$+\left[\frac{k}{\Gamma}\left(\frac{T_{n+1} - T_{n-1}}{2\Delta x}\right)\right]\frac{\Delta t}{\rho C_s} + \frac{\Delta t}{\rho C_s}\beta q_{0r}\exp(-\beta x) \qquad \text{(VI-14)}$$

Applying the techniques of explicit finite differences, the materials are treated as a series of elemental volumes through the cylinder. The mass of each volume is considered to be concentrated at a point referred to as a nodal point. Fig. 38 illustrates an elemental volume and its nodal point, n. The area at $x - \Delta x/2$ is A_{in}, the area at $x + \Delta x/2$ is A_{out}, and the area at x is $\bar{A}$. The heat transferred into the left side of the elemental volume is

$$Q_{IN} = A_{IN} q_{IN} = -A_{IN} k (T_n - T_{n-1})/\Delta x \qquad \text{(VI-15)}$$

The heat transferred out of the right side is

$$Q_{out} = A_{out} q_{out} = -A_{out} k (T_{n+1} - T_n)/\Delta x \qquad \text{(VI-16)}$$

The temperature T_n is the bulk temperature of the nodal volume whose heat capacity is $C_s \rho \Delta x \quad (A_{in} + A_{out})/2$. The heat flux at the center of the elemental volume; i.e., at the position x, is approximated as the mean heat flux

$$q(x) = \frac{(q_{IN} + q_{out})}{2} \qquad \text{(VI-17)}$$

Substituting Eqs. (VI-15) and (VI-16) into Term III of Eq. (VI-14) yields

$$\left[-\frac{Q_{out}}{A_{out}} + \frac{Q_{IN}}{A_{IN}}\right]\frac{\Delta t}{\Delta x \rho C_s} \qquad \text{(VI-18)}$$

where ρ and C_s are evaluated at T_n.

Term IV in Eq. (VI-14) can be expressed as

$$-\left[\frac{k}{r}\left(\frac{\frac{q_{out}}{A_{out}}-\frac{q_{IN}}{A_{IN}}}{2}\right)\right]\frac{\Delta t}{\rho C_s} \qquad \text{(VI-19)}$$

Term II accounts for motion with respect to some fixed reference point. In this analysis the solid-phase material is maintained at a fixed position in space and the burning surface moves at the calculated burning rate relative to that fixed position in space. As the solid-phase layers are consumed, the nodal points within a material are repositioned so that the incremental distances between the nodal points, Δx, are equal. As the thickness of the solid phase is decreased, the number of nodal points in solid phase is decreased so as to maintain the stability of the numerical solution. Two factors control the increment sizes Δt and Δx: 1) the desired accuracy of the solution; and, 2) the stability criterion for the finite difference equations. By decreasing the increment size Δx, the solution can be made more accurate, but the time required for the calculations increases disproportionately since the time increment Δt must also be decreased to maintain the stability of the solution. A sufficient condition for stability is to insure that the sum of all the factors multiplying the temperature at a particular nodal point is greater than or equal to zero. In the method presented here, the time increment does not vary as different materials are considered. Thus, it is sufficient to consider the stability of the critical nodal point. The numerical solution is set up so that the critical nodal point for stability is the nodal point at the surface of the fuel. Accordingly, stability is insured when

$$1-\frac{2\Delta t}{C_s\rho\Delta x^2}\left(k+h_{CONV}\Delta x\right)\geq 0 \qquad \text{(VI-20)}$$

Numerous check calculations were performed on all portions of the numerical solution. In several instances it was possible to compare the values calculated by the numerical solution with the values from closed-form solutions and series solutions.

VI-B: Simulation of a Hybrid Motor Test Firing

The purpose of the parametric study was threefold (1) to compare the thermal profiles in the solid fuel established during steady-state operations to those established during shut-down and reignition, (2) to compare computed

regression rate behaviors during restarts following different shut-down durations with the regression rate behaviors following initial ignition and (3) to evaluate and compare the thermal response of several hypothetical high energy fuels.

The initial task was to prescribe sufficient input conditions to the computer program to simulate an experimental firing. Run 18 was chosen as the datum case for comparison purposes, and the sequence that follows outlines the approach used to simulate the O_2-Plexiglas system.

1. The physical properties of the Plexiglas fuel, the properties of the chamber gases and the grain dimensions were input to the program. No parameter was input to the initial datum case to consider the heating of subsurface layers by radiation. However, as further discussed in Appendix I, our experiments showed that radiant heating to the subsurface layers of the Plexiglas fuel was significant and must be accounted for in future investigations.

2. The gas-torch igniter was simulated by applying a heat flux to the surface of the fuel in a step function initiated at $t = 0.0$. After 100 m sec, the step function was followed by a decreasing ramp function to zero at 300 m sec. The magnitude of the igniter heat flux was fixed at a value that produced ignition delays that agreed approximately with the experimental results.

3. The pressure-time history recorded during Run 18 was also an input to the program. From the pressure-time history, the program calculated an effective convective heat transfer coefficient, h, and then a heat flux to the surface, Q. The heat flux to the surface determined the regression rate. Small corrections were made to computed convection coefficients to make the regression rates agree with experimental results. This sequence summarizes the inputs to the datum case; a complete list of input parameters is given in Table II.

VI-C: Calculated Results for a Plexiglas Fuel

The calculated results of the datum case partially simulated the experimental results of Run 18. The computed steady-state regression rates were within 1% of the measured

average regression rate. Ignition delays of 0.077 sec were computed and were approximately equal to those recorded and photographed during the experiments. However, as was indicated by a comparison of measured and calculated thermocouple responses, radiant heating to the subsurface regions should be included in the solution to the heat conduction equation.

An important advantage of the computer simulation was that thermal responses can be compared for a range of fuel properties. The thermal profiles for the nonradiative datum case are presented in two forms, Figs. 39a and 40a. In Fig. 39a, the results of the passage of a thermal wave penetrating through the fuel during shut-down to preheat the sublayers above their respective steady-state temperatures is clearly illustrated. Curve 1 represents the steady-state profile at $t = 4.0$ sec. Superimposed on the same axis, curve 2 is the thermal profile 2.0 seconds after shut-down just prior to restart. The temperatures in the layers adjacent to the surface have diminished slightly; however, the thermal wave has preheated the subsurface layers considerably. Curve 3 is the thermal profile at $t = 9.0$ sec, less than two seconds after reignition. This thermal profile is slowly approaching its original steady-state condition. In Fig. 40a, the same profiles are shown at their instantaneous surface locations. At $t = 5.0$ sec, the reaction stops and the surface ceases to ablate. Therefore, the profiles at $t = 6.0$ and $t = 7.0$ sec are shown at the same surface.

The results obtained from the temperature-time histories at the thermocouple locations did not agree with the experimental results of Run 18. The computed temperature-time histories lagged in response to ignition and were below the experimental values recorded. It was concluded that the poor agreement resulted from considering only convective heating in the computed temperatures, while the experimental results were obtained by sensing convective and radiative heat to the subsurface layers.

Therefore, two additional heating relationships were considered to account for the subsurface radiant heating. They were

(1) a radiative heat flux to the fuel

$$q_r = A_{ss}\sigma(T_f^4 - T_w^4)$$

and (2) subsurface heating by radiation using Beer's Law[24]

$$q_x = q_r \exp(-\beta x)$$

This introduced two additional parameters to the study, the overall radiation interchange factor, A_{fs}, and the Beers' Law parameter, β.

With these two appropriate values added, Case I becomes the modified datum case considering a radiative system. The temperature-time responses of the locations corresponding to the thermocouples were in reasonable agreement. A comparison of the measured and computed temperature-time responses for two thermocouples is shown in Fig. 41. The lack of better agreement between the two temperature-time responses was probably due to the uncertainty of the true location of each thermocouple and unknowns associated with radiation effects. Further considerations of the thermocouple technique is given in Appendix I.

A comparison of the thermal profiles for the non-radiative datum case and the radiative Case I is shown in Figs. 39 and 40. As already described, Figs. 39a and 40a are for the nonradiative datum case, while Figs. 39b and 40b show the effects of radiation on the system. A faster regression rate is noticeable by the more advanced positions of the instantaneous surfaces in Fig. 40b. Also, the chemical reaction in the system does not stop at t = 5.0 sec. Instead, a slow continuous surface reaction occurs causing a low regression rate during the shut-down period. As a result, additional heat is transferred to the fuel during shut-down, and, as compared with the thermal profiles in Fig. 40a, profiles now have less of a slope and more heat stored in the fuel.

The results of Case I were considered an accurate representation of the experimental firing. The major purpose of the parametric study could now be accomplished: to compare the calculated instantaneous regression rate behaviors on restarts following varied shut-down durations. Three shut-down durations were considered: Case I with a 2.0 sec shut-down, Case II with a 0.9 sec shut-down and Case III with a 4.0 sec shut-down. The instantaneous regression rate behaviors are presented in two graphical forms.

First, in Fig. 42, a nondimensional form similar to that used by Marxman, Wooldridge and Muzzy in Ref. 12, the transient regression rate behaviors for Cases I, II and III are compared. Results indicate that increasing shut-down duration (up to an undetermined time) increases the degree of overshoot. Second, in Fig. 43, if the results are presented in the dimensions of regression rate and time, the results are more obvious. The steady-state regression rates for the radiative and nonradiative systems are shown in dashed and solid lines respectively. The regression rate tail-off associated with the drop in chamber pressure should lead to extinction. However, slow

burning is continued during the shut-down. The restart pressurizations were initiated at 5.9, 7.0 and 9.0 sec for Cases I, II, and III respectively. The computed transient regression rates are plotted for comparisons. The regression rate overshoots are now obvious and are clearly increasing with increased shut-down durations. The restart of the nonradiative datum case is also plotted for comparison. Results such as ignition delay and the time to reach 90% of initial steady-state regression rate on restart are tabulated for comparison in Table III. It should be noted that the time to reach 90% of the initial regression rate on restart following any shut-down duration is nearly one-fifth of the time to reach 90% of the steady-state regression rate on ignition. That is, steady-state regression rates on reignition are achieved five times as fast as on initial ignition.

VI-D: Hypothetical High Energy Fuel

The physical properties of a hypothetical fuel, whose physical ingredients were similar to a fuel consisting of 50% Boron, 20% ammonium perchlorate, AP, and 30% binder, were substituted for the Plexiglas properties for a series of calculations to determine the regression rate overshoots that may occur in a practical high energy fuel. The fuel was assumed to be opaque to thermal radiation. Surface temperature and latent heat were varied for three cases, and the values for each case is listed in Table III (Case IV, V and VI). The transient regression rates are plotted in Fig. 44. The regression rate overshoots are increased as the latent heats are decreased and the surface temperatures increased.

An additional case, similar to Case V, was considered with a 4.0 sec shut-down duration. As all the other initial parameters were equal, the regression rate transients following ignition were similar. However, the regression rate behavior following the 2.0 sec and 4.0 sec shut-downs were different and are compared in Fig. 45. The overshoot following the 2.0 sec shut-down was 18% greater than steady-state, whereas the overshoot following a 4.0 sec shut-down was 20% greater.

CHAPTER VII

SUMMARY AND CONCLUSIONS WITH SUGGESTIONS FOR FUTURE WORK

VII-A: Summary and Conclusions

From an analytical study of the shut-down and restart processes, it was concluded that if proper attention is focused on the inter-relationships between: (1) the non-steady thermal state of the fuel during shut-down, (2) the instantaneous regression rate behaviors following a shut-down duration and (3) the pressure transients following reignition, the pressure-time histories and fuel consumption following reignition may be anticipated. Experimental results have provided conclusive evidence that such relations between the thermal state of the fuel, the instantaneous regression rate, and the transient chamber pressure do exist.

The thermocouple probes, especially fabricated for this study, provided accurate subsurface temperature histories and consistent surface temperature measurements. Thermocouple studies showed that a nonsteady, nonuniform thermal state exists in the fuel during shut-down and a deeper thermal profile develops. Chamber pressures measured during the transient and chamber filling interval following reignition of a preheated fuel have everywhere exceeded their respective initial ignition transient pressures. From these experimental results, we can infer that the higher chamber pressures are a result of the higher rates of fuel mass addition, and therefore faster instantaneous regression rates, caused by the preheating of the fuel.

However, experimental conditions have precluded any measurement of the instantaneous regression rates to verify our inference. Therefore, an additional parametric study, using a computer to simulate an experimental firing of the O_2-Plexiglas hybrid rocket motor, was performed to determine the effects of preheating and shut-down on instantaneous regression rate behavior. The computer results were conclusive and as expected; the calculated restart regression rate transients had overshoots as large as 21% above steady-state values. The times to reach 90% of equilibrium chamber conditions following reignition were one-fourth as long as the times on initial ignition. The regression rate overshoots increased as the shut-down duration was increased for the shut-down intervals investigated (0.9 sec to 4.0 sec.). The same computer simulation was applied to three hypothetical high energy fuels to determine the influence of the shut-down duration on reignition

regression rate transients in a practical hybrid fuel. The results were similar to those obtained from the PMM study.

The combined results from the parametric computer study and the experimental O_2-Plexiglas motor study proved that radiant heating to the subsurface layers is not negligible and cannot be ignored as previous researchers have assumed. Radiant heating to the subsurface layers of the fuel must be considered in the heat conduction equation in order for experimental results to agree with calculated predictions. The effects of radiation in the PMM system increased the instantaneous regression rates and increased the depths of the thermal profiles in the fuel.

In conclusion, the effects of a preheated fuel (as a consequence of a previous ignition and a temporary shut-down) will greatly influence the chamber filling interval and the instantaneous regression rates following reignition. Therefore, attention must be focused on the overall thermal distribution during shut-down in order to predict satisfactory pressure-time histories and design the reliable structural components capable of withstanding the excessive rates of pressurization following reignition.

VII-B: Suggestions for Future Work

Future experimental work should be directed at:

1. determining the upper limit of the shut-down duration needed to eliminate the influence of the preheated fuel,

2. extending the computer simulation to predict the time when the preheated fuel no longer contributes to an overshoot on reignition,

3. investigating the minimum time for steady chamber conditions to be regained following step changes in the oxidizer flow and chamber pressure, thereby simulating throttling maneuvers,

4. incorporating the experimental results from a simple polymeric fuel (Plexiglas) and the computer predictions for a metal loaded fuel (for example, 40% Al, 60% Plexiglas) to predict the restart process for a metal loaded hybrid rocket motor.

REFERENCES

1. Marxman, G. A. and Wooldridge, C. E., "Research on the Combustion Mechanism of Hybrid Rockets," Advances in Tactical Rocket Propulsion, AGARD CP No. 1, Aug. 1968, pp. 421-478.

2. Barrère, M. and Moutet, A., "Résultats Récents Obtenus sur les Systèmes Hybrides ou à Lithergols," ONERA, Chatillon, France, Oct. 1966.

3. Moutet, A. and Barrère, M., "Contribution a l'Étude de la Combustion dans les Fusées à Lithergol on Hybrides," Advances in Aeronautical Sciences, Pergamon Press, New York, 1961, p. 465.

4. Summerfield, Martin, Design Principles for Predicting Start-Stop Performance of Solid and Hybrid Rocket Motors, (NASA Grant NGR 31-001-109), Princeton University, Department of Aerospace and Mechanical Sciences, May 1970, pp. 15-20, (a proposal for research, unpublished).

5. Lees, L., "Combustion and Propulsion," Third AGARD Colloquium, Pergamon Press, New York, 1958, p. 451.

6. Marxman, G. and Gilbert, M., "Turbulent Boundary Layer Combustion in the Hybrid Rocket, "Ninth Symposium on Combustion, Academic Press, New York, 1963, p.371.

7. Anderson, Stanley E., "A Discussion of the Parameters Affecting the Burning Rate of Hybrid Fuels," Rohm and Haas, Huntsville,Ala., Second ARPA Hybrid Meeting, Jan., 1963.

8. Hurt, L. J. and Anderson, S. E., "Hydrodynamic Factors Influencing the Combustion of Hybrid Propulsion System," Chemical Engineering Progress Symposium Series No. 61, Vol. 62.

9. Smoot, L. D. and Price, C. F., "Regression Rates of Nonmetalized Hybrid Fuel Systems," AIAA Journal, Vol. 3, No. 8, Aug. 1965, pp. 1408-1413.

10. Smoot, L. D. and Price, C. F., "Regression Rates of Metalized Hybrid Fuel Systems," AIAA Journal, Vol. 4, No. 5, May 1966, pp. 910-915.

11. Kosdon, F. A. and Williams, F. A., "Pressure Dependence of Nonmetalized Hybrid Fuel Regression Rates," AIAA Journal, Vol. 5, No. 4, April 1967, pp. 774-778.

12. Marxman, G. A., Wooldridge, C. E. and Muzzy, R. J., "Fundamentals of Hybrid Boundary-Layer Combustion," Heterogeneous Combustion, Progress in Astronautics and Aeronautics, Vol. 15, Academic Press, New York 1964, p. 485.

13. Connaughton, J. W., Wilson, B. F. and Wharton, W. W., "An Experimental Study of Hypergolic Ignition and Restart in a Unique Hybrid Window Motor," AIAA Paper, No. 66-69, Jan. 1966.

14. Drew, Walter B., "An Analytical Method for Determining the Melt Layer Thickness and Regression Rates for a Hybrid or Tribrid Rocket Motor," NASA TN-D-5699, Langley Research Center, Hampton, Va., May 1970.

15. McAlevy, R. F. and Lee, S. L., "The Linear Pyrolysis of PMM," Technical Report ME-RT66006, Stevens Institute of Technology, Hoboken, N. J., July 1966.

16. Zabelka, R. J. and Brink, D. F., "Studies in Hybrid Combustion," (NOTS TP 3550, NAWWEPS 8541), Naval Ordnance Test Station, April 24, 1968, pp. 19-29, 92, 202, 207-208.

17. Rabinovitch, B., "Regression Rates and the Kinetics of Polymer Degradation," Tenth Symposium (International) on Combustion, Cambridge, England, 1965, pp. 1395-1402.

18. Fineman, Stephen, "Some Analytical Considerations of the Hybrid Rocket Combustion Problem," Princeton University, Department of Aerospace and Mechanical Sciences, MSE Thesis, 1962.

19. Houser, T. J. and Peck, M. V., "Research in Hybrid Combustion," Heterogeneous Combustion, Progress in Astronautics and Aeronautics, Vol. 15, Academic Press, New York, 1964, p. 559.

20. Most, William J., "Ignition Transient Prediction and Control of Solid Propellant Rocket Motors," Princeton University, Department of Aerospace and Mechanical Sciences, Ph.D. Thesis, June 1969, p. 43.

21. Courtney, W. G., Kineyko, W. R. and Dawson, B. E., "Combustion During Perpendicular Flow," Heterogeneous Combustion, Progress in Astronautics and Aeronautics, Vol. 15, Academic Press, New York, 1964, p. 523.

22. Caveny, L. H., "Generalized Moving Boundary Heat Conduction Solution - A Fortran IV Program", Princeton University, Department of Aerospace and Mechanical Science, in preparation.

23. Eckert, E. R. C., "Survey on Heat Transfer at High Speeds", University of Minnesota, December 1961.

24. Hottel, H. C. and Sarofim, A. F., Radiative Transfer, McGraw-Hill, New York, 1967, pp. 199-235.

25. Brewer, W. D., "Effect of Thermocouple Wire Size and Configuration on Interval Temperature Measurements in a Charring Ablator", NASA TN-D-3812, Langley Research Center, Va., March 1967.

26. Strittmater, R. C., and Holmaes, H. E., and Watermeier, L. A., "Lead Loss Problem for a Thermocouple Imbedded in a Burning Propellant", Journal of Spacecraft and Rockets, Vol. 3, No. 8, August 1966, pp. 1302-1303.

Compendium of Hybrid Motor Firings

Runs 1-19 were at O_2 Flux = 0.1 lbm/in^{2}sec

Run #	t_{ign} (sec)	t_{run} (sec)	t_{shd} (sec)	t_{rei} (sec)	p_c psig	$t_{.9p_c}$ (sec)	Ignition Delay (sec)	$\dot{r}_5 \times 10^2$ (in/sec)	Thermocouple Depths (in) ($\pm$ 0.002 inches)
1	0.500	5.0			600	1.470	0.075	1.19	
2	0.250	5.0			645	1.130	0.070	1.21	
3	0.100	2.0			650	1.150	0.080	2.37	
4	0.050	5.0			675	1.150	0.075	1.39	
5	0.040	5.0			620	1.320	0.070	1.20	
6	0.100	2.0			610	1.100	0.065		
7	0.250	5.0			670	1.385	0.070		
8	0.250	5.0			600	1.40	0.070		
9	0.250	4.0			700	0.960			
10	0.250	5.0			600		0.065	1.22	
11	0.100	4.0			315	1.750	0.075		
12	0.100	5.0			320	1.350	0.065		
13	0.050	5.0			325	1.120	0.078	1.090	
14	0.050	5.0			77	0.70	0.080		
15	0.100	5.0			76	0.53	0.075		
16	0.050	5.0			70	0.65	0.070	0.828	
17	0.050	5.0	2.0	5.0	85 *(90)	2.70 (0.40)	0.070 (0.045)		0.025/0.035/0.060/0.075
18	0.050	5.0	2.0	5.0	340 (350)	1.23 (0.520)	0.065 (0.055)		0.040/0.070/0.100/0.130
19	0.050	5.0	2.0	5.0	300 (310)	1.34 (0.58)	0.065 (0.050)		all at 0.125

Runs 20-23 were at O_2 Flux = 0.05 lbm/in^{2}sec

20	0.100	5.0			640	2.71	0.085	0.946	
21	0.050	5.0			600	3.36	0.080	0.687	
22	0.100	5.0	2.0	5.0	380 (385)	2.14 (1.50)	0.085 (0.070)		0.018/0.035/0.065/0.090
23	0.050	5.0	2.0	5.0	60 (70)	2.85 (0.72)	0.090 (0.050)		0.020/0.030/0.040/0.055

*All items in parenthesis are the respective values for the reignition process.

Table II

Datum Case Properties Used in the Calculations for the O_2-Plexiglas System

Thermal Conductivity, k, cal/cm K sec	0.001213
Specific Heat of gas, c_p, cal/g-c	0.35
Density, ρ_f, g/cm^3	1.683
Thermal Diffusivity, α, cm^2/sec	0.002325
Ratio of Specific Heats, γ,	1.2
Average Molecular Weight, combustion gases g/g-mole	28.0
Initial Temperature, T_0, C	21.1
Throat Diameter of Nozzle, d_t, cm	0.434
Diameter of Motor Port d, cm	2.54
Maximum Chamber Pressure, P_c, atmos	24.80
Surface, Temperature, T_s, C	372.0
Latent Heat, ΔH, cal/g	-351.0
Igniter Heat Flux, Q, cal/cm^2 sec	13.65
Flame Temperature, T_f, C	2732.0

Table III

Calculated Parameters for the Ignition and Reignition Processes

	Datum	Case I	Case II	Case III	Case IV	Case V	Case VI	Case VII
Fuel	PMM	PMM	PMM	PMM	Boron	Boron	Boron	Boron
Surface Temperature, T_s, C	372	372	372	372	372	372	500	372
Latent Heat, ΔH, cal/g	351	351	351	351	351	100	100	100
Radiation Considered YES/NO	NO	YES	YES	YES	NO	NO	NO	NO
Shut-down Duration, t_{shd}, sec	2.0	2.0	0.9	4.0	2.0	2.0	2.0	4.0
Ignition Delay sec,	0.078	0.075	0.075	0.075	0.514	0.516	0.864	0.516
$\dot{r}$ at t = 4.95 sec cm/sec	0.0271	0.0306	0.0315	0.0306	0.0194	0.044	0.0311	0.044
Time to 90% $\dot{r}$ (1st IGN) t_2, sec	1.75	1.55	2.05	1.55	2.5	2.0	1.9	2.0
Reignition Delay (sec)					0.15	0.2	0.3	0.2
Maximum $\dot{r}_t$ on Restart cm/sec	0.0313	0.0343	0.0358	0.0372	0.020	0.052	0.0401	0.0539
Regression Rate Overshoot, %	15.0	12.0	14.0	21.6	3.1	18.1	29.0	20.0
Time to 90% of Initial $\dot{r}$ (Restart) t_2, sec	0.50	0.45	0.45	0.40	0.5	0.4	0.45	0.38
Decrease in Ignition Interval t_2/t_1	0.286	0.29	0.22	0.258	0.20	0.20	0.236	0.19

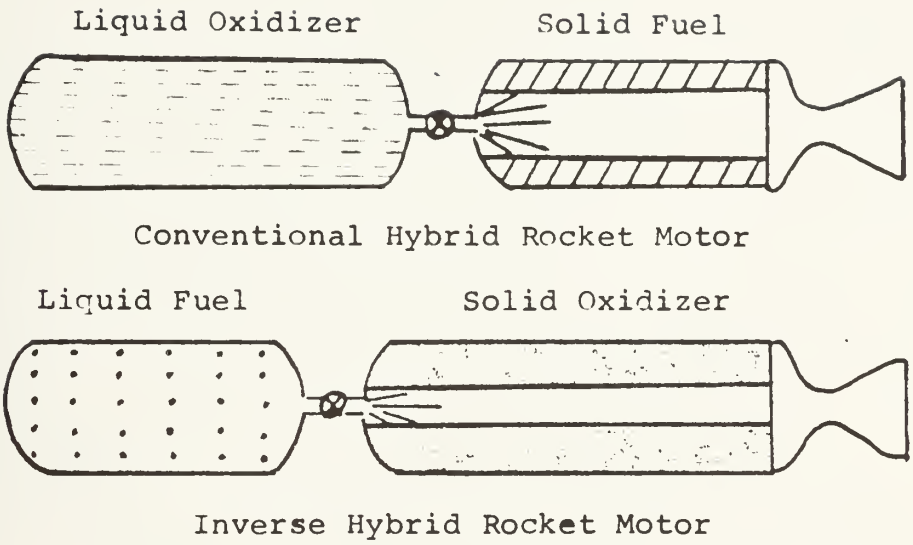

Fig. 1 Conceptual Representation of a Conventional and an Inverse Hybrid Rocket Motor

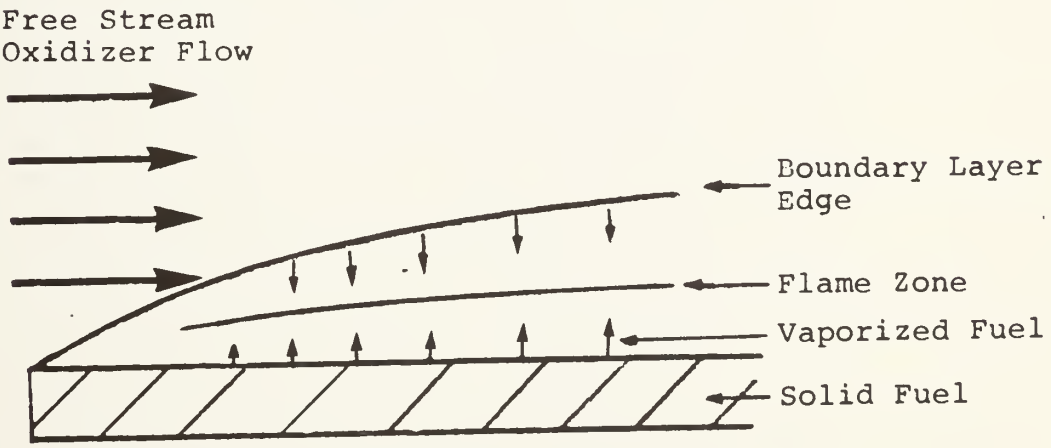

Fig. 2 Simplified Hybrid Combustion Model for Flow over a Flat Plate

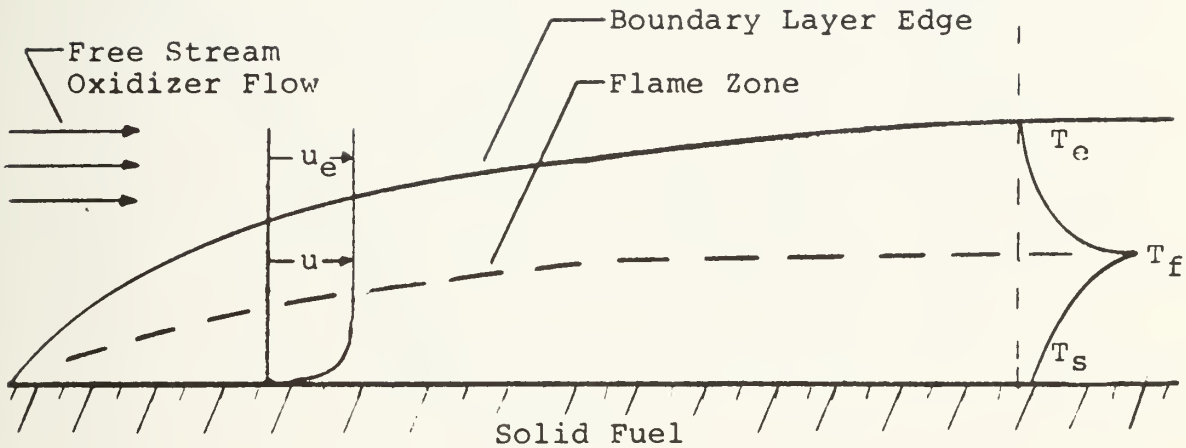

Fig. 3 Turbulent Boundary Layer Combustion Model (taken from Marxman and Gilbert, Ref. 6)

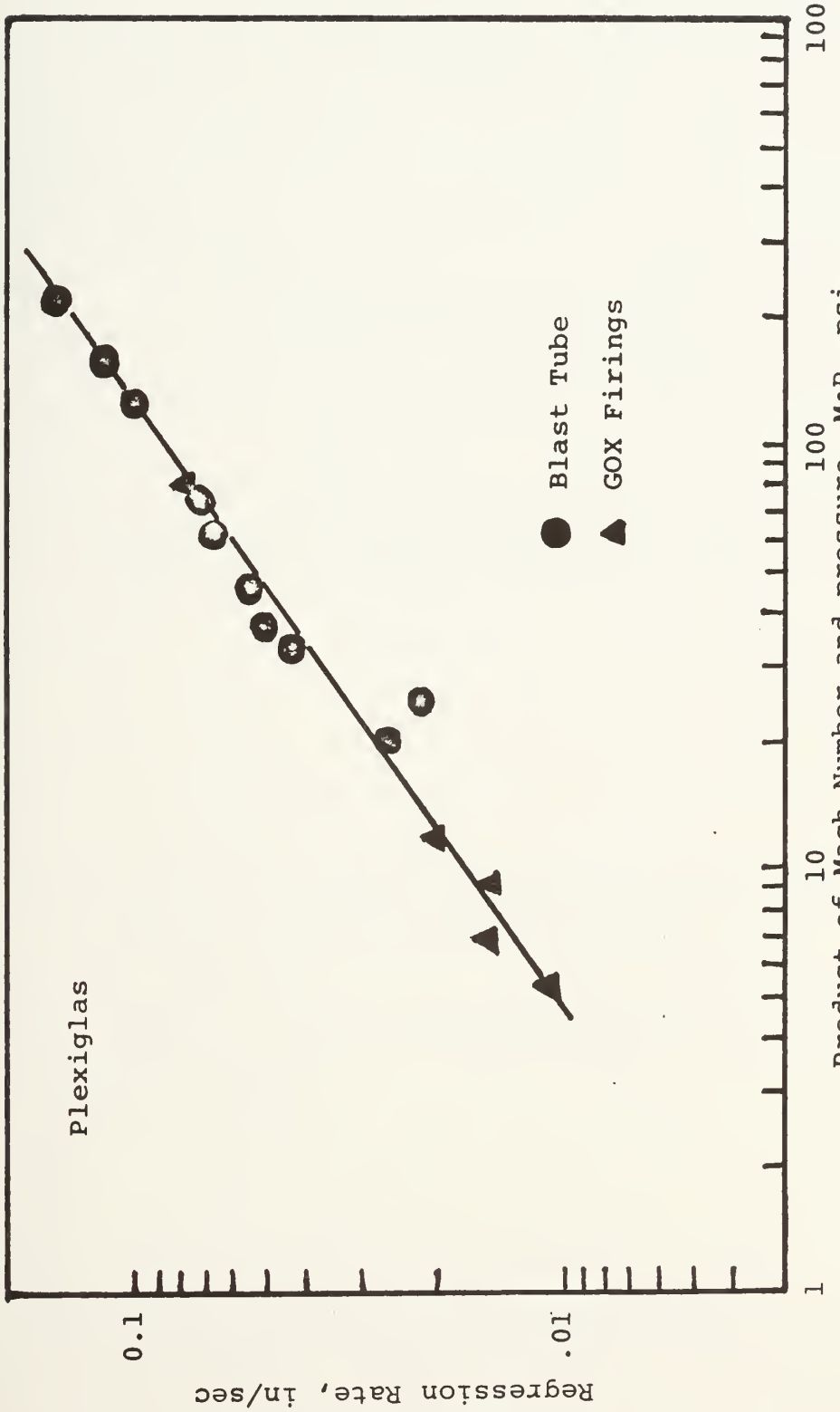

Fig. 4 Variation of Regression Rate with MP for Plexiglas (taken from Anderson, Ref. 7)

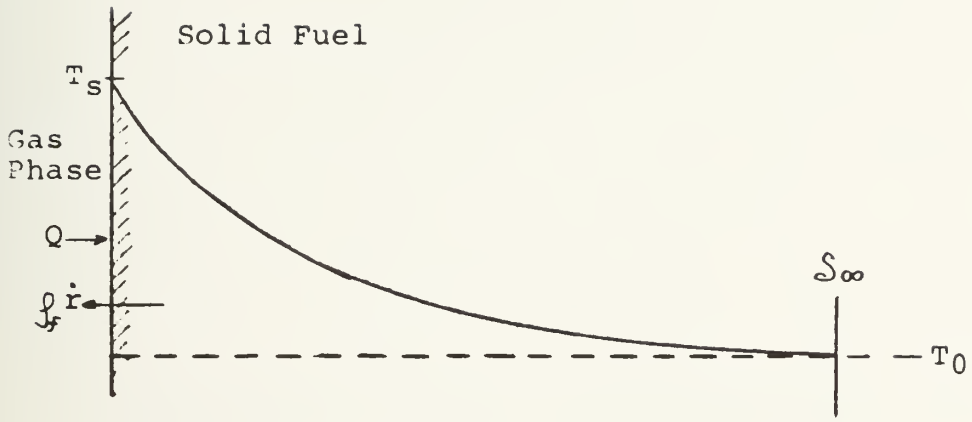

Fig. 5 Steady-State Thermal Profile in a Hybrid Rocket Fuel

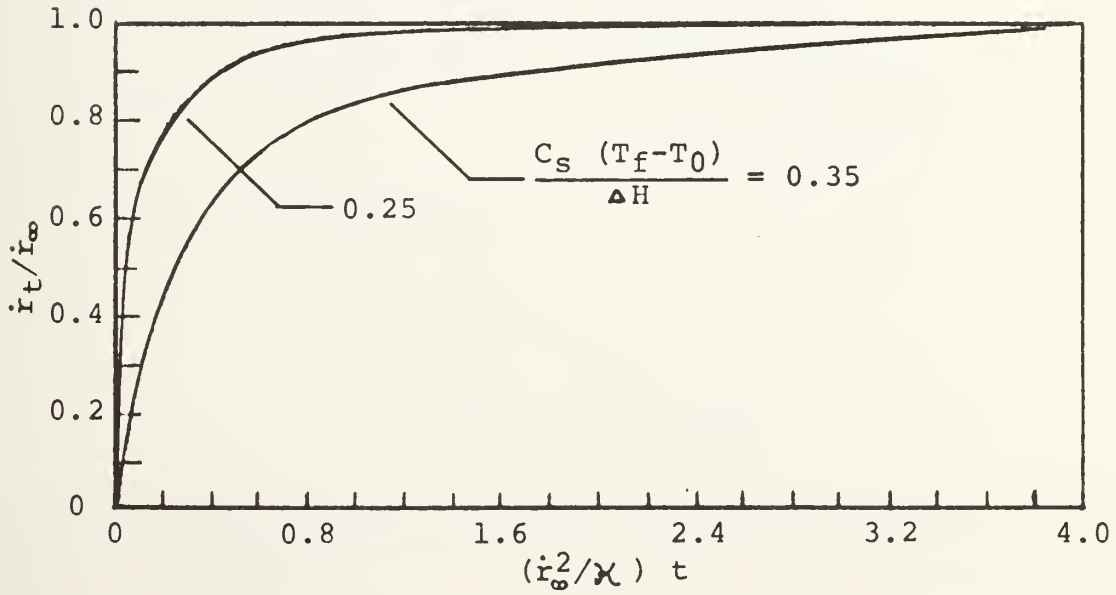

Fig. 6 Transient Regression Rate Behavior during the Establishment of a Thermal Profile in a Hybrid Fuel (taken from Marxman et al., Ref. 12)

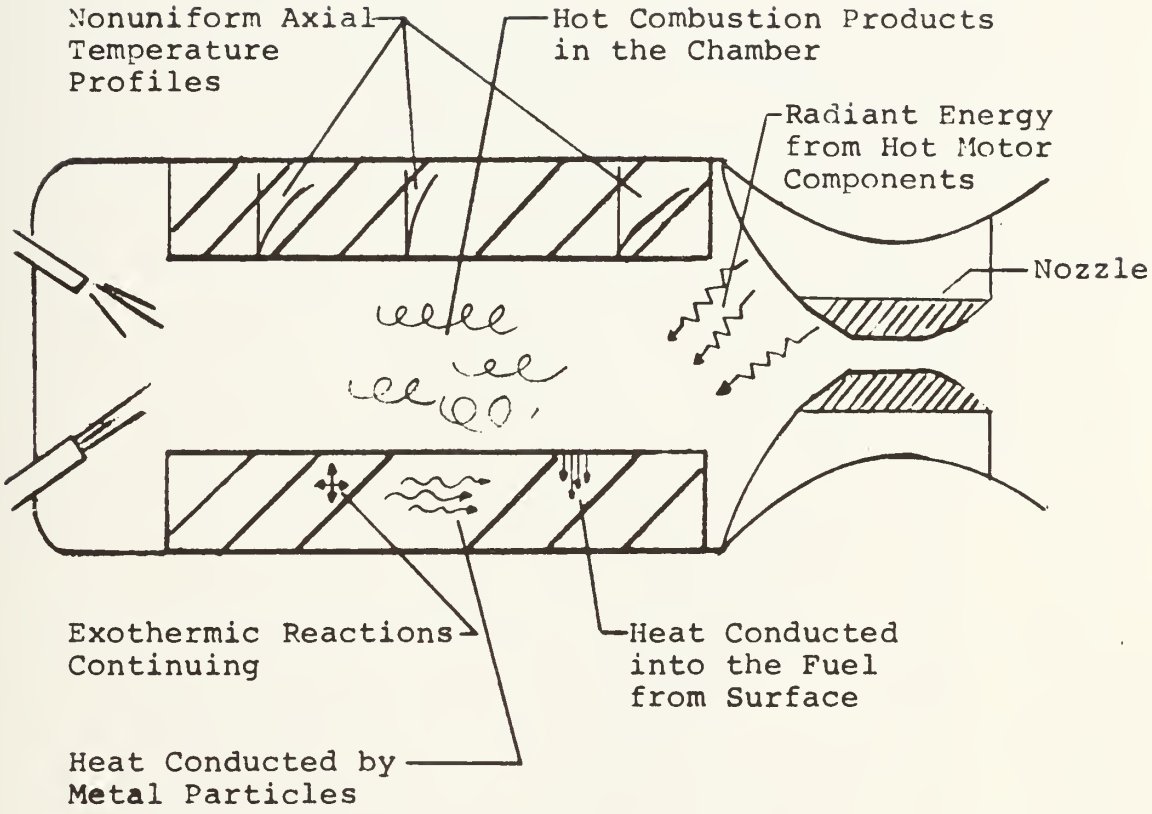

Fig. 7 Model of the Nonuniform Heat Distribution during Shut-down

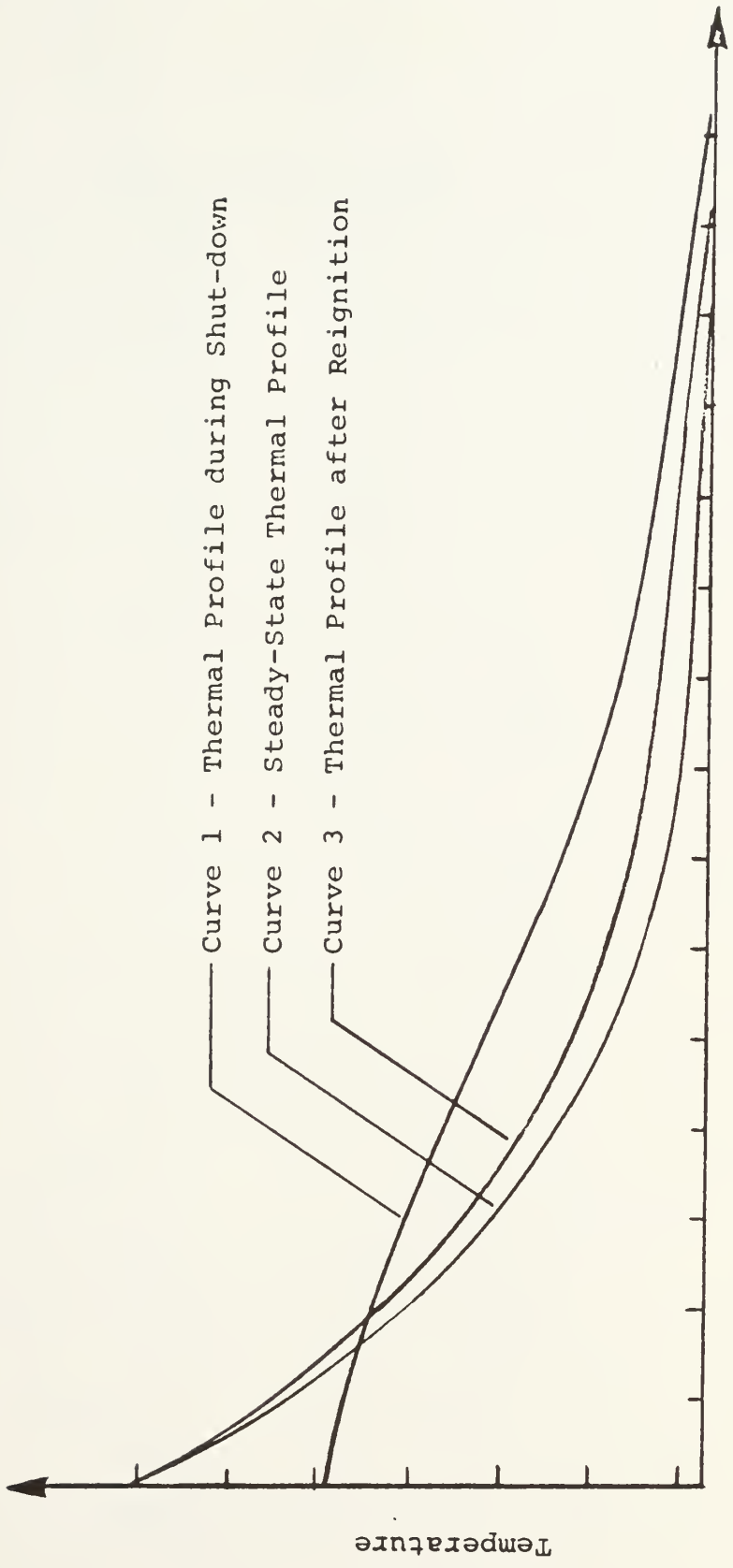

Fig. 8 Changes in the Steady-State Thermal Profile as a Result of Shut-down and Reignition

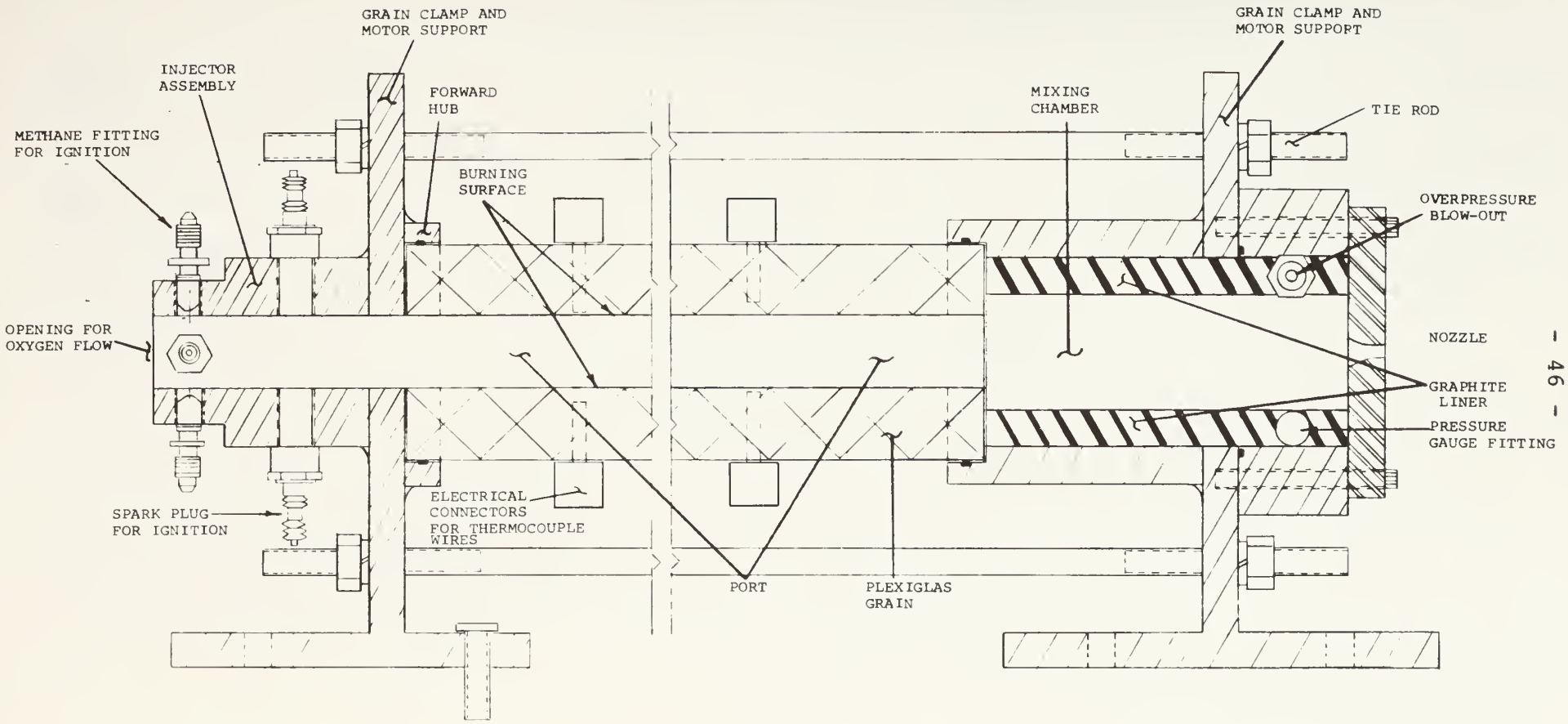

Fig. 9 Schematic Drawing of Hybrid Motor Assembly

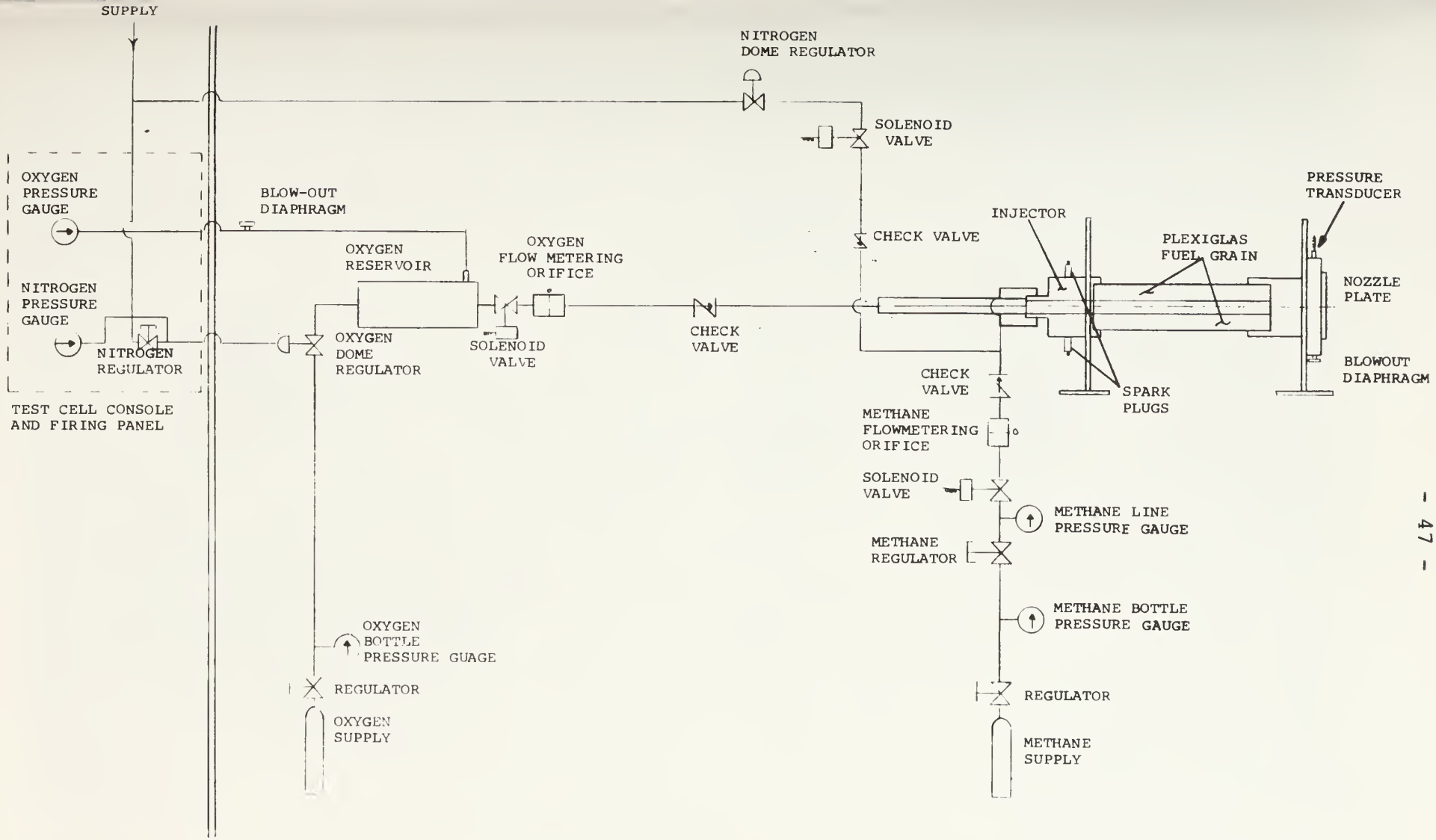

Fig. 10 Gas System Schematic Drawing

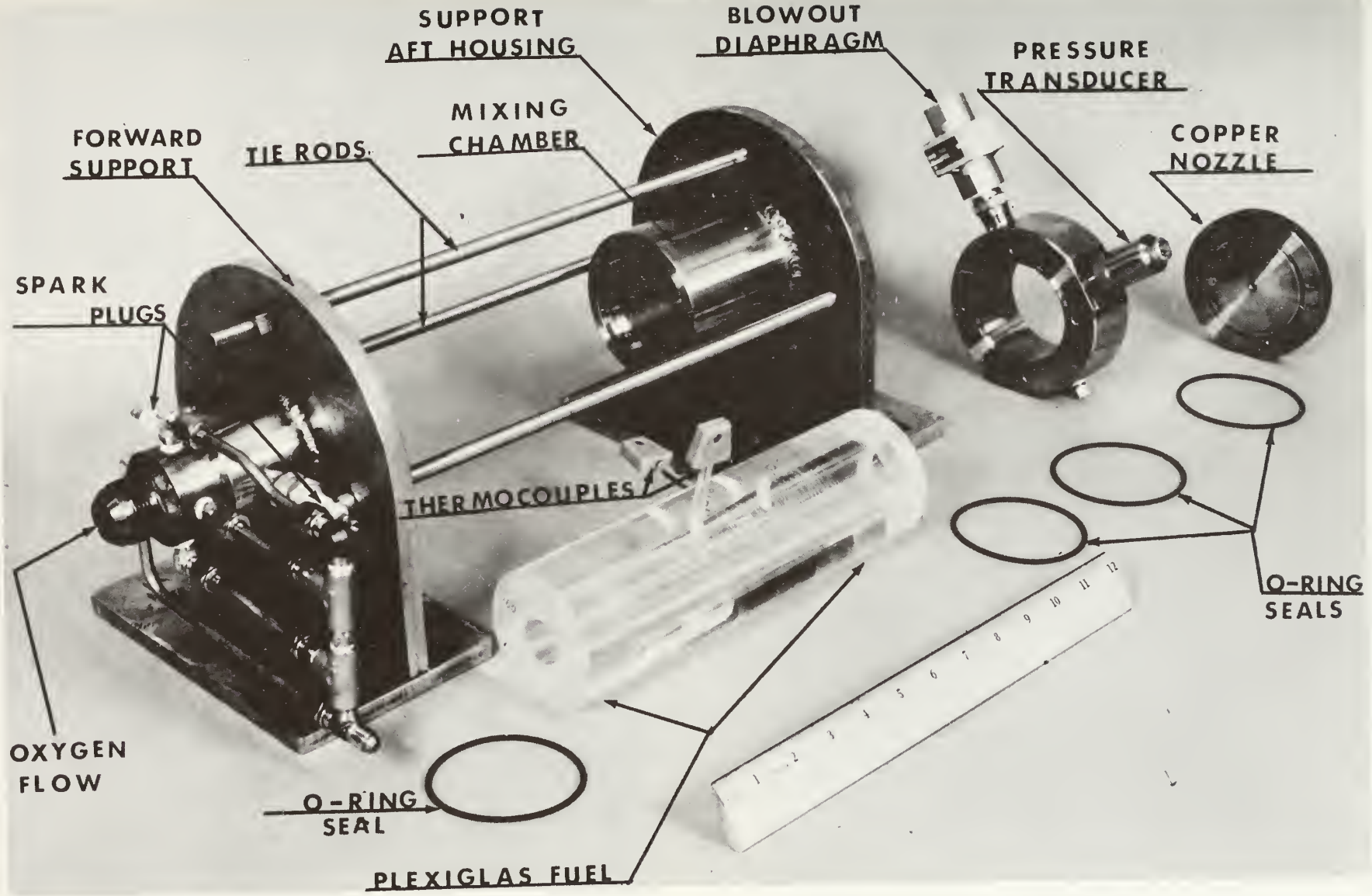

FIG. 11 EXPLODED VIEW OF THE HYBRID MOTOR

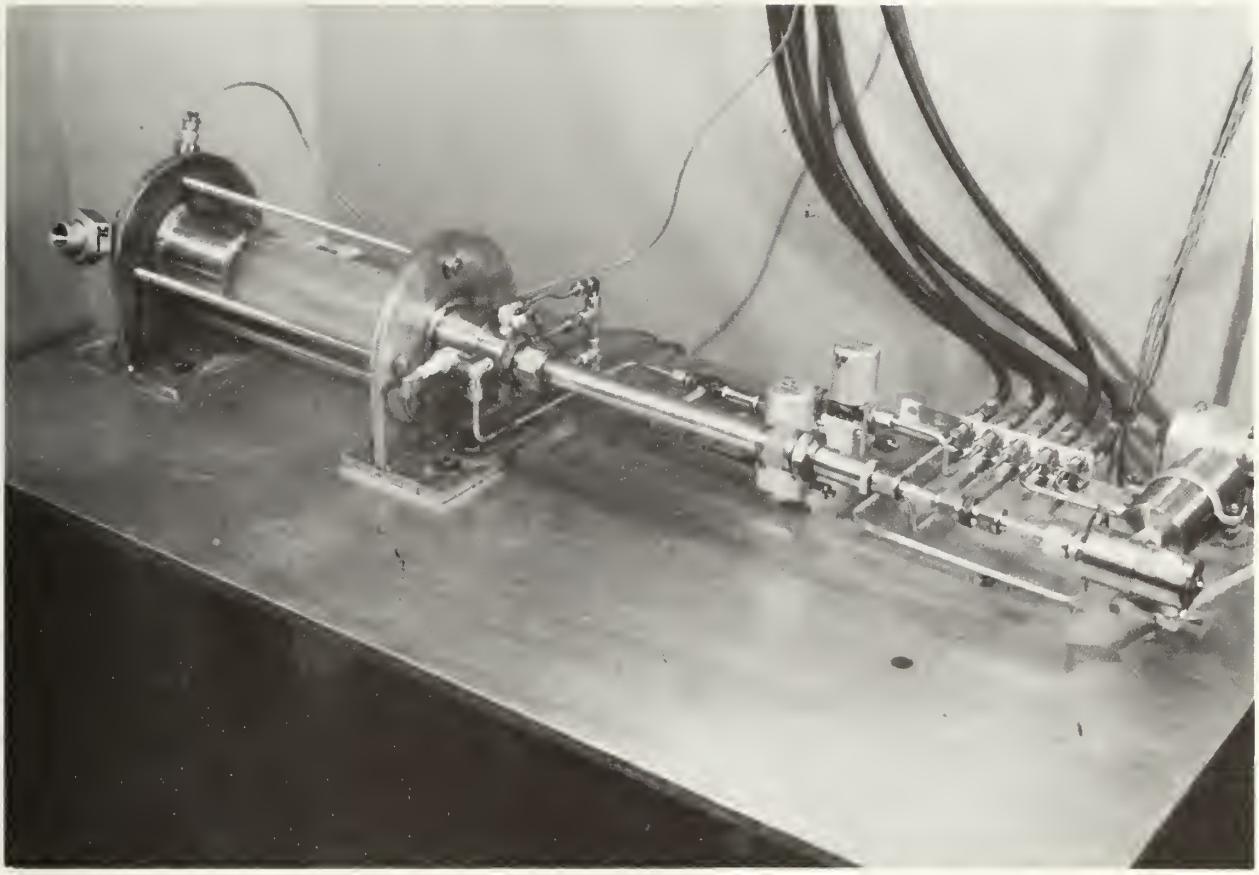

Fig.12 Photograph of hybrid motor mounted in test bay

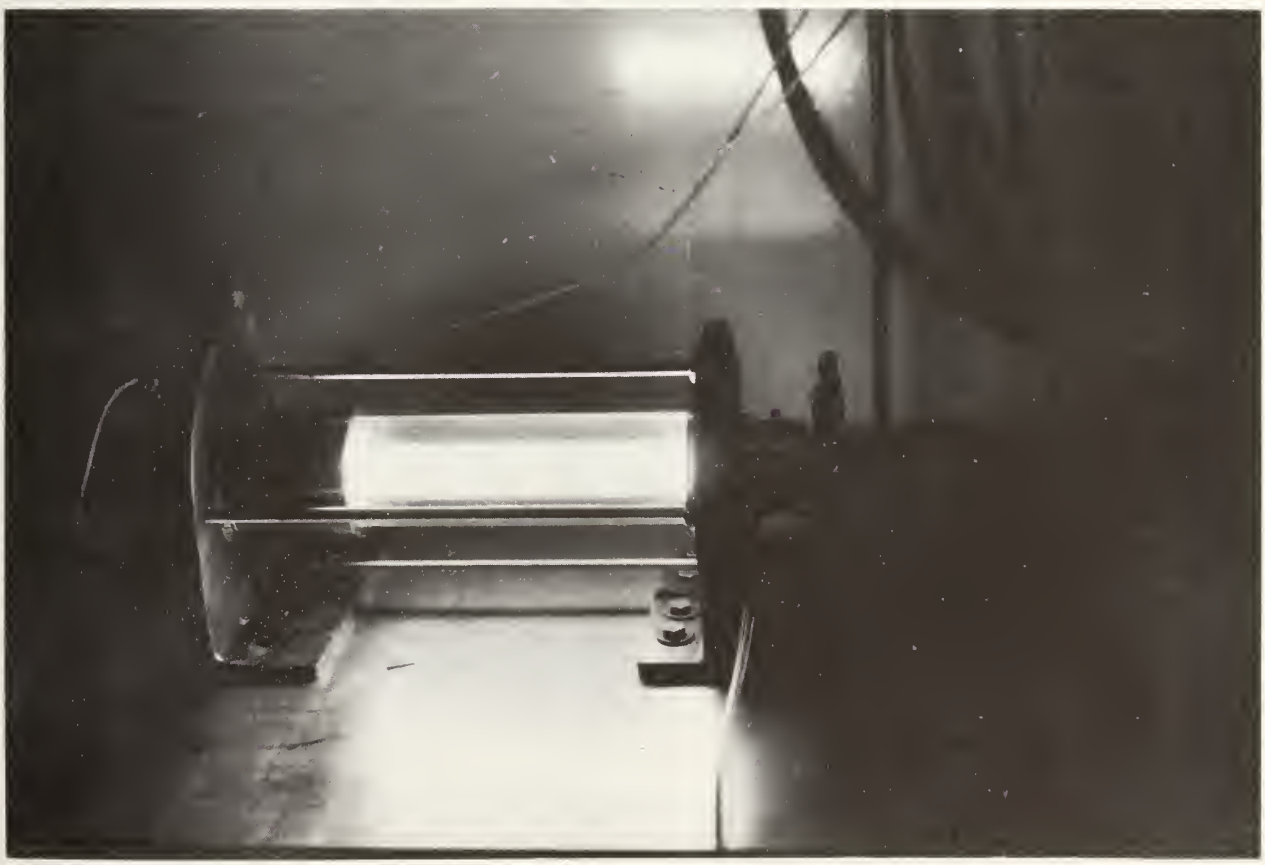

Fig.13 Photograph of test bay with hybrid motor mounted

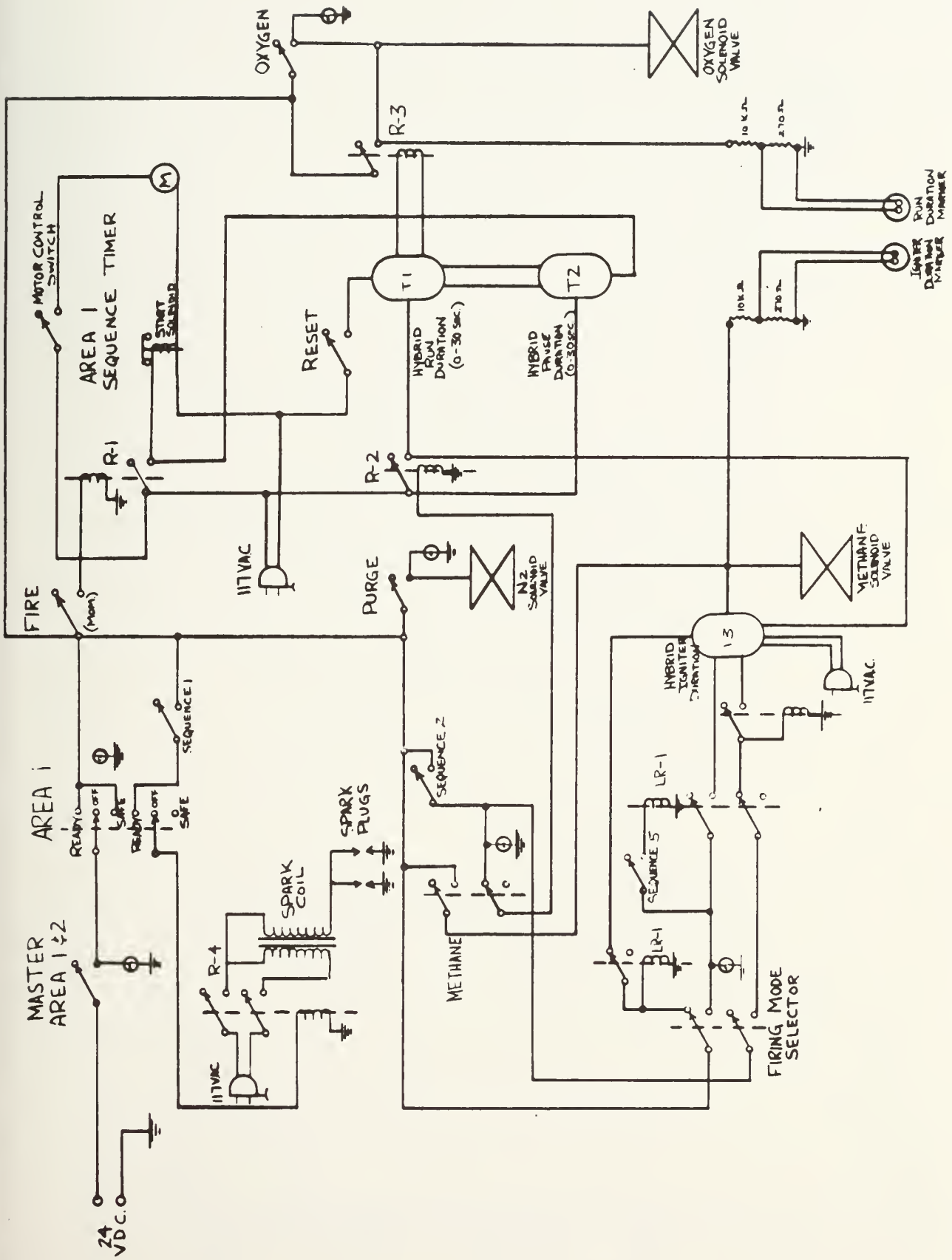

Fig. 14 Electrical Schematic Drawing

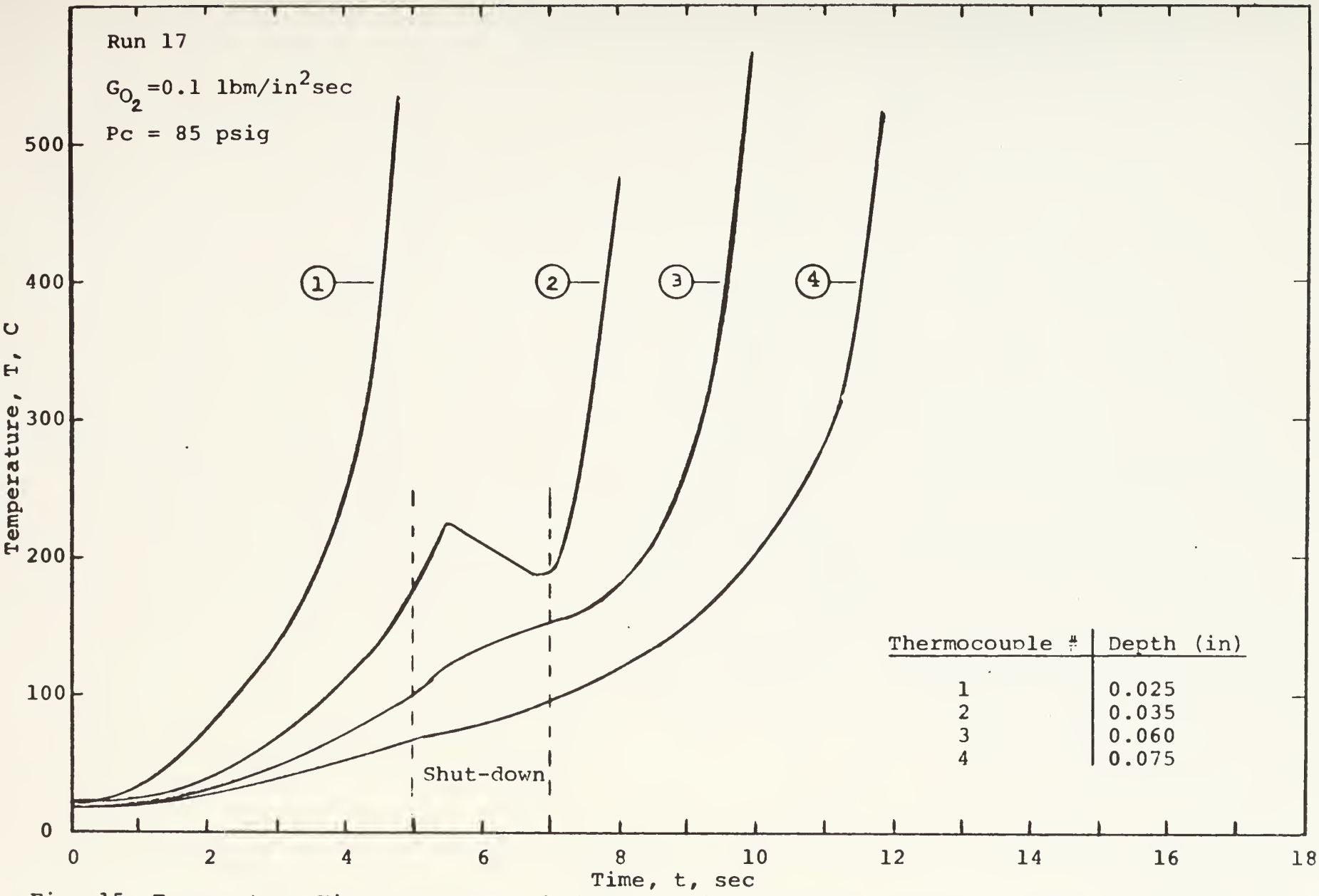

Fig. 15 Temperature-Time Responses of Thermocouples Located 4.0 to 6.0 Inches from Injector

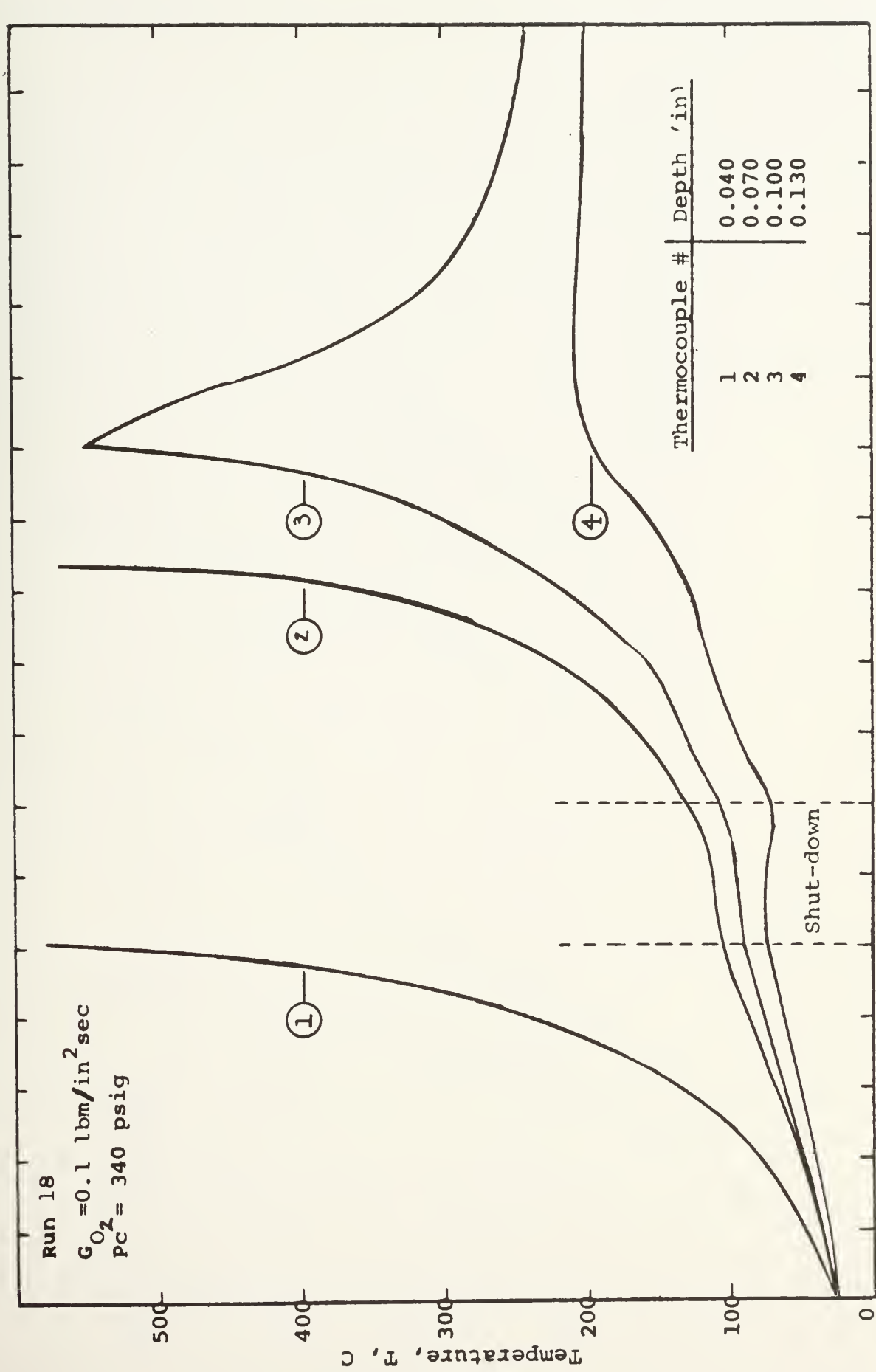

Fig. 16 Temperature-Time Responses of Thermocouples Located 4.0 to 6.0 Inches from Injector

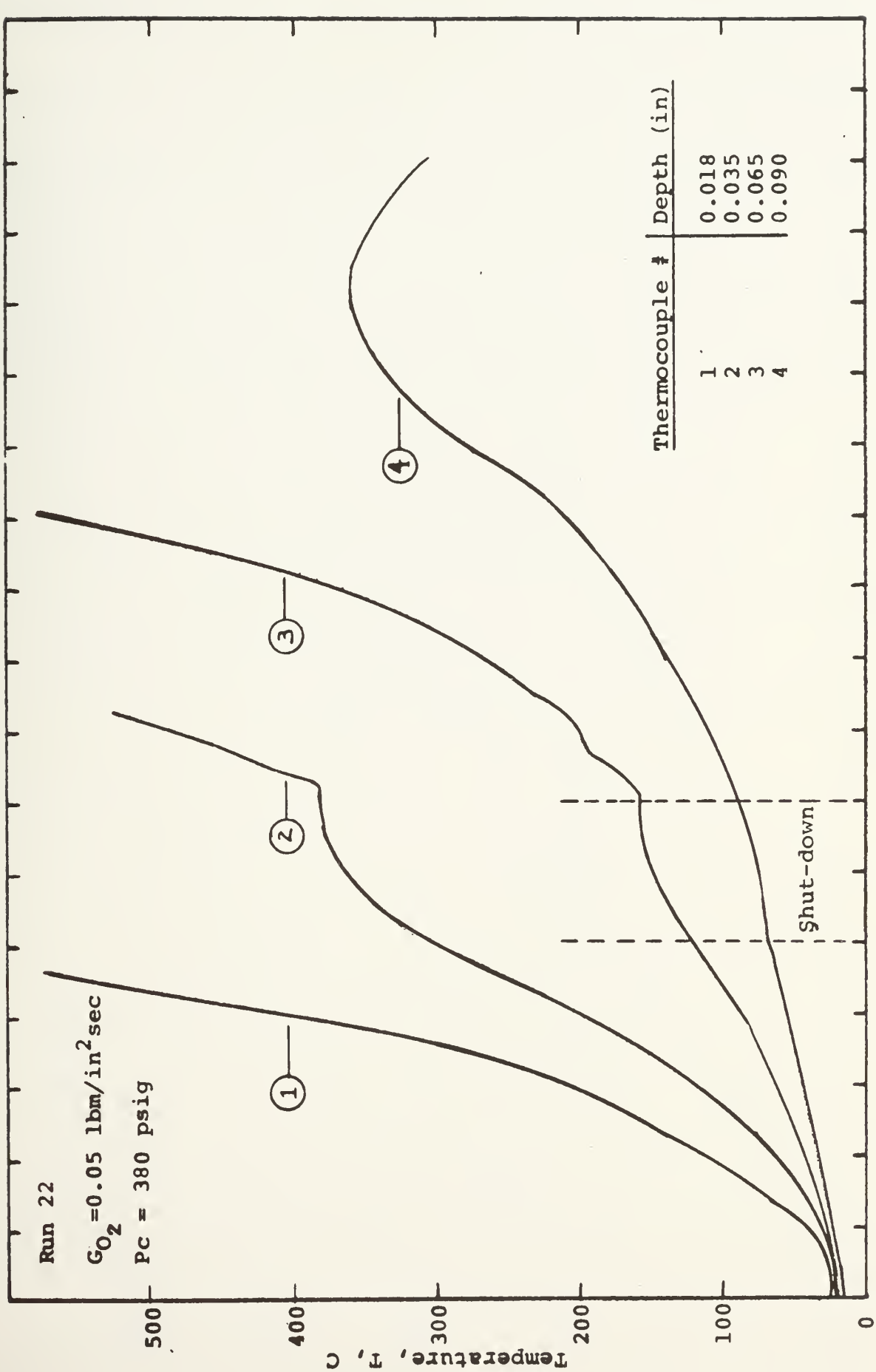

Fig. 17 Temperature-Time Responses of Thermocouples Located 4.0 to 6.0 Inches from Injector

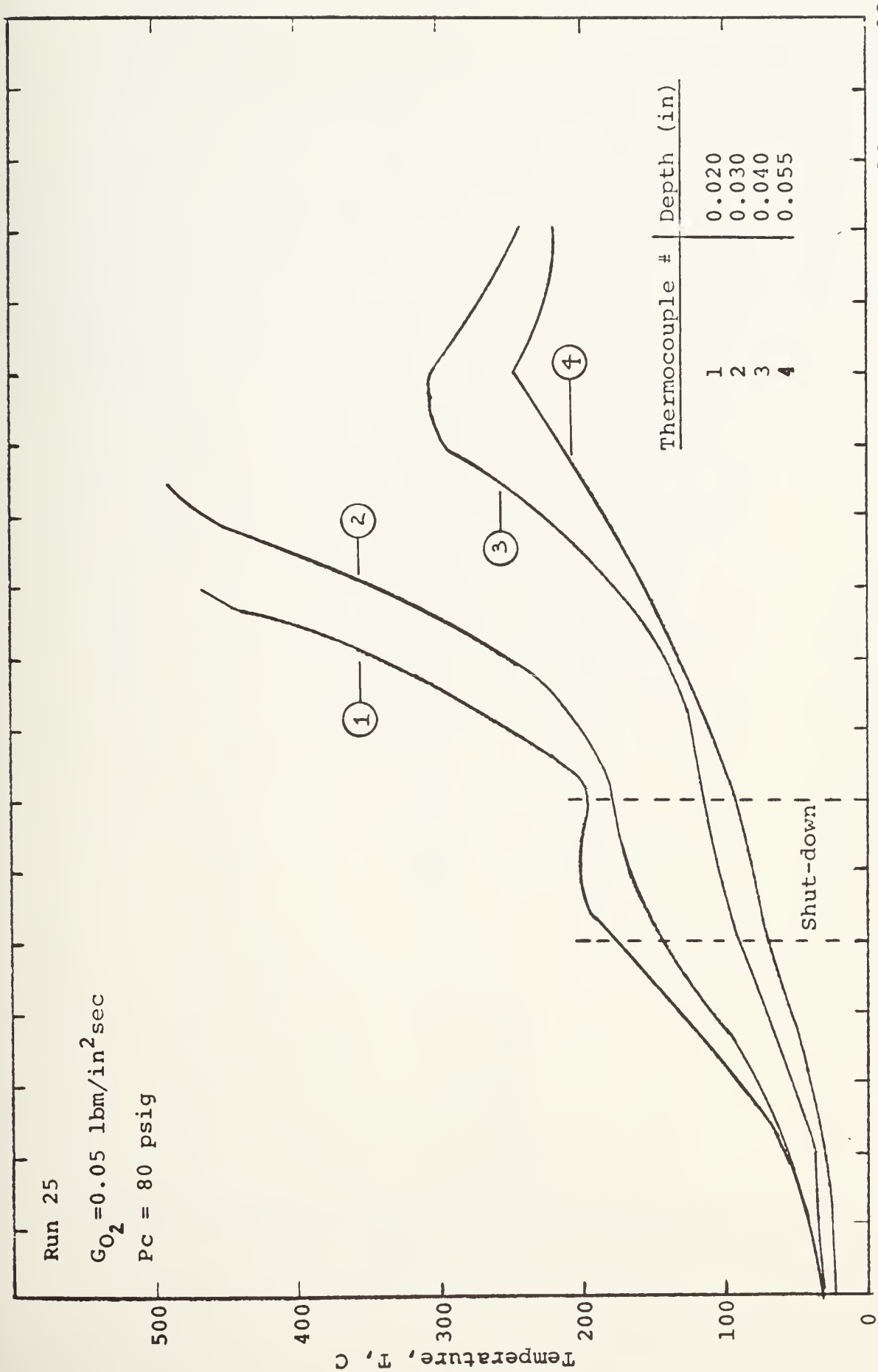

Fig. 18 Temperature-Time Responses of Thermocouples Located 4.0 to 6.0 Inches from Injector

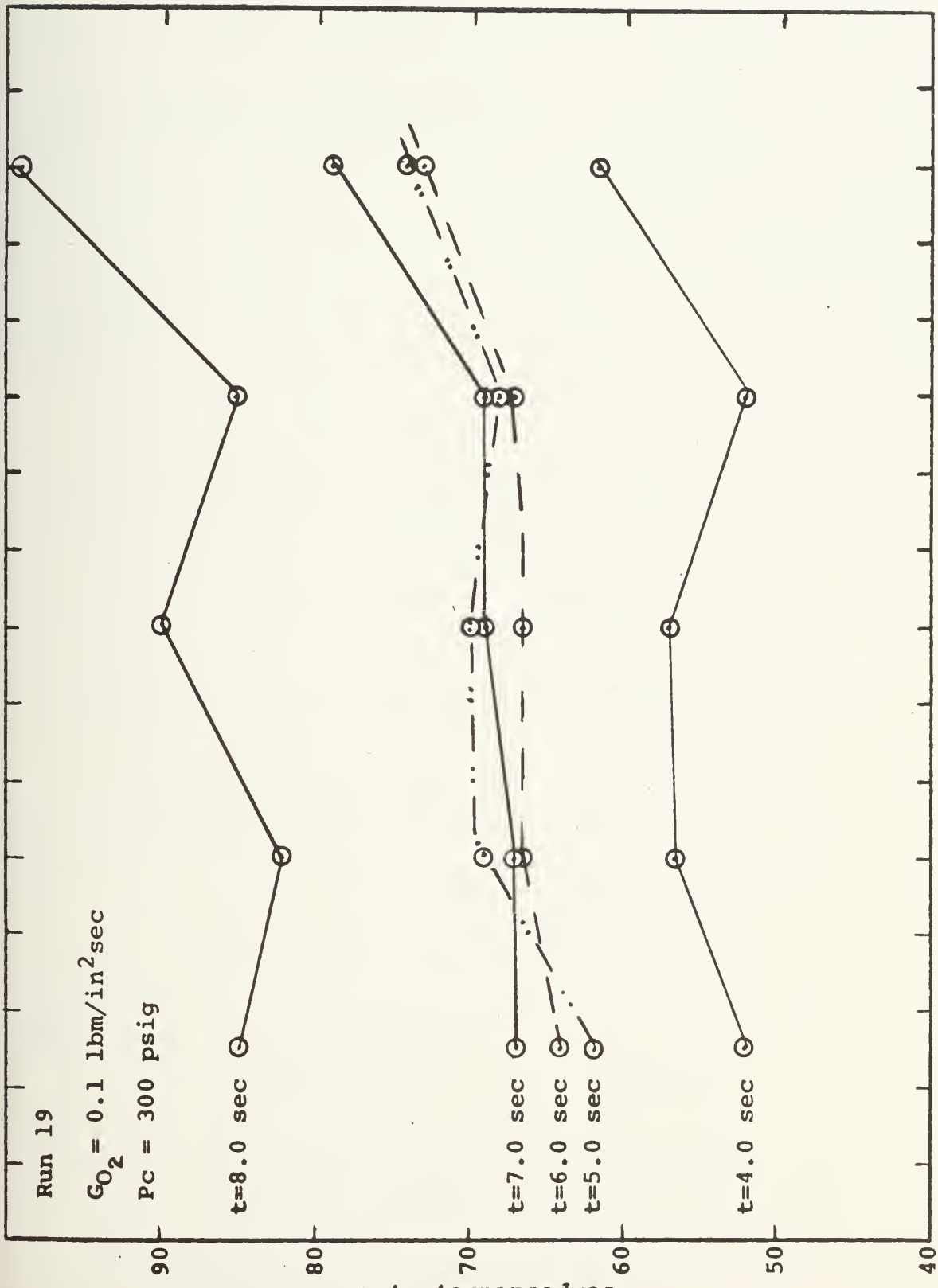

Fig. 19 Nonsteady and Nonuniform Heat Distribution to the Fuel during the Shut-down Duration (Shut-down between 5-7 sec)

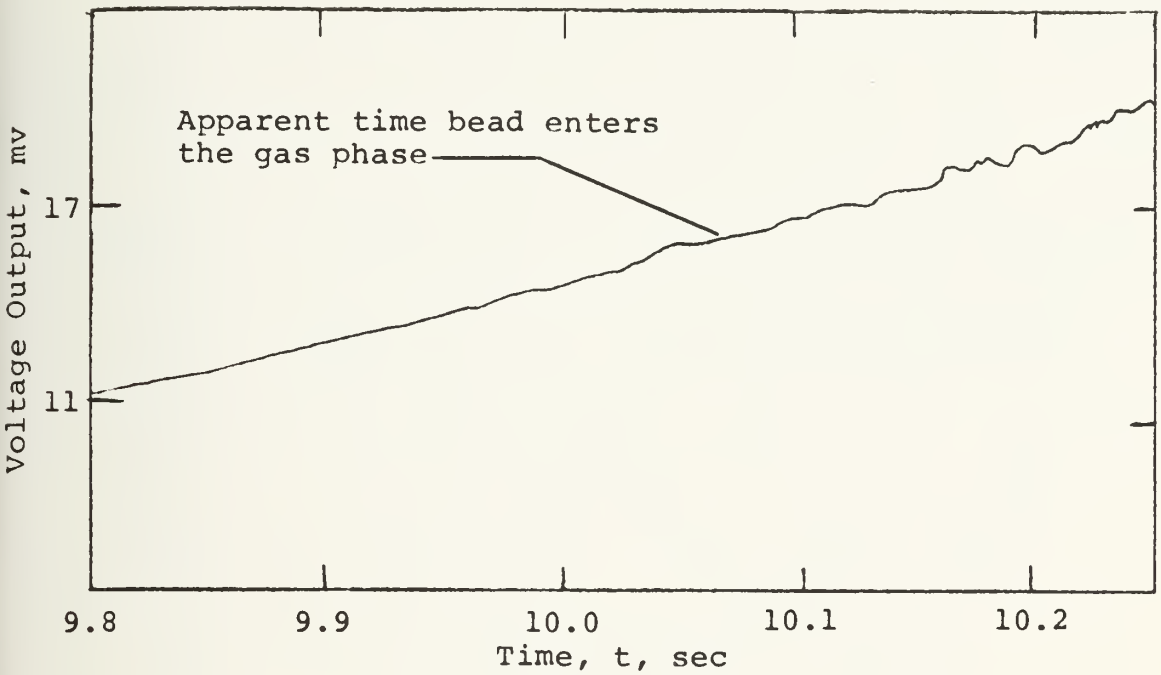

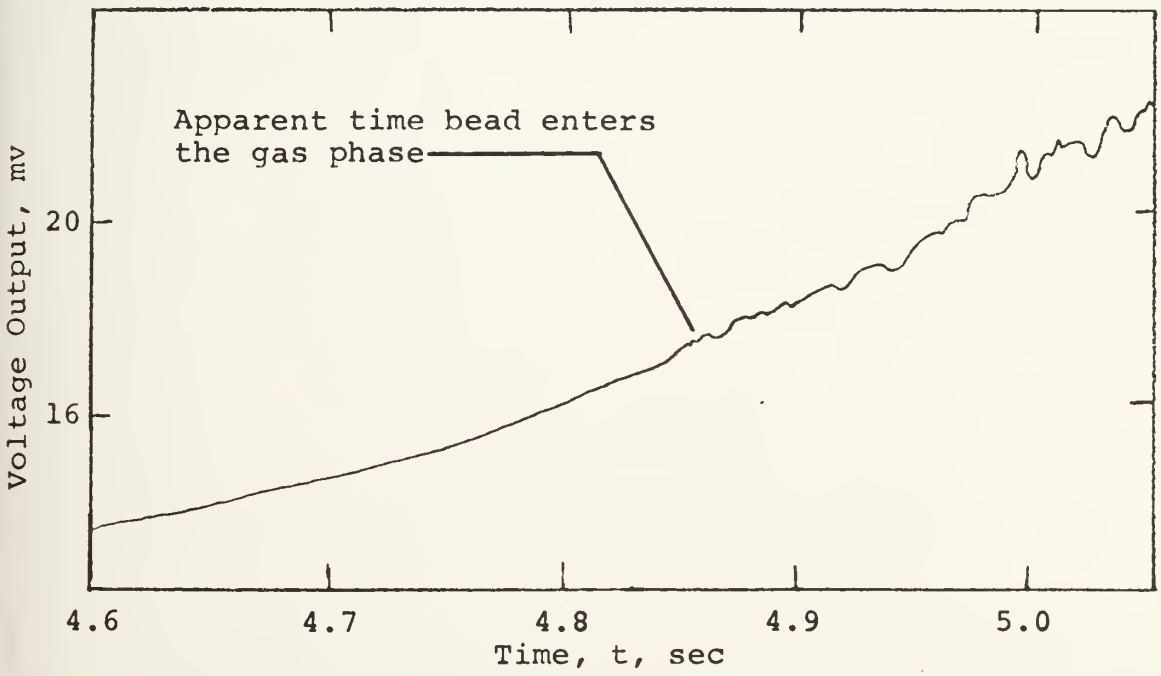

Fig. 20 Examples of the Change in Thermocouple Output as the Bead Enters the Gas Phase

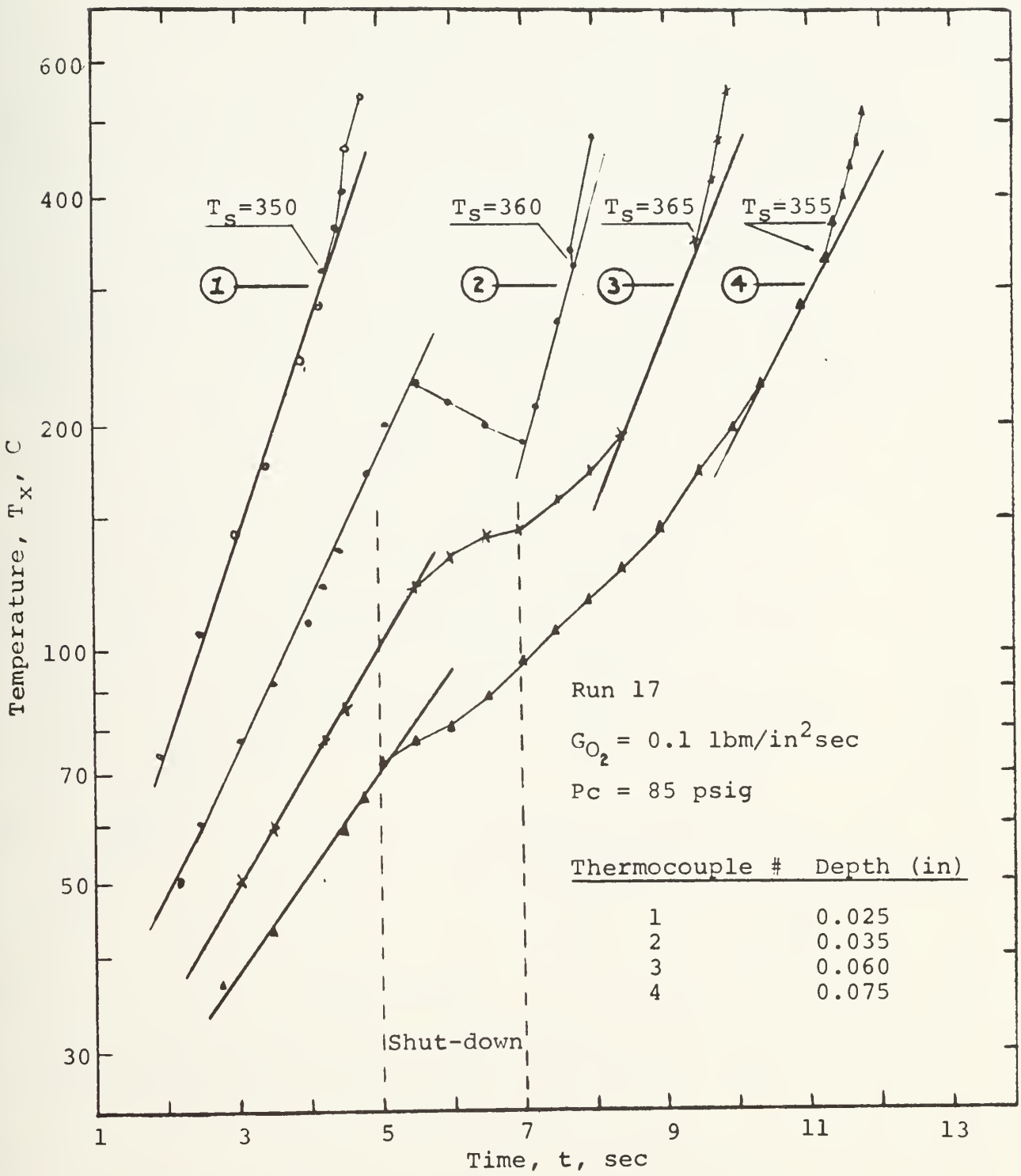

Fig. 21 Log T_x vs Time for Run 17 with Measured Surface Temperatures Indicated

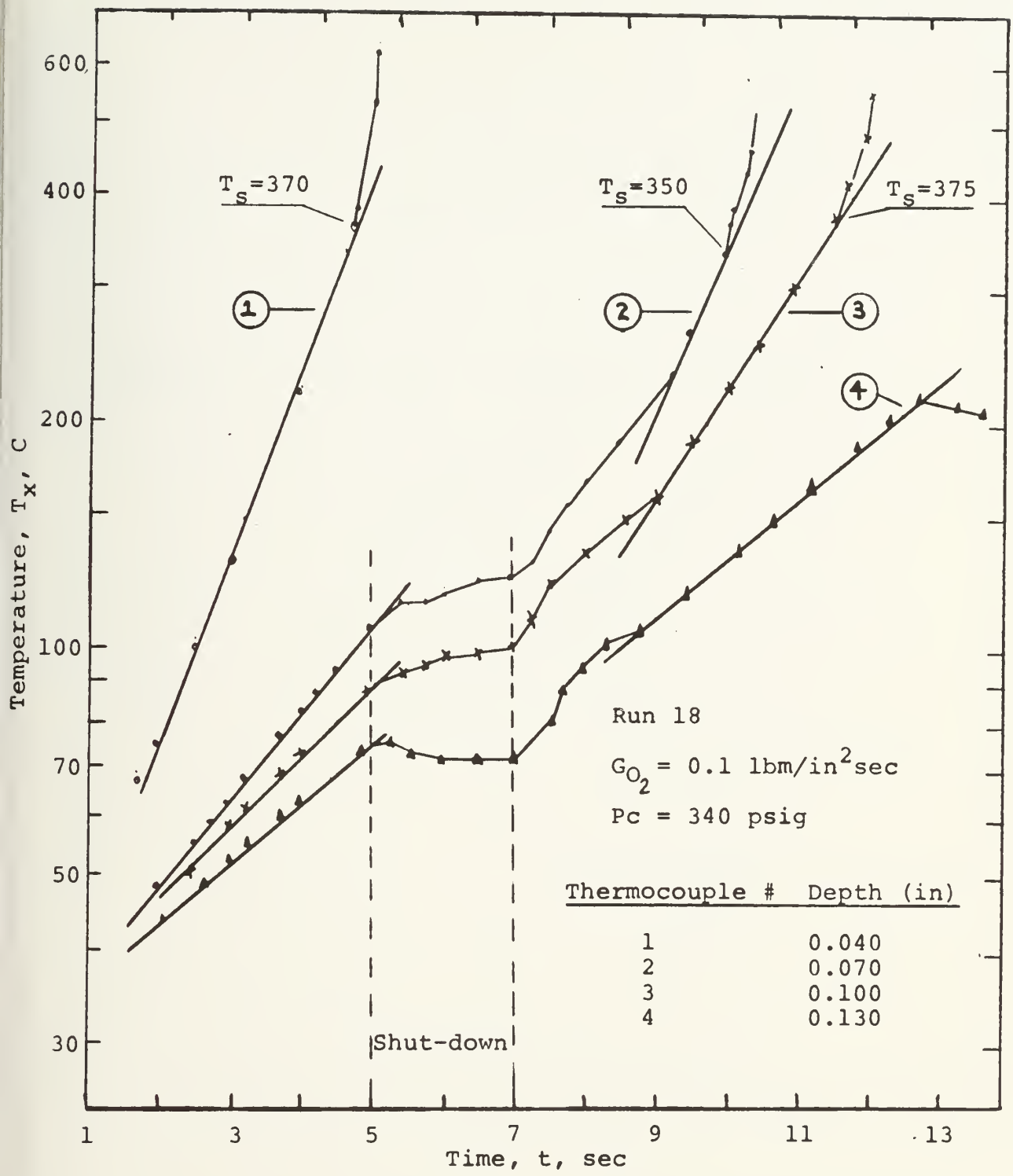

Fig. 22 Log T_x vs Time for Run 18 with Measured Surface Temperatures Indicated

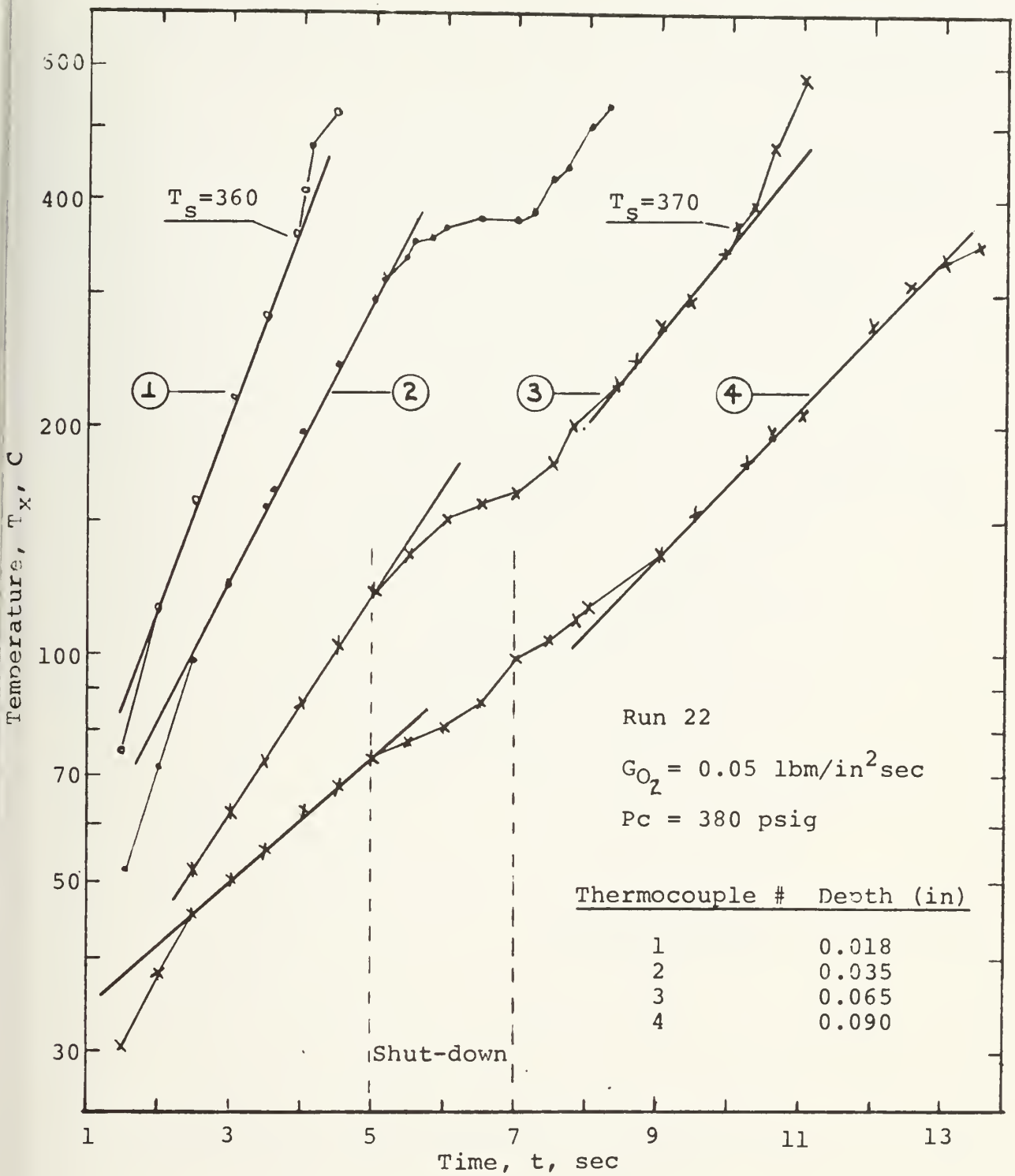

Fig. 23 Log T_x vs Time for Run 22 with Measured Surface Temperatures Indicated

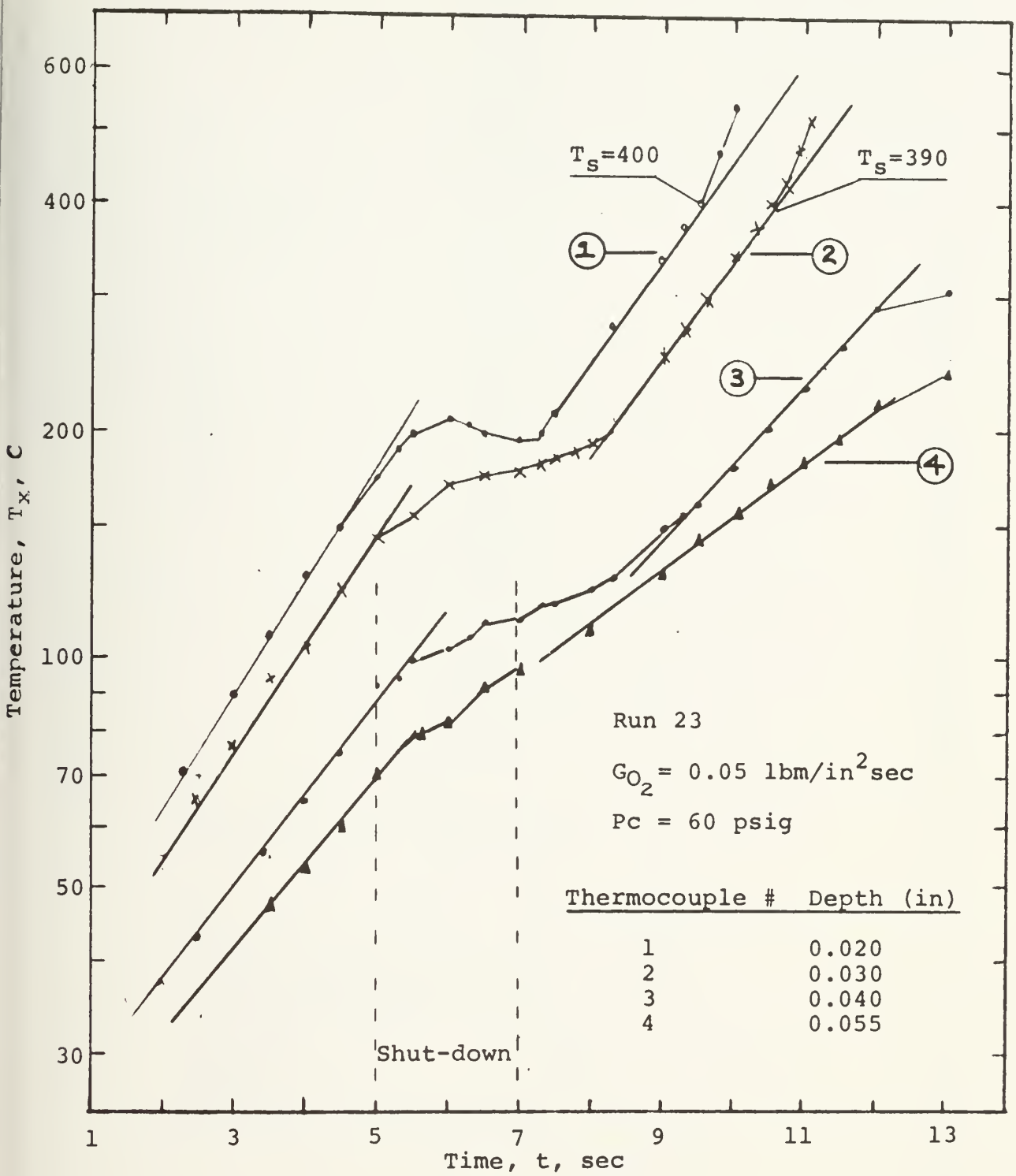

Fig. 24 Log T_x vs Time for Run 23 with Measured Surface Temperatures Indicated

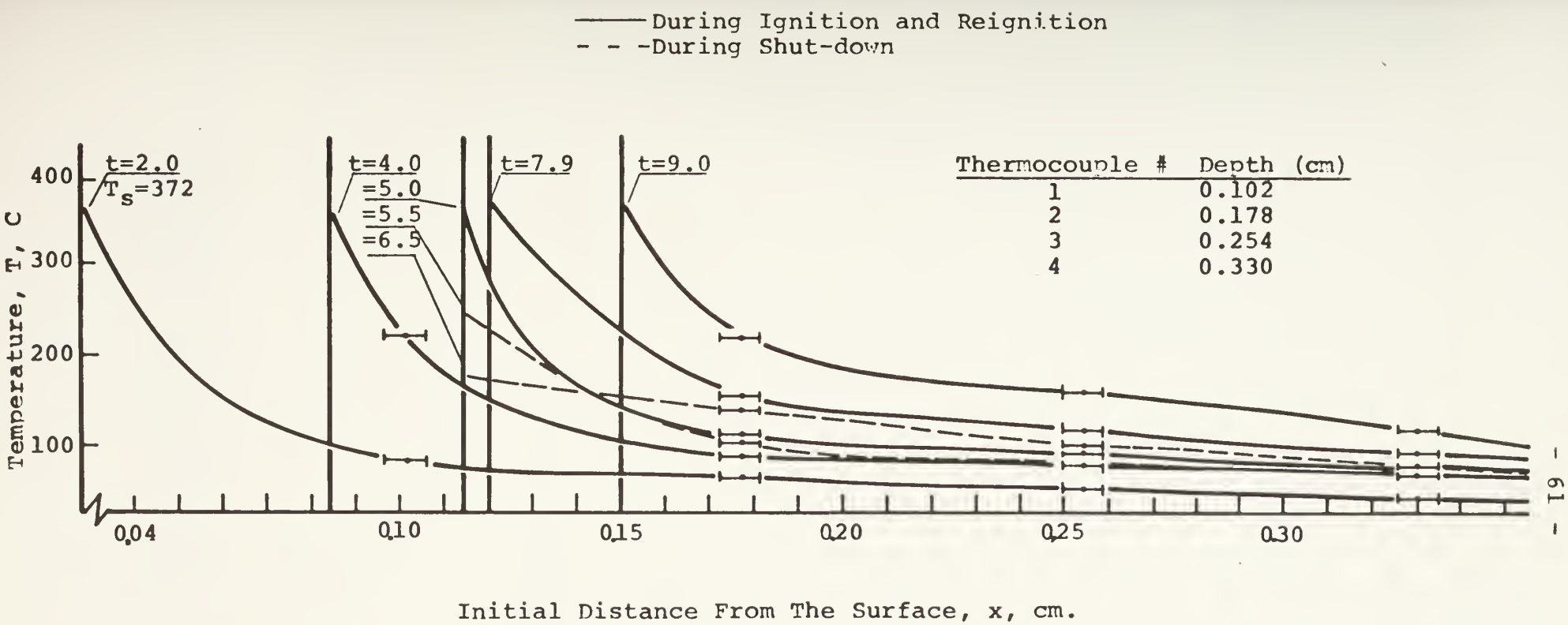

Fig. 25 The Thermal Profiles Measured by Four Thermocouples during Run 18. Surface Temperature, T_s, during Firing Intervals Was Assumed to be Constant.

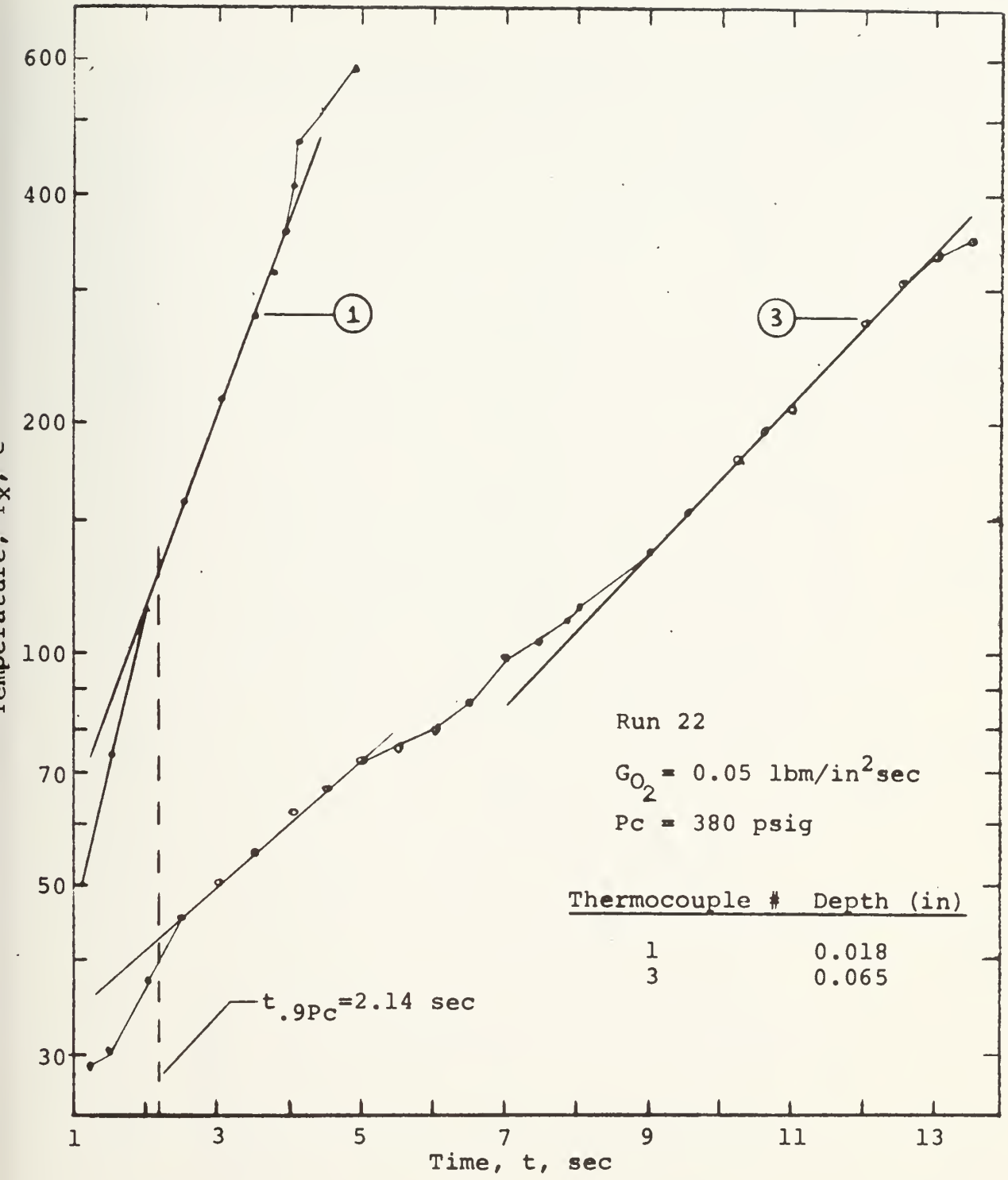

Fig. 26 Log T_x vs Time for Run 22 to Compare the Time to Establish Thermal Equilibrium, as Indicated by the Straight Line Approximation, with Time to Establish 90% of the Steady-State Chamber Pressure, $t_{.9Pc}$

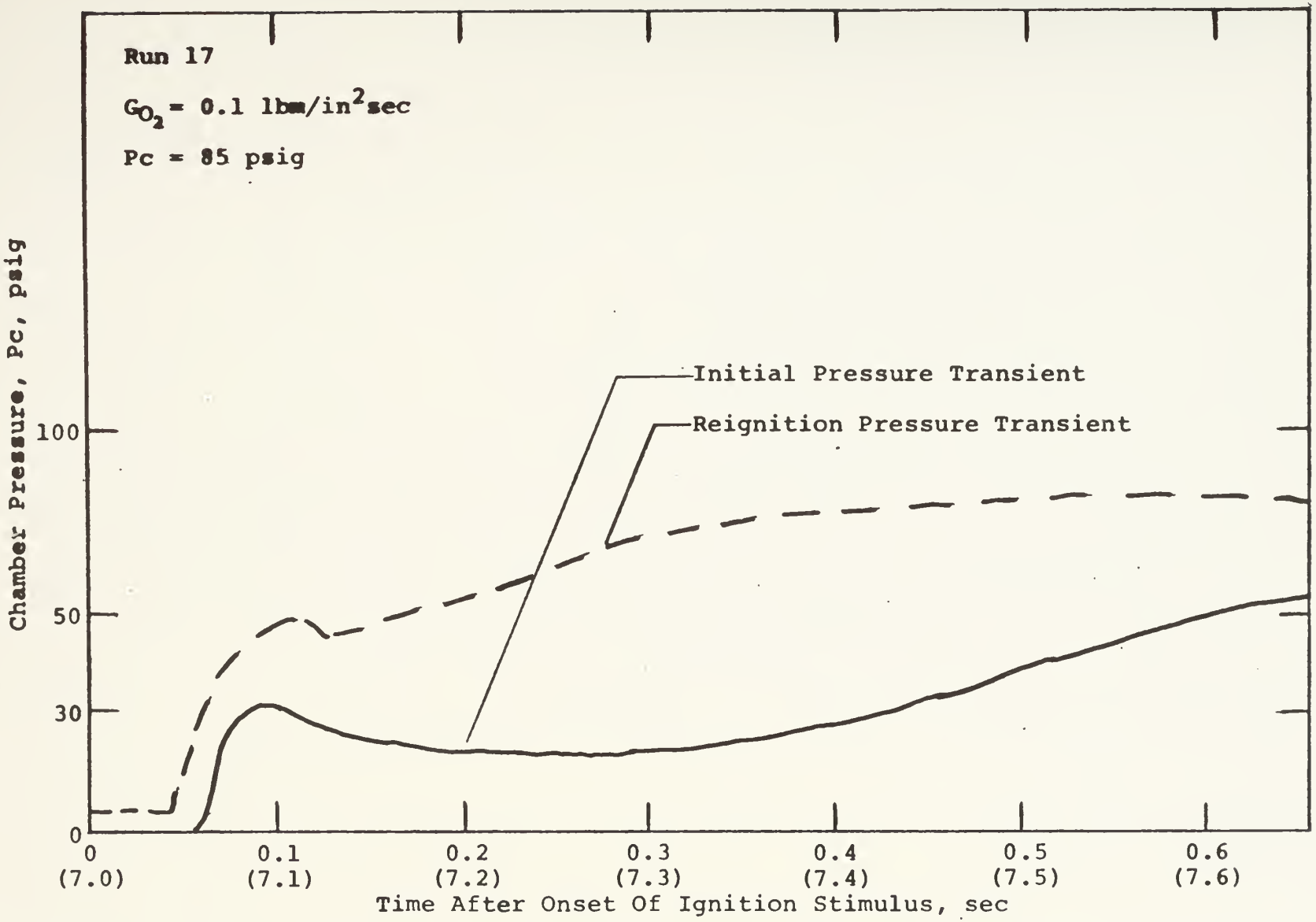

Fig. 27 Effect of a 2.0 sec Shut-down on the Pressure Transient following Reignition

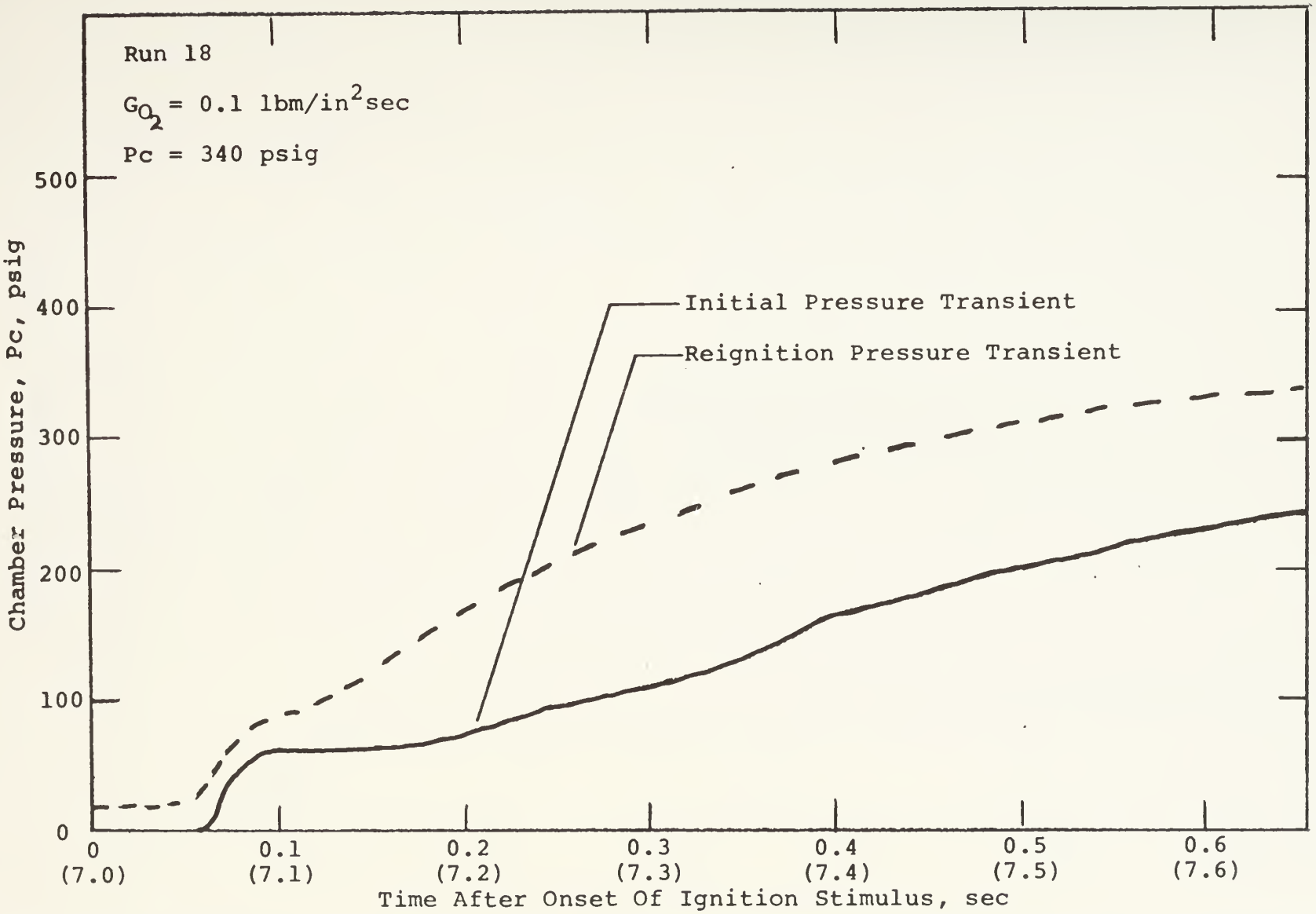

Fig. 28 Effect of a 2.0 sec Shut-down on the Pressure Transient following Reignition

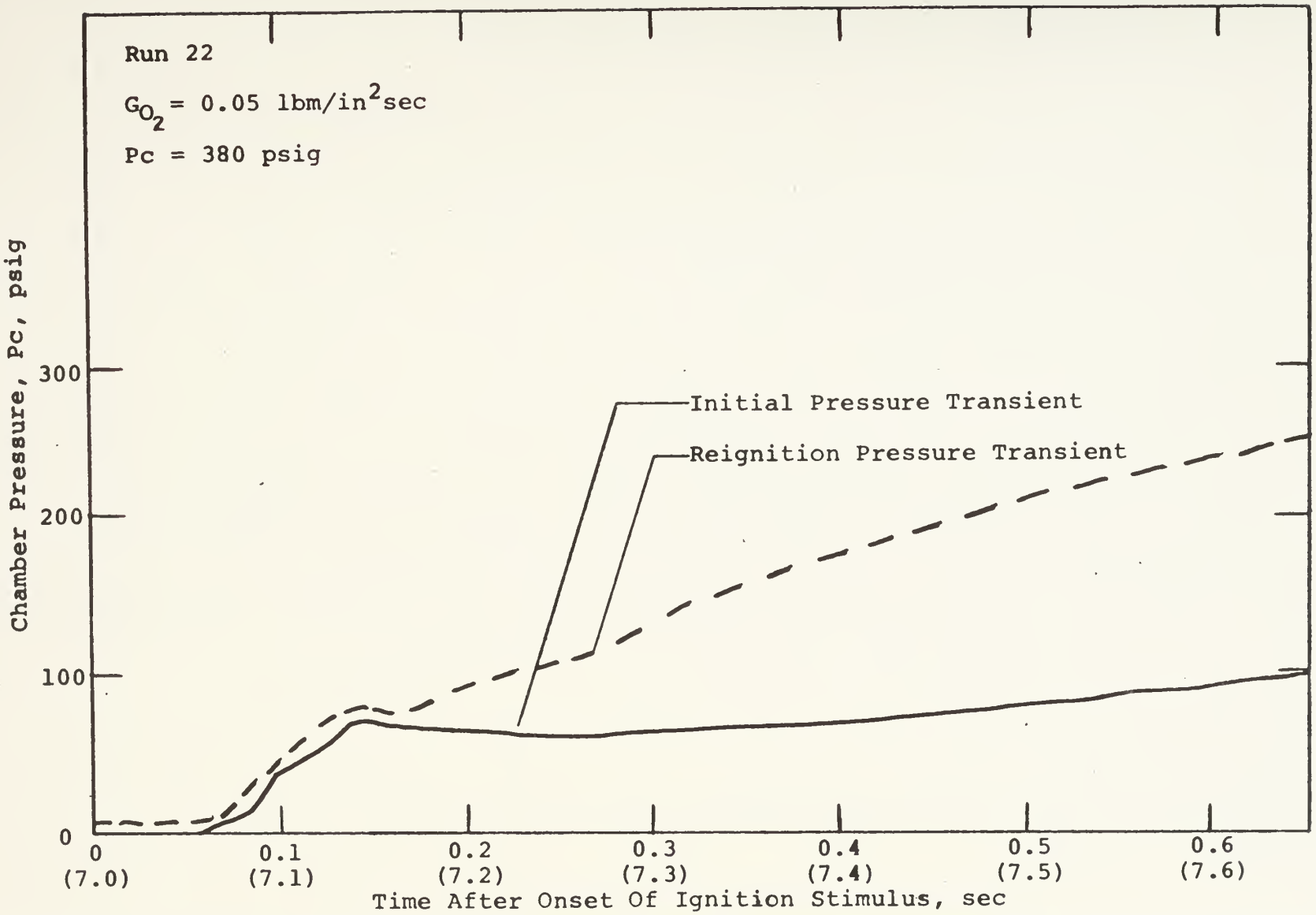

Fig. 29 Effect of a 2.0 sec Shut-down on the Pressure Transient following Reignition

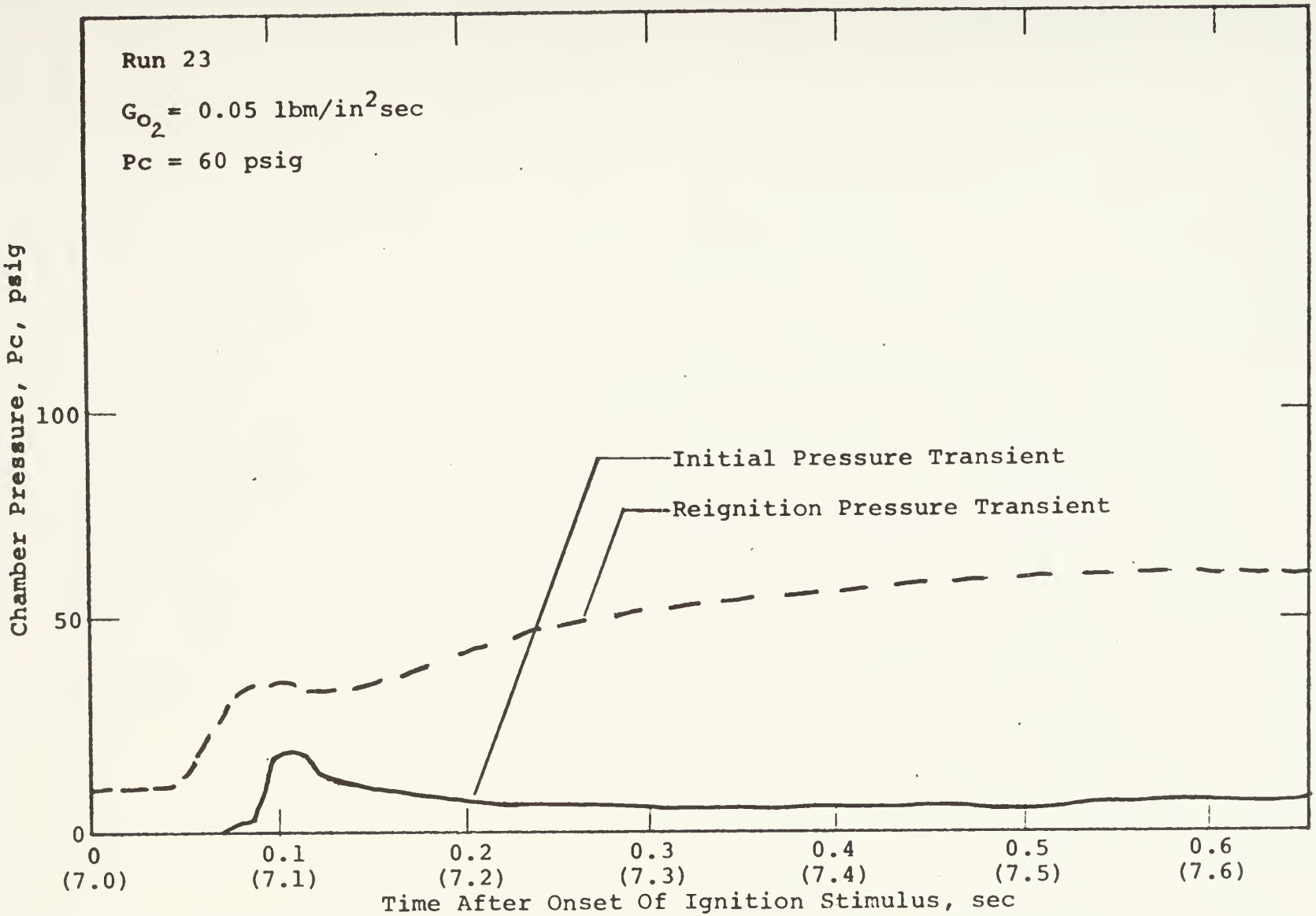

Fig. 30 Effect of a 2.0 sec Shut-down on the Pressure Transient following Reignition

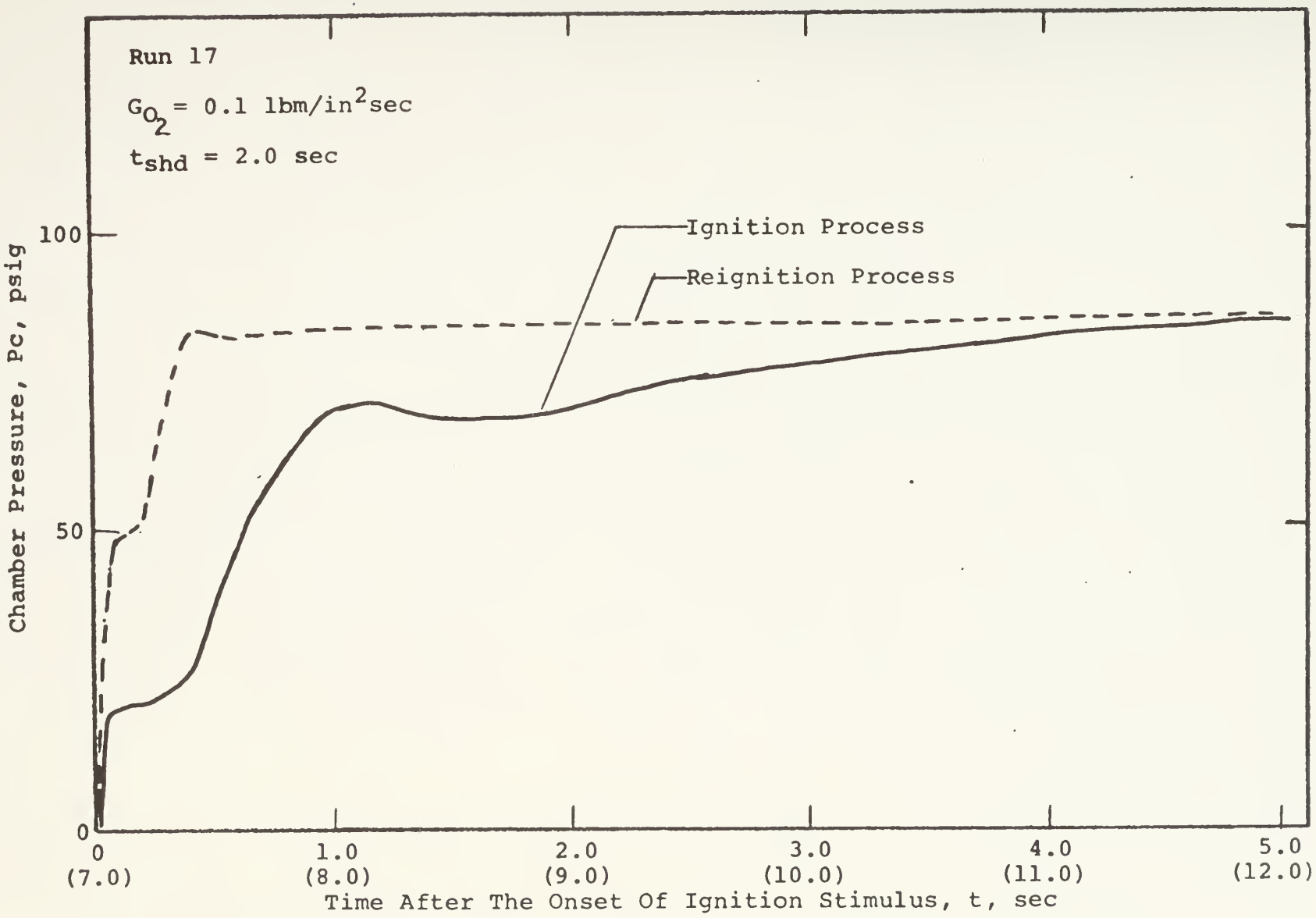

Fig. 31 Pressure-Time Histories of the Ignition and Reignition Processes

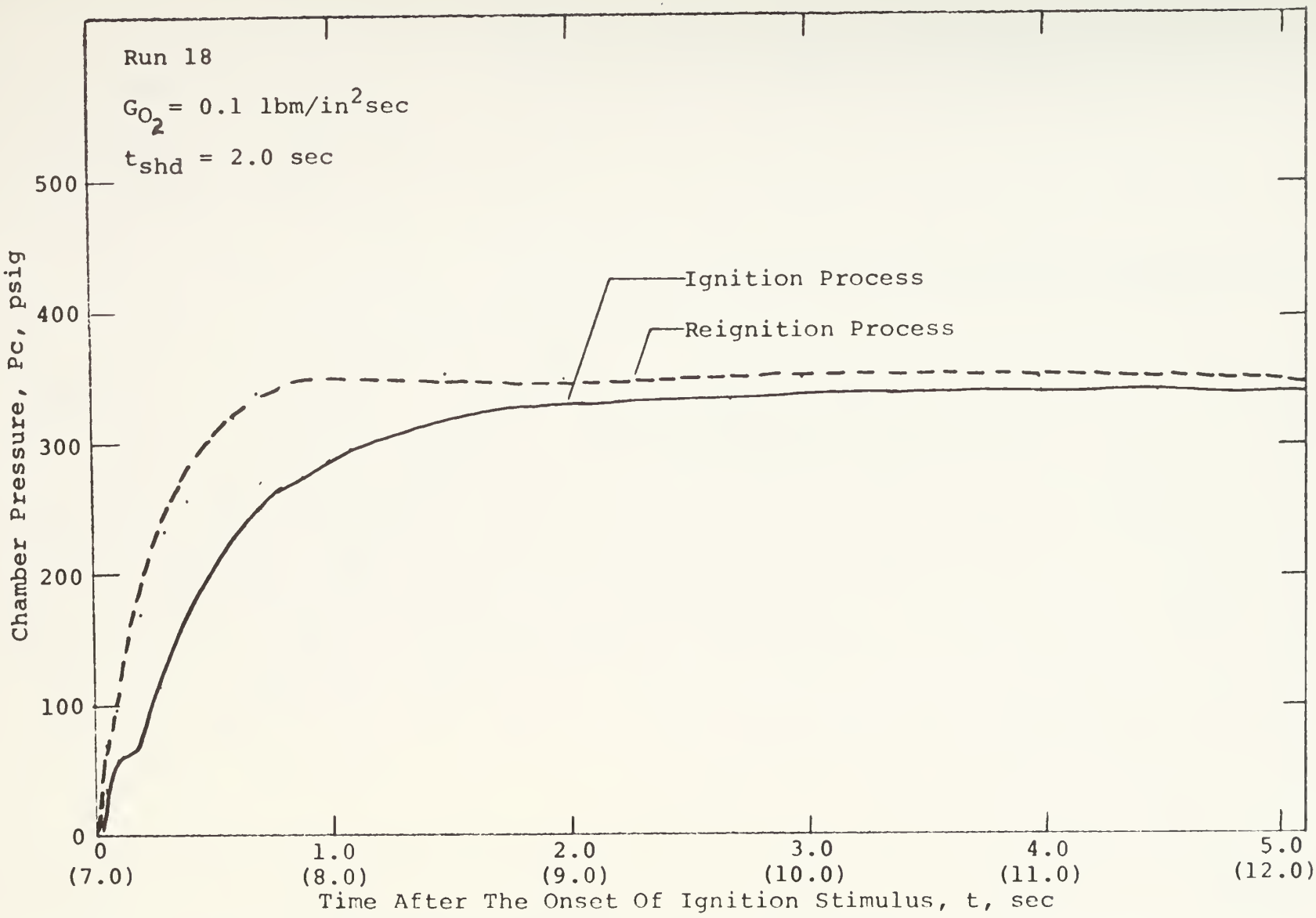

Fig. 32 Pressure-Time Histories of the Ignition and Reignition Processes

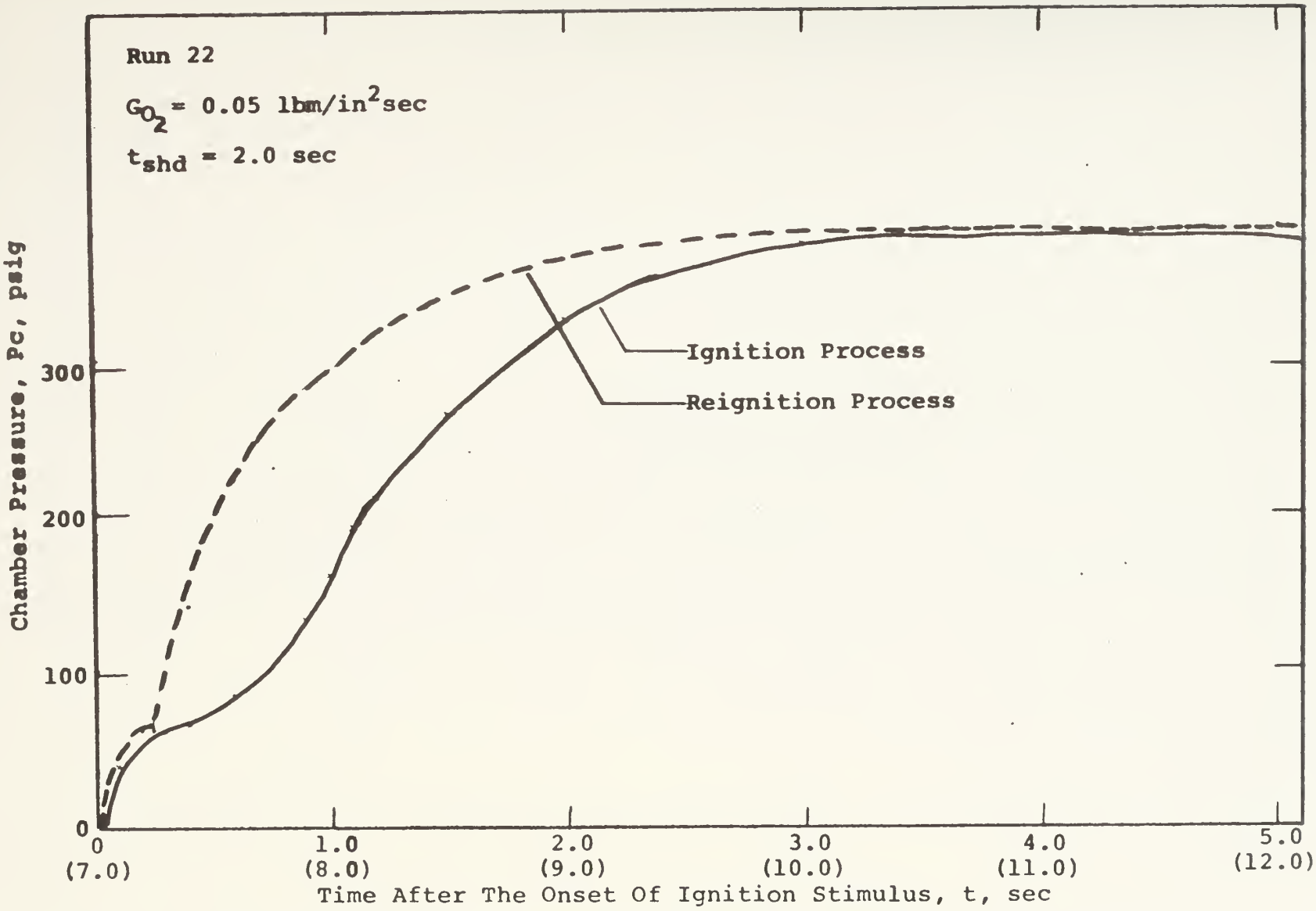

Fig. 33 Pressure-Time Histories of the Ignition and Reignition Processes

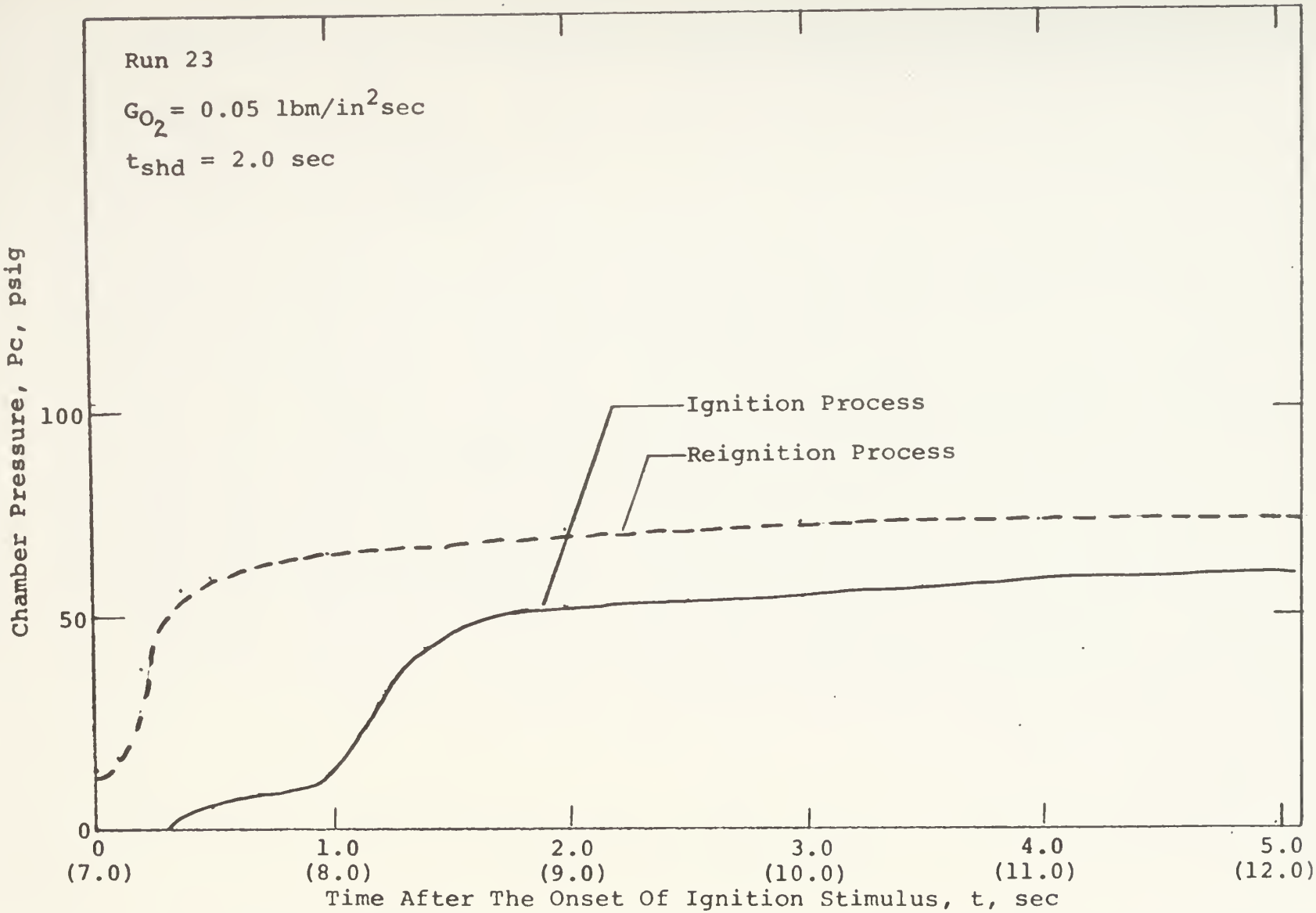

Fig. 34 Pressure-Time Histories of the Ignition and Reignition Processes

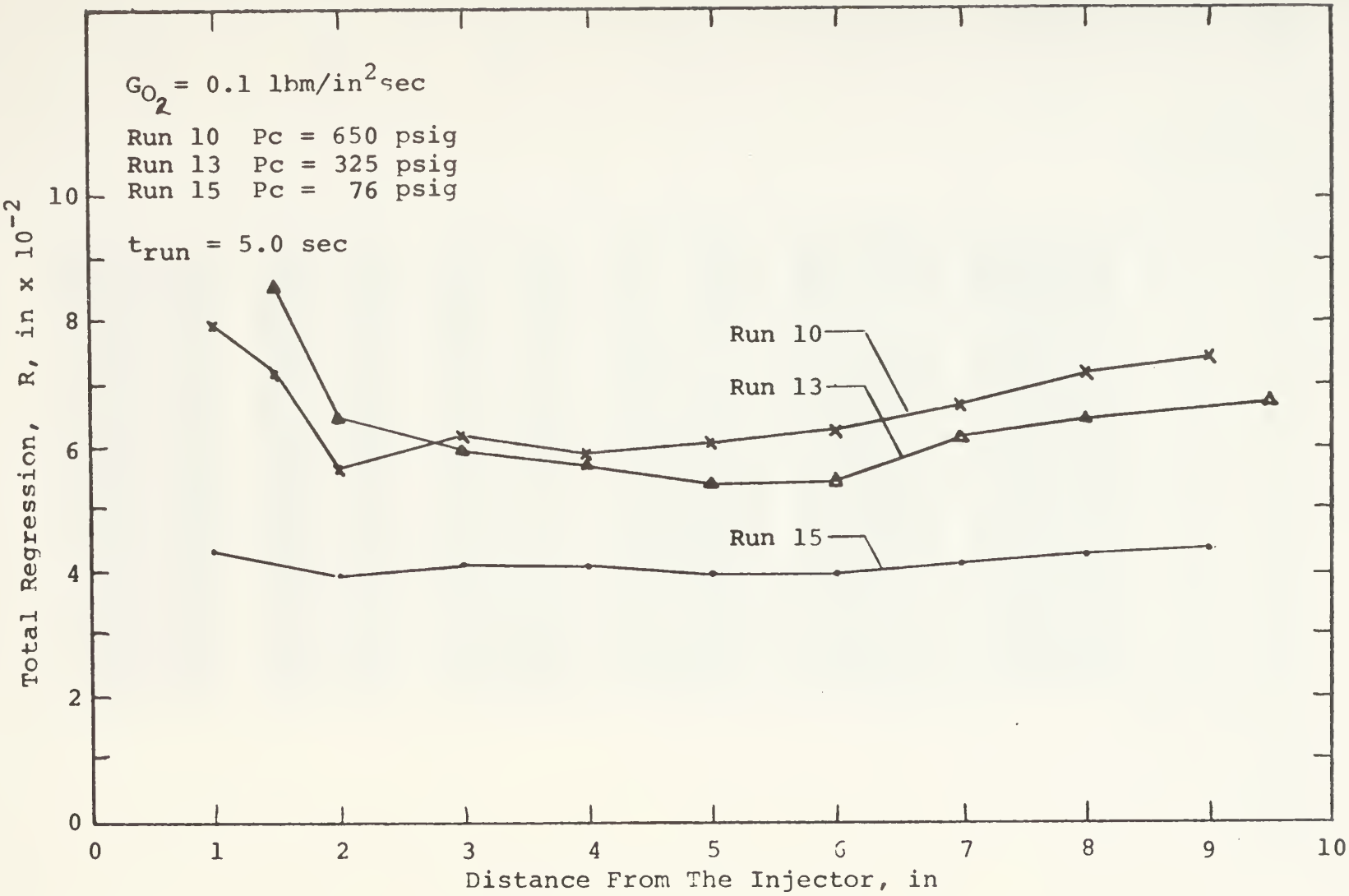

Fig. 35 Effects of Pressure on Total Regression, and Its Axial Dependence along the Grain

FLAME SPREADING DURING HYBRID IGNITION

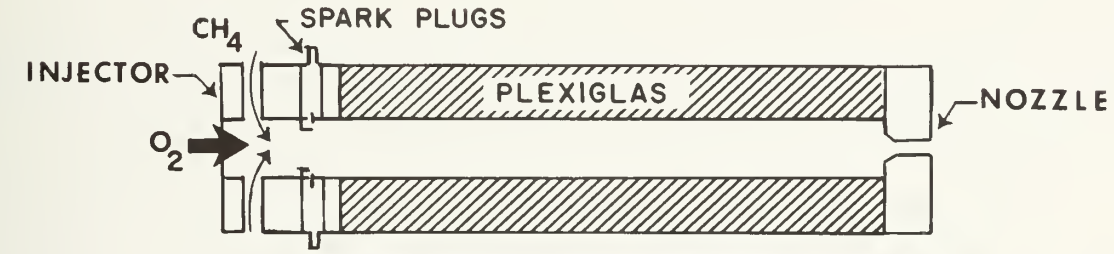

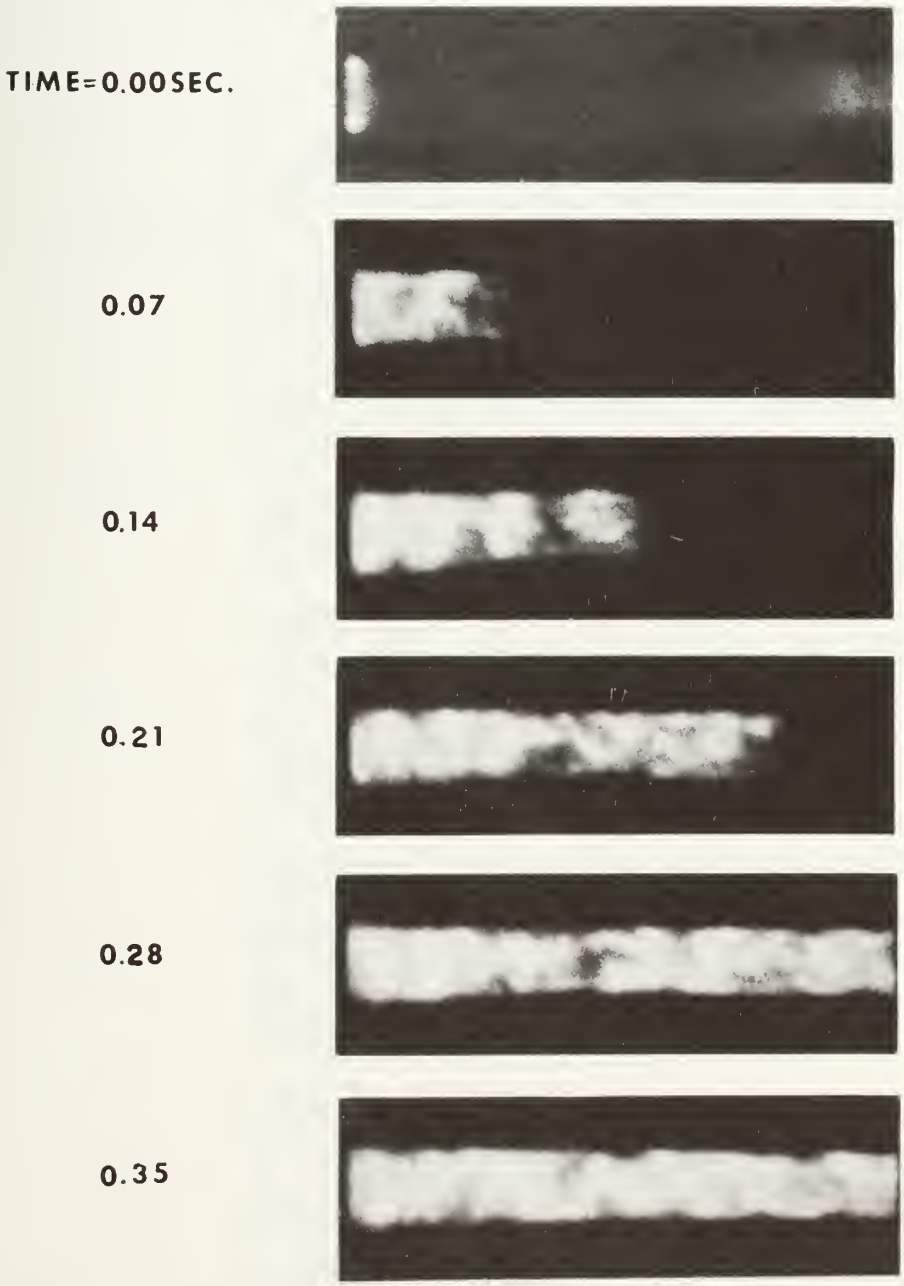

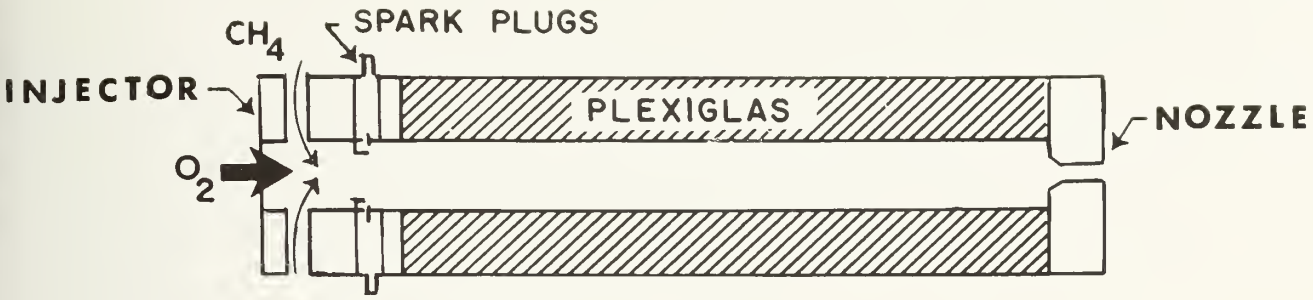

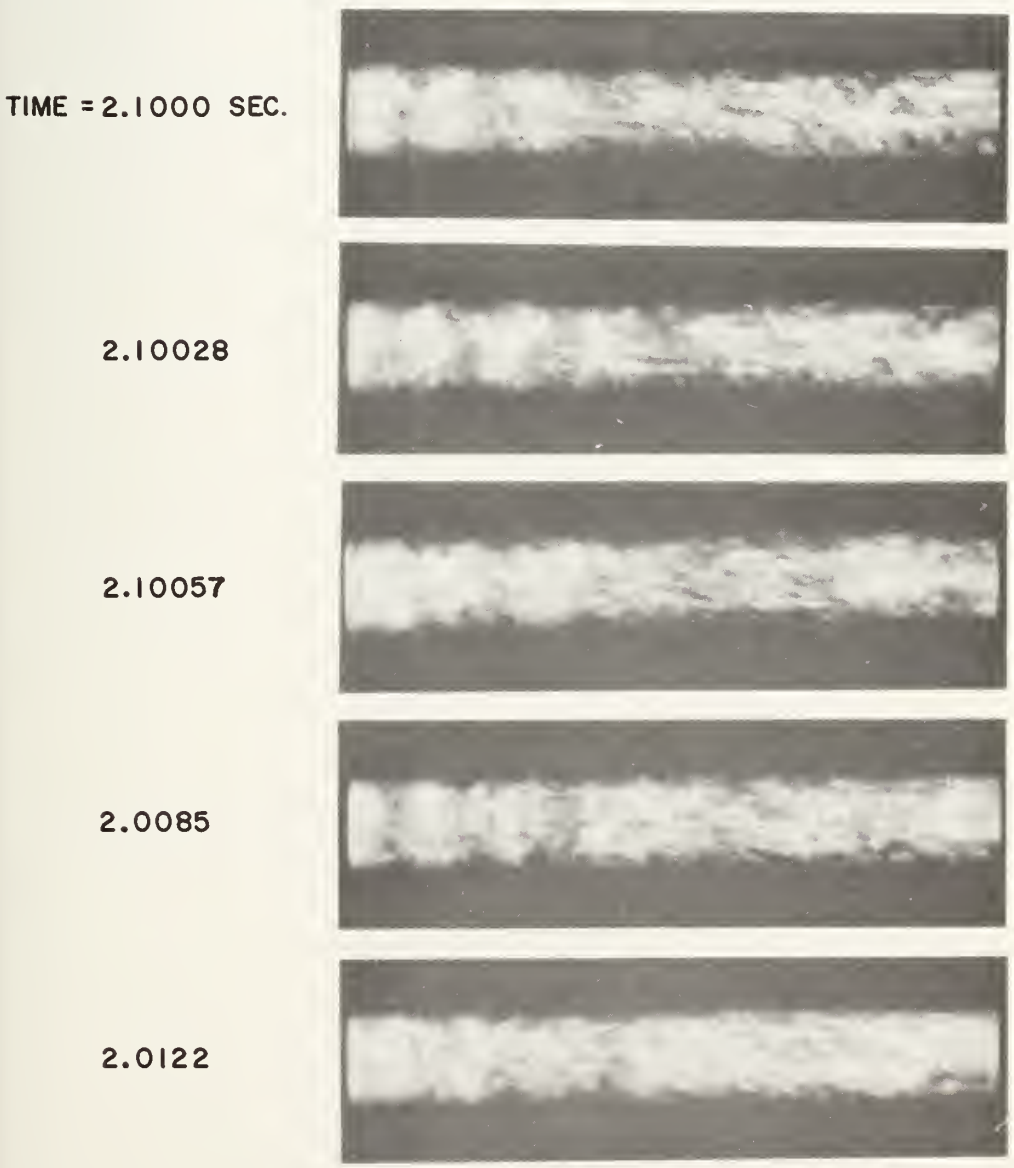

Fig. 37 Flame Distribution During Steady Burning of Hybrid Rocket

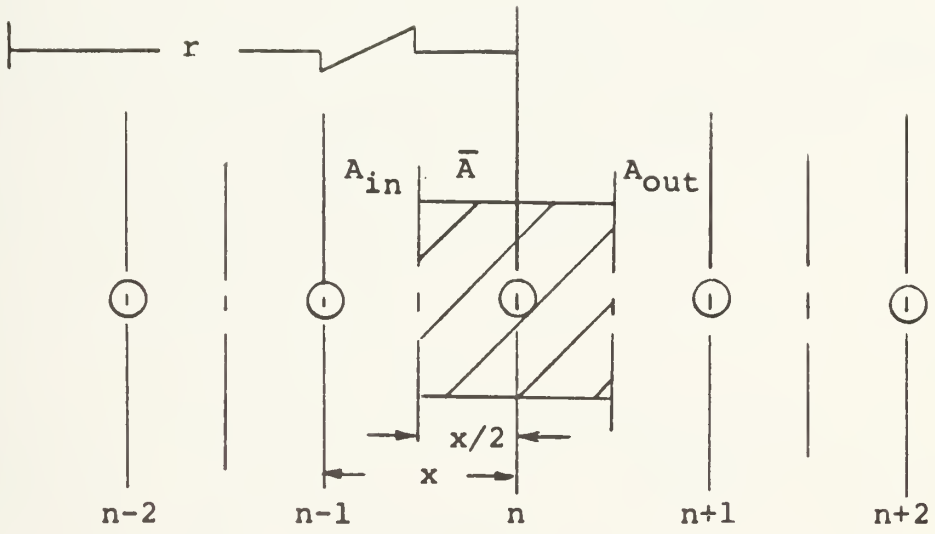

Fig. 38 Schematic of the Nodal Point Array within the Hollow Cylinder

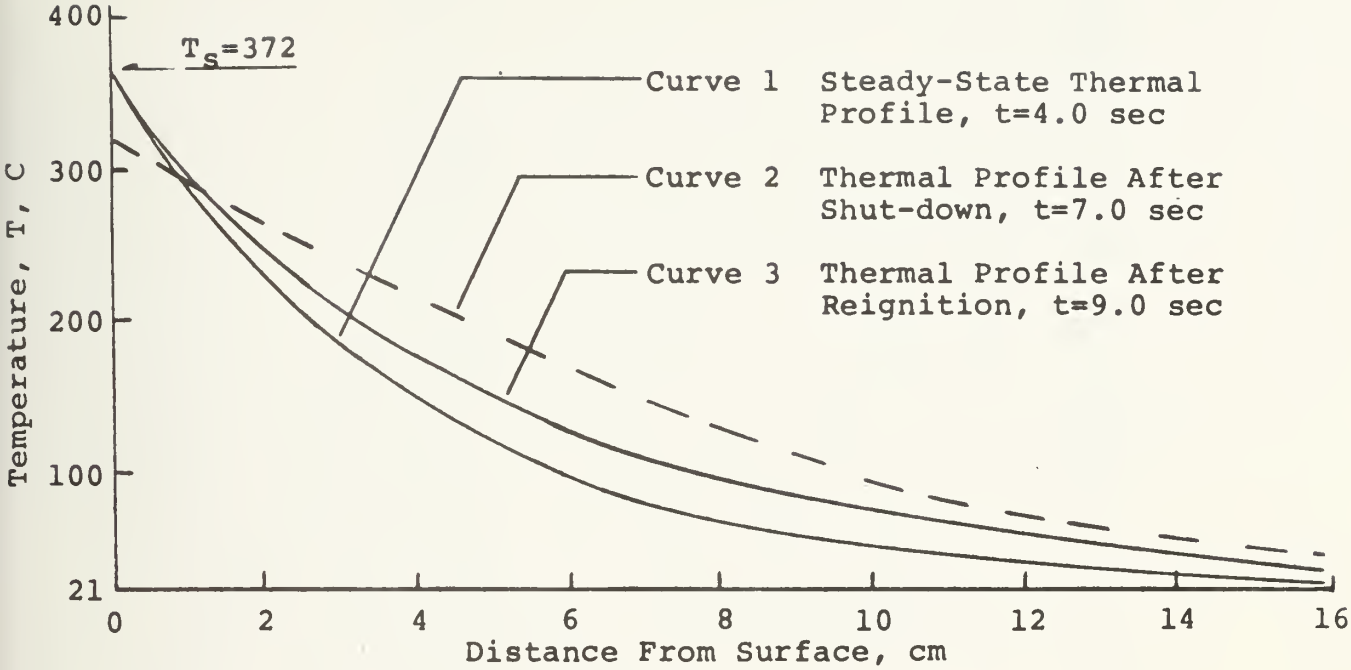

(a) Nonradiative Datum Case

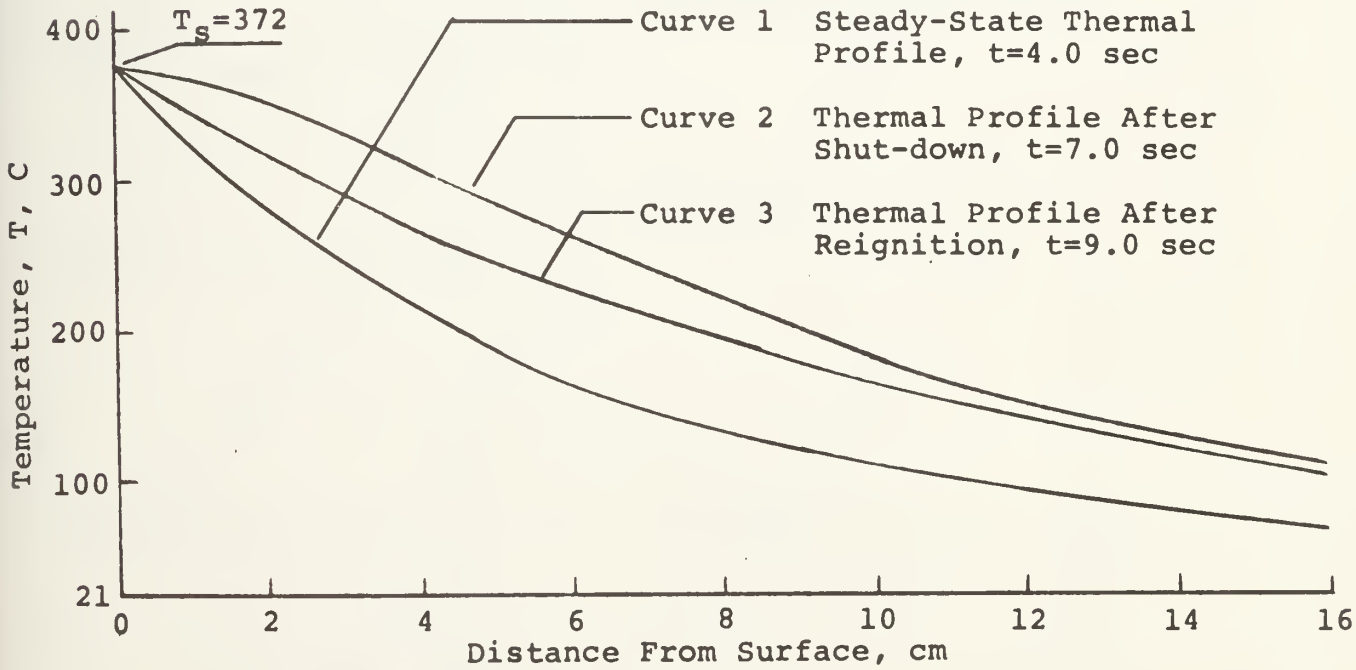

(b) Case I, Radiation Included

Fig. 39 Effects of Shut-down and Reignition on the Calculated Steady-State Thermal Profile for the Nonradiative and Radiative Cases

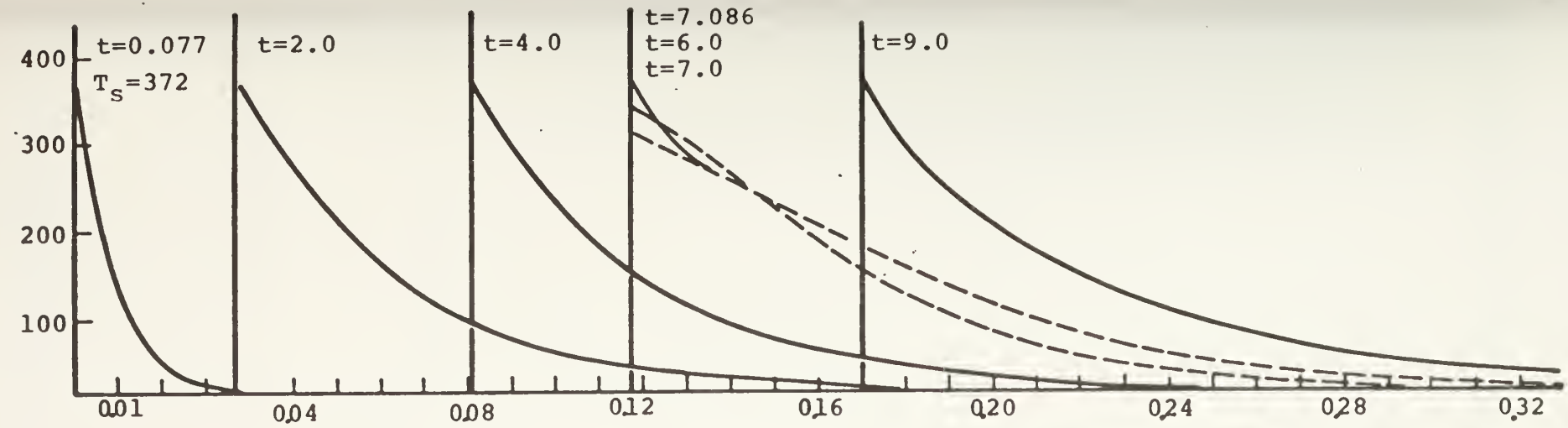

Initial Distance From The Surface, cm

(a) Nonradiative Datum Case

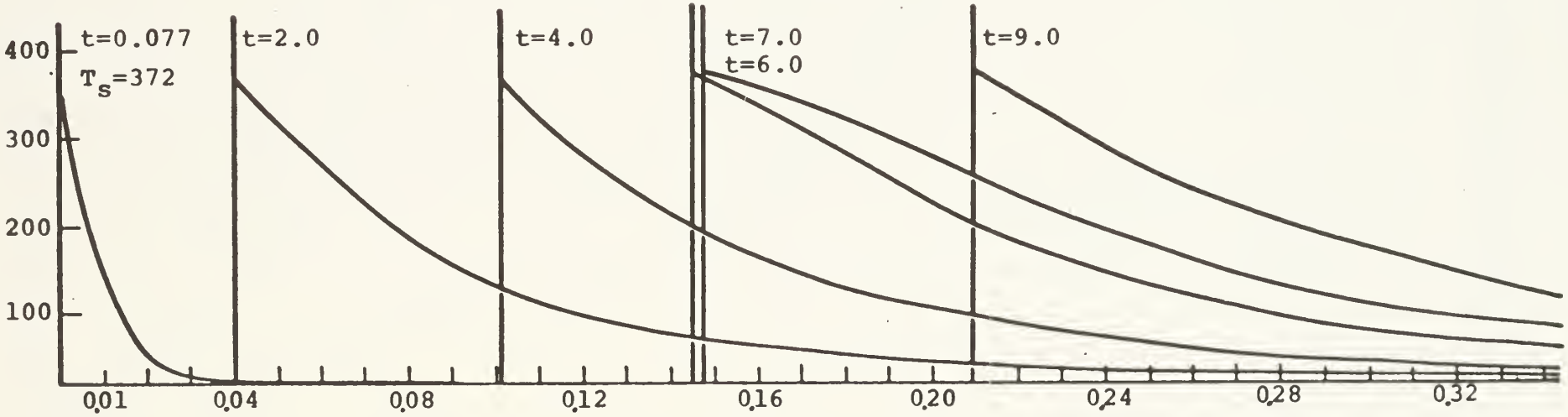

Initial Distance From The Surface, cm

(b) Case I, Radiation Included

Fig. 40 Calculated Thermal Profiles Shown at Their Respective Instantaneous Surface Locations

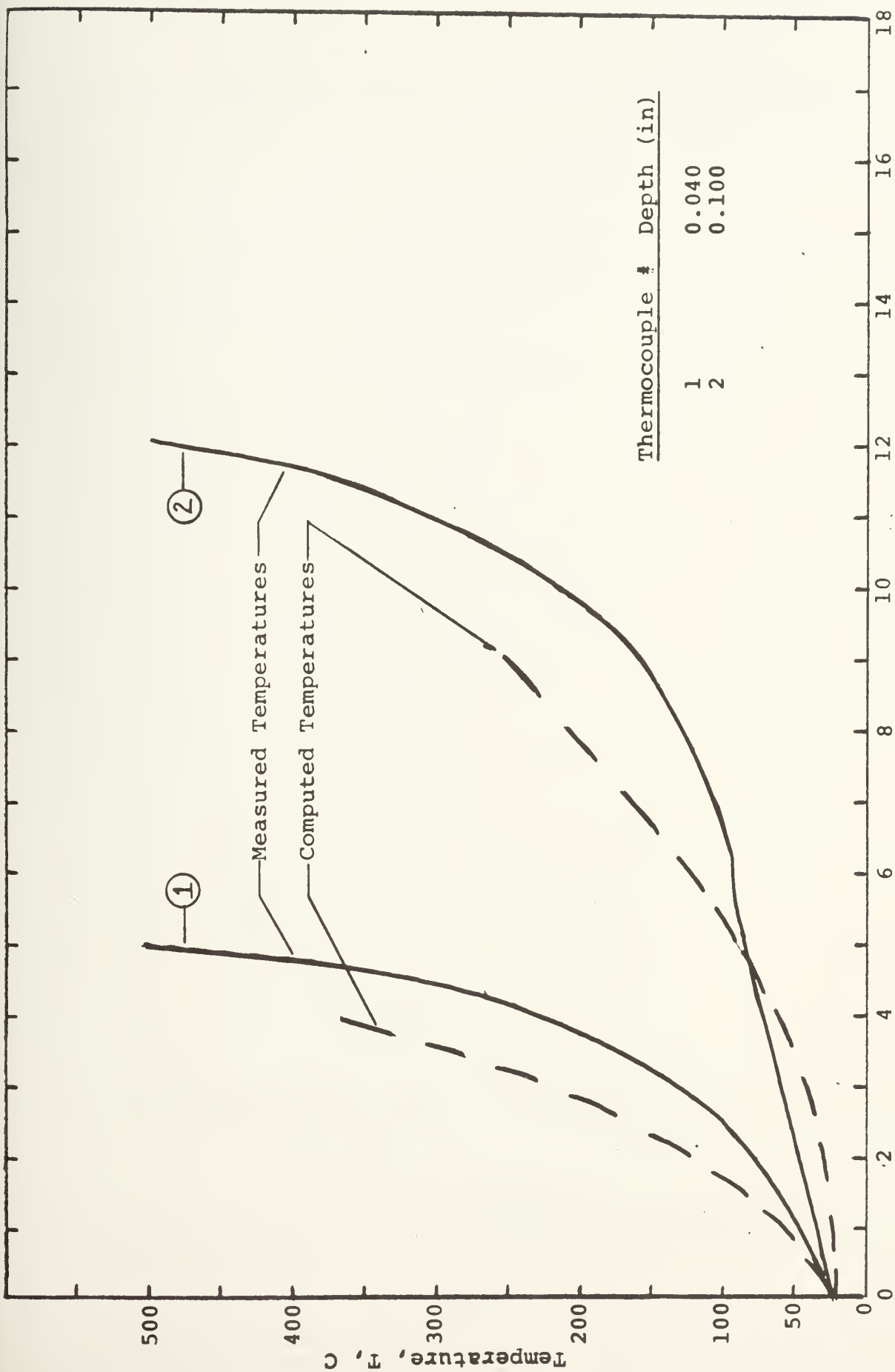

Fig. 41 Measured and Calculated Temperature-Time Responses for Two Thermocouples

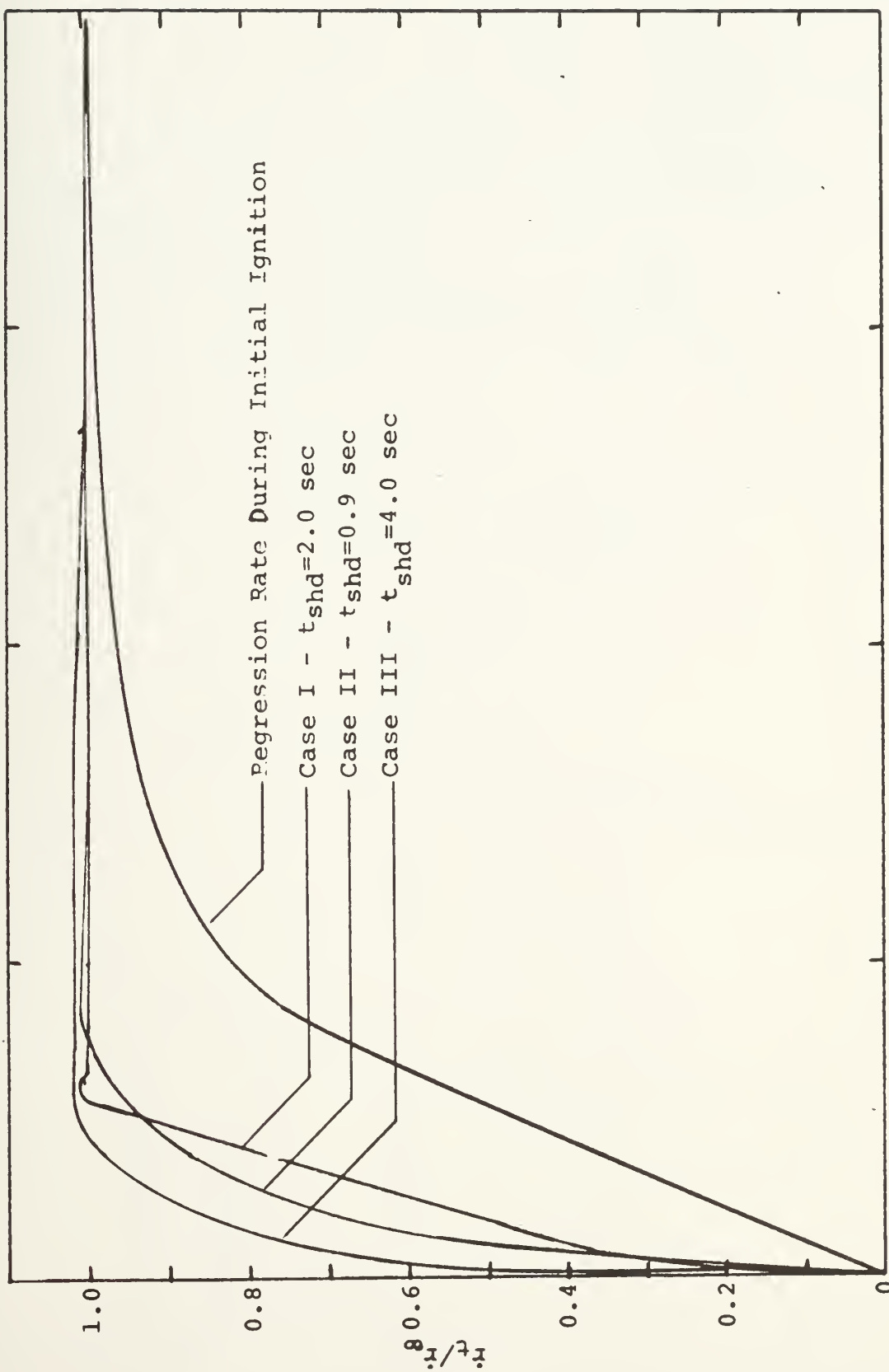

Fig. 42 The Effect of Shut-down Duration on the Transient Regression Rate Behavior following Reignition

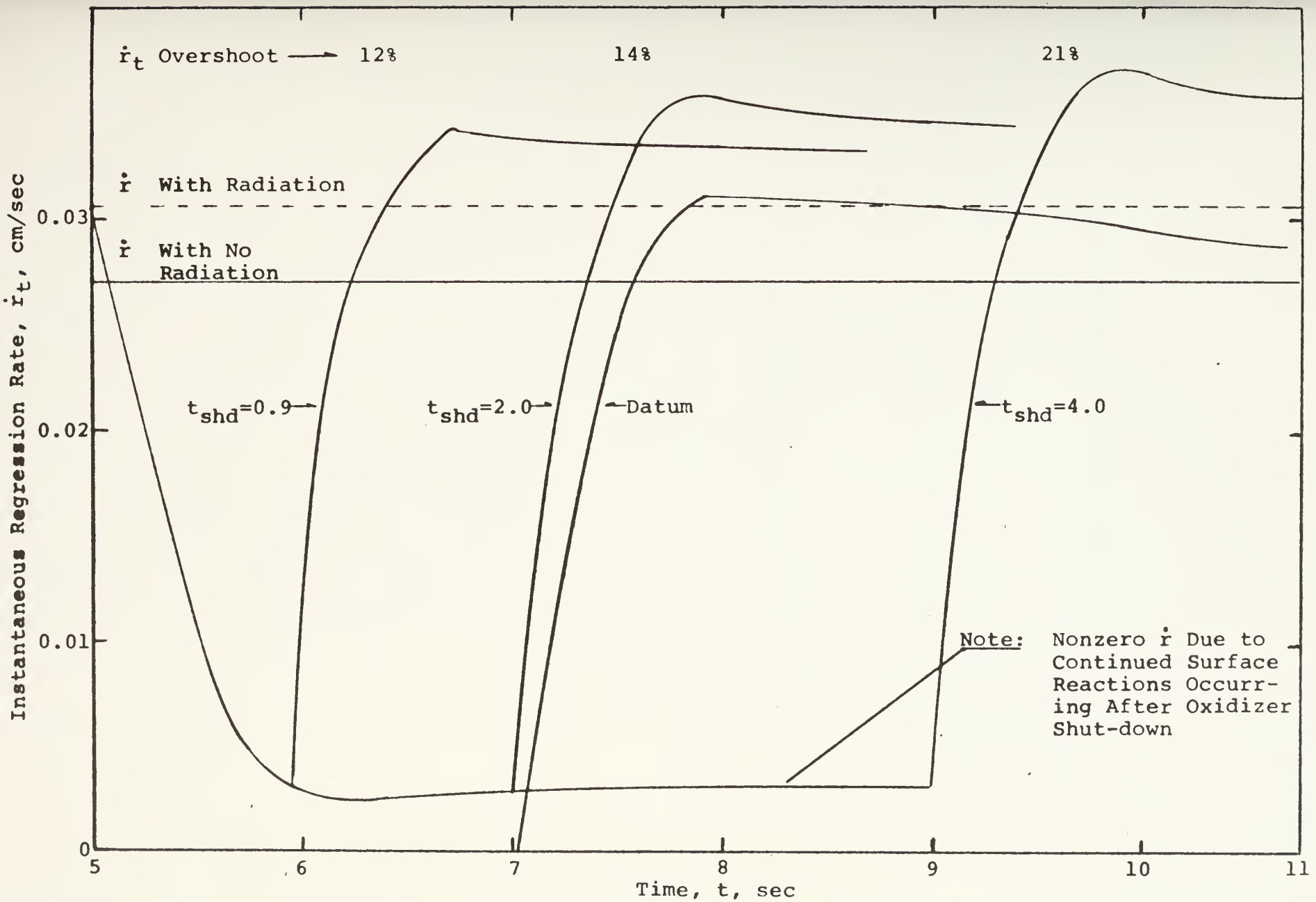

Fig. 43 Effect of Shut-down Duration on the Transient Regression Rate Behavior following Reignition

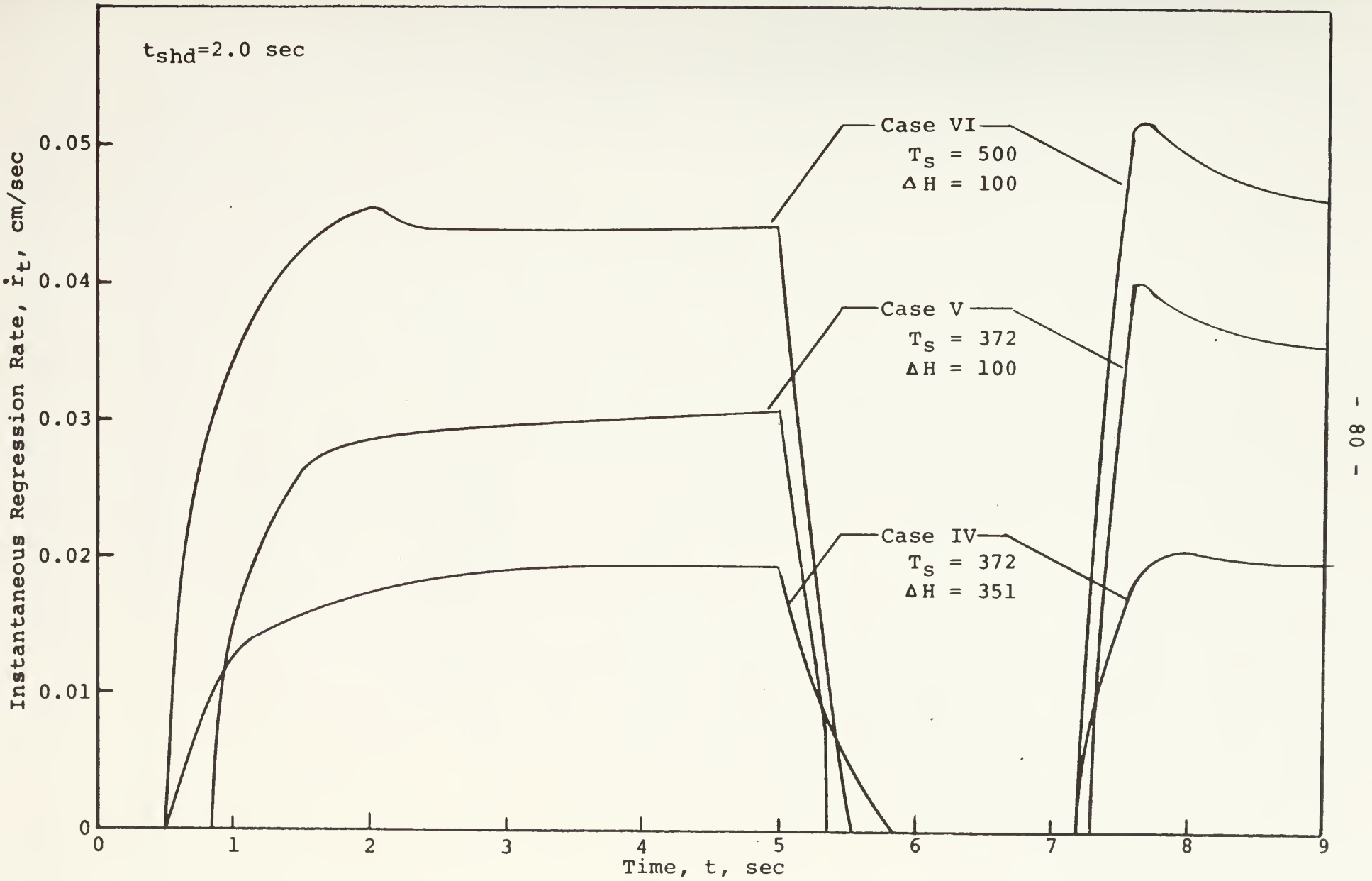

Fig. 44 Calculated Transient Regression Rate Behaviors for High Energy Fuels

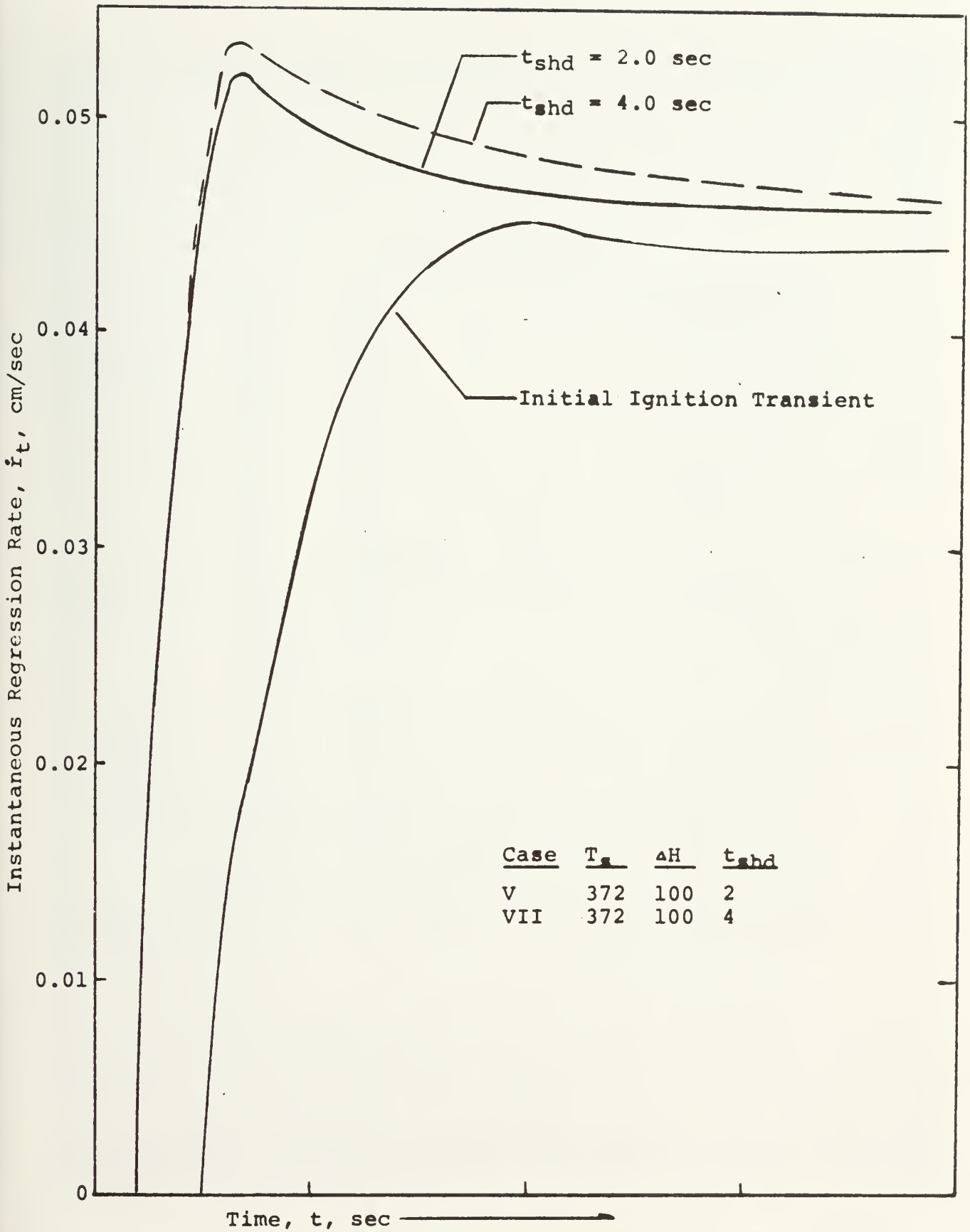

Fig. 45 Effect of Shut-down on the Calculated Transient Regression Rate Behaviors for High Energy Fuels

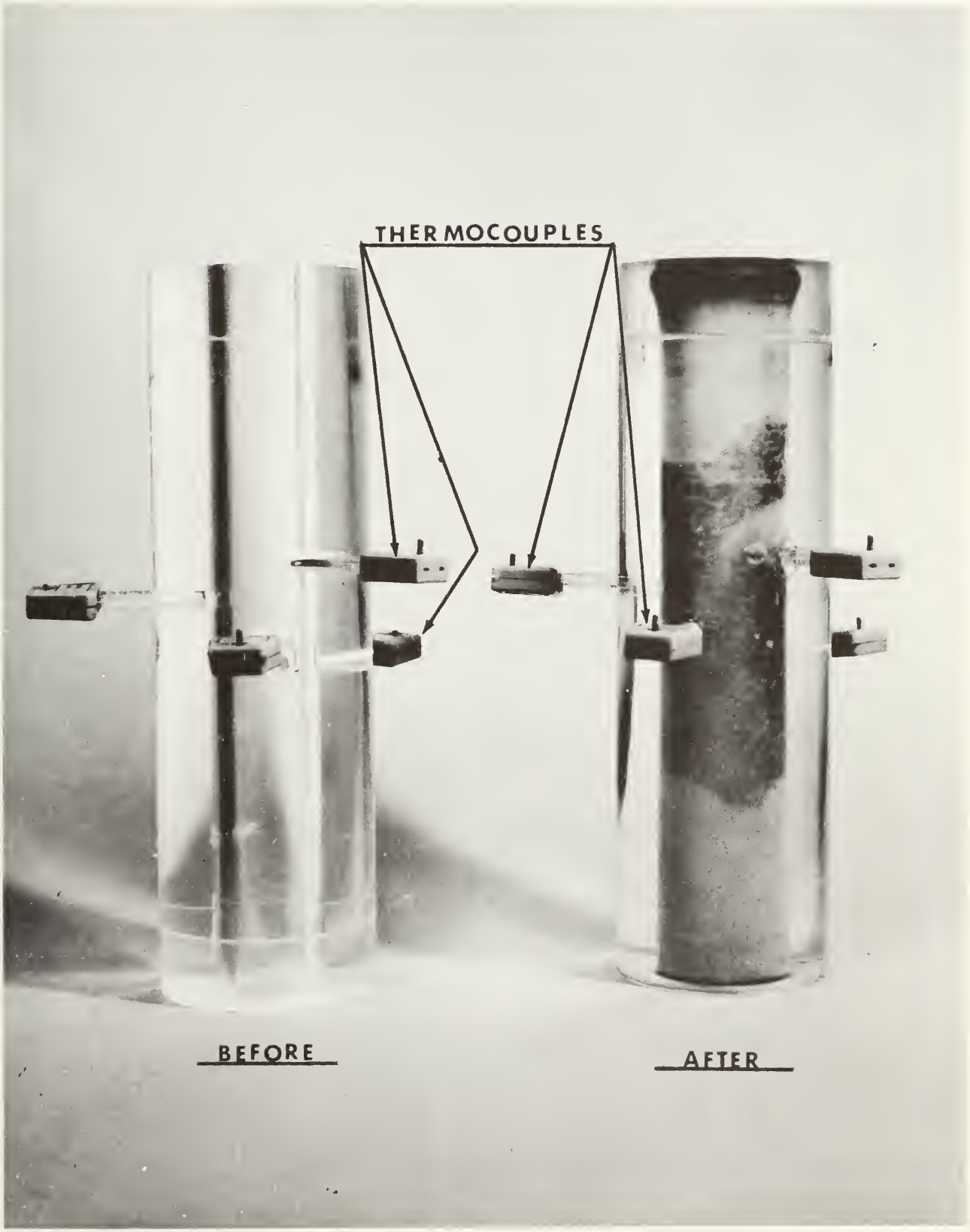

FIG. 46 PLEXIGLAS FUEL INSTRUMENTED WITH 4 THERMOCOUPLES

(FIRING SEQUENCE: $t_{run} = 5.0$, $t_{shd} = 2.0$, $t_{rel} = 5.0$ sec.)

APPENDIX A

THERMOCOUPLE TECHNIQUE

App. A-1: Considerations of the Possible Errors in Thermocouple Data

The 1-mil chromel-alumel thermocouples used in this study were purchased from Omega Engineering Inc., Stamford, Connecticut. These thermocouples provided accurate responses over the temperature range of interest and small enough wire diameter to enable temperatures to be measured without greatly disturbing the surrounding material. Yet, they were strong enough to withstand positioning on Plexiglas rods and embedding in the fuel. A Plexiglas grain instrumented with four thermocouples embedded in the fuel is shown before and after firing in Fig. 46.

Certain errors are inherent to every temperature study. A brief listing follows to describe some of these.

(1) The major problem associated with any procedure is the uncertainty in location of the point at which the temperature is being measured. The uncertainty arises from two factors. The first uncertainty is locating the actual position of the thermocouple at a prescribed depth from the surface. Each successive measured dimension used to locate the bead compounds the tolerance errors given on the previous dimension. The second uncertainty is the error in locating the effective junction of the thermocouple. The effective junction, as defined by Brewer,[25] is the point in the material whose temperature corresponds to the measured temperature output of the thermocouple. For example, the recorded temperature may be assumed to be the temperature on the surface of the bead when in fact it is the temperatures at the center of the bead.

(2) Considerable errors in temperature measurements may result from the disturbance in the material caused by the presence of the temperature probe itself. In particular, lead wires can cause considerable heat to be conducted away from the point of measurement. Studies of this conduction error made by Brewer[25] show that the errors are significant if the thermocouple lead wires near the bead are parallel to the direction of heat flow. Strittmater, et al.[26] agree that it is attractive to consider directing the leads along an isotherm to prevent heat losses through them. However, as the authors[26] indicate, an isotherm could be difficult to locate due to nonuniform burning surfaces resulting from propellant roughness. Also, as the entire surface is seldom ignited all at once, placement of the lead wires parallel to the initial grain surface involves the risk that the burning surface will reach the lead wire before the bead and preheat it by conduction.

A compromise between the two considerations mentioned above was made for this study. Lead wires in the vicinity

of the bead were oriented perpendicular to the heat flow to minimize the conduction error. At a sufficient distance away from the bead, the lead wires were directed away from the surface plane to avoid their heating before the bead.

(3) The temperature recorded by a sensing probe is dependent on its surrounding environment. The influence of radiative heating can produce large increases in temperature responses because the radiation effect is proportional to the temperature of the source raised to the fourth power minus the temperature of the sink raised to the fourth power. However, it was initially assumed for these experiments that the radiation effect on the thermocouple outputs would be insignificant and could be ignored. This assumption was based on two factors: 1) the emissivities of PM in the temperature range of interest is close to unity[15] and 2) the temperature sensing probes were made from materials that would reflect most of the radiant energy reaching the bead. Therefore, as previous workers have assumed[6,15,18], the radiation effects would be negligible. However, as discovered from the results of the thermocouple data, radiation to the subsurface regions of the fuel is significant. Thus, a solution to the heat conduction equation considering only convective heating would yield poor results when compared to experimental data, but when two radiation parameters are considered, the solution produced favorable results. Therefore, it has been an incorrect assumption by previous researchers to disregard the radiative influence on temperature measurements in Plexiglas systems.

App. A-2: Thermocouple Mounting Procedure

A mounting procedure was devised to minimize all the errors. The thermocouples were positioned and maneuvered with the aid of a micromanipulator and a Stereo-zoom microscope. The procedure used for mounting and installing are discussed in the following.

(1) The thermocouple was placed on a 1/4 inch diameter rod in a machined groove 0.005 inches in depth across the diameter of the face. Plexiglas rods 1/4 x 2 inches were used so as not to effect the properties of the fuel. The thermocouple was positioned in the groove with the bead as close to center as possible. A drop of PS-18, a plexiglas cement, was used to fasten the thermocouple bead to the rod. This cement was used since it hardens to the same material as the surrounding fuel. Therefore, it should not effect ablation in the areas of the bead or the fuel surrounding the bead.

(2) The lead wires were also cemented across the face of the 1/4 inch rod. When embedded in the fuel, the lead wires will be perpendicular to the heat flow in the vicinity of the bead and thereby minimize the conduction error described earlier. The remaining lengths of lead wire were drawn along the sides of the rod and cemented into 0.132 inch groove. An Omega, 1/4 inch Chromel-Alumel, adapter was fitted to the end of the rod and the lead wires were connected to their respective terminals. The rod, complete with thermocouple, was ready for installation in the fuel.

(3) Radial holes with flat bottoms to assure positive depth locations were drilled into the Plexiglas fuel grains. Normally each hole was measured to locate each thermocouple at a different depth. The holes were half filled with the same Plexiglas cement, PS-18, and the rods were carefully inserted, forcing some of the cement and most of the air bubbles to the surface. This procedure assured a gas-tight seal near the bead. The rods were secured with tape and at least 24 hours was allowed for drying before firing the instrumented grain.

The mounting procedure, although an arduous task requiring enduring patience, produced a reliable thermocouple probe. One hundred percent of the thermocouples installed in the fuel functioned property.

APPENDIX B

COMMERCIALLY AVAILABLE EXPERIMENTAL APPARATUS AND EQUIPMENT

Item	Use	Manufacturer or Distributor
Plexiglas (PMM)	Hybrid Rocket Fuel	Commercial Plastics & Supply Trenton, N. J.
Thermocouples (CHAL-001)	Subsurface temperature histories	Omega Engineering, Inc. Stamford, Conn.
Methane regulator (Two-stage) (MOD-3:Ser.3050)	Regulate flow of ignition gas	The Matheson Co., Inc. East Rutherford, N. J.
Pressure Transducer (PT-76-2M)	Measure chamber pressure	Dynisco, Division of American Brake Shoe Company Cambridge, Mass.
Solenoid Valves (MV-74)	Electrically operated on-off valves	Marotta Valve Corp. Boonton, N. J.
High Speed Film (931-A)	16 MM High Speed Reversal Films	DuPont Photo Products Wilmington, Del.
Plexiglas Cement (PS-18)	Embedding thermocouples	Commercial Plastics & Supply Trenton, N. J.
Wollensak Model WF-16 Fastex Camera	High Speed Movies	Wollensak Rochester, N. Y.

APPENDIX C

OPERATING PROCEDURE

FOR

HYBRID MOTOR

A. Pre Firing Procedure

1. Turn on all electrical equipment to allow for 30 min. warm up.
2. Select and install O_2 orifice.
3. Select and install CH_4 orifice.
4. Weigh and install graphite insert.
5. Install pressure transducers: include RTV ¼ disk where needed.
6. Clean, weigh, and install grain.
7. Install nozzle plate.
8. Connect all recording devices.
9. For Electrical hookup procedure go to Section B.
10. Turn on main N_2 pressure (Mechanical Room).
11. Open N_2 control pressure valve (Test Cell).
12. For calibration procedure go to Section C.
13. Open CH_4 bottle valve and set CH_4 regulator.
14. Open O_2 bottle valve and record pressure.
15. Plug in ignitor control box at wall outlet.
16. Plug in spacing grid hamp.
17. Ignitor control safe switch to on.
18. Install exhaust duct.
19. Remove keys and clear area #Z.
20. Open blower vent and vacate test cell.
21. Turn on blower.

B. Electrical Procedure

1. Plugs from test area #Z (4 pins) to transducer input #I.
2. Calibrate voltmeter @ 9000.
3. Zero voltmeter @ 0000.
4. Zero amplifiers @ 10 volts with shunts.
5. Calibrate transducers with 10 volts thru input conductioners using volt button.
6. Balance transducer thru amplifier output with balance buttons to zero.
7. Connect marker blips using reversed (bronze) cords.
8. Fl to CH_2.
9. Ol to CH_4.

C. N_2 Calibration

1. From A #11.
2. Check N_2 line supply from area 4.
3. Turn on 24 volt power.
4. N_2 supply switch on panel to on.
5. Calibrate @ pressures.
6. Dump N_2 pressure from panel switch.

D. Firing Procedure

1. Turn on circuit breaker 14, 17, 12, and DC supply.
2. Turn on N_2 supply switch on panel.
3. Set O_2 reservoir pressures.
4. Check ignitor mode switch, ignitor timer and run duration timer.
5. Reset automatic O_2 switch to down position.
6. Power to area.
7. Warning lights on.
8. Siren on.
9. Firing mode switch to READY.
10. Firing sequence.
11. Terminate sequence with reset O_2 switch to up position.

E. Shut Down Procedure

1. N_2 purge for 2 sec.
2. Siren off.
3. Firing mode switch to off.
4. Remove keys from console.
5. Turn off circuit breaker #17.
6. Blower on for 15 sec.
7. Enter test cell and turn off ignitor safety switch.
8. Remove ignitor control box plug from wall outlet.
9. Close CH_4 and O_2 bottle valves.
10. Vacate test cell and turn blower on.
11. Insert keys.
12. Firing mode switch to SAFE.

13. Bleed O_2 line and reservoir pressure.
14. Bleed CH_4 line intermittent N_2 purge.
15. Firing mode switch to off.
16. Remove keys from console.
17. Turn off N_2 control pressure valve.
18. Insert keys.
19. Firing mode safety switch to safe.
20. Bleed purge pressure.
21. Console N_2 supply switch to off.
22. Warning lights off.
23. 24 volt DC power off.
24. Circuit BK #14 off.
25. Break down and clean motor.
26. Clean up test cell.

Thesis 122325
S1665 Saraniero
Combustion anomalies
in stop-restart fir-
ing of hybrid rocket
engines.